NUREG/CR–5343
PNL–6806

Radionuclide Characterization of Reactor Decommissioning Waste and Spent Fuel Assembly Hardware

Progress Report

Prepared by
D. E. Robertson, C. W. Thomas, N. L. Wynhoff, D. C. Hetzer

Pacific Northwest Laboratory
Operated by
Battelle Memorial Institute

Prepared for
U.S. Nuclear Regulatory Commission

NUREG/CR--5343

TI91 007071

Radionuclide Characterization of Reactor Decommissioning Waste and Spent Fuel Assembly Hardware

Progress Report

Manuscript Completed: December 1990
Date Published: January 1991

Prepared by
D. E. Robertson, C. W. Thomas, N. L. Wynhoff, D. C. Hetzer

Pacific Northwest Laboratory
Richland, WA 99352

Prepared for
Division of Regulatory Applications
Office of Nuclear Regulatory Research
U.S. Nuclear Regulatory Commission
Washington, DC 20555
NRC FIN B2880

NUREG/CR-5343
PNL-6806

MASTER

DISTRIBUTION OF THIS DOCUMENT IS UNLIMITED

ABSTRACT

This study is providing the NRC and licensees with a more comprehensive and defensible data base and regulatory assessment of the radiological factors associated with reactor decommissioning and disposal of wastes generated during these activities. The objectives of this study are being accomplished during a two-phase sampling, measurement, and assessment program involving the actual decommissioning of Shippingport Station and the detailed analysis of neutron-activated materials from commercial reactors. Radiological characterization studies at Shippingport have shown that neutron activation products, dominated by ^{60}Co, comprised the residual radionuclide inventory. Fission products and transuranic radionuclides were essentially absent. Waste classification assessments have shown that all decommissioning materials (except reactor pressure vessel internals) could be disposed of as Class A waste. Measurements and assessments of spent fuel assembly hardware have shown that ^{63}Ni, ^{59}Ni, and ^{94}Nb sometimes greatly exceed the 10CFR61 Class C limit for some components, and thus would require disposal in a high level waste repository. These measurements are providing the basis for an assessment of the disposal options for these types of highly radioactive materials. Comparisons of predicted (calculated) activation product concentrations with the empirical data are providing an assessment of the accuracy of calculational methods. Work is continuing on radiological characterization of spent PWR and BWR control rod assemblies. Additional work is planned on current issues/problems relating to reactor decommissioning. These efforts will be reported on in future supplements to this report.

EXECUTIVE SUMMARY

This study has been implemented to provide the NRC and licensees with a more comprehensive and defensible data base and regulatory assessment of the radiological factors associated with reactor decommissioning and disposal of wastes generated during these activities. The objectives of this study are being accomplished during a two-phase sampling, measurement, and assessment program involving the actual decommissioning of Shippingport Station and the detailed analysis of neutron-activated materials from commercial reactors. Radioactive materials have been obtained from Shippingport Station and from a number of commercial stations for comprehensive radionuclide and stable element analyses.

The decommissioning of Shippingport Station, completed in 1989 under the direction of the Department of Energy, has provided a valuable opportunity to conduct a rather detailed study of the residual radionuclides in contaminated components of a nuclear power plant during an actual dismantling and disposal of a plant. Although it is recognized that there were differences between Shippingport Station and other commercial nuclear power stations, the similarities were such that an examination of the residual radionuclides associated with dismantled Shippingport components has provided valuable information for helping to assess the technology, safety, and costs of decommissioning commercial stations. Radiological characterization studies have shown that neutron activation products, dominated by ^{60}Co, comprised the residual radionuclide inventory at Shippingport Station. Fission products and transuranic radionuclides were essentially absent. Waste classification assessments have shown that all decommissioning materials (except reactor pressure vessel internals) could be disposed of as Class A waste. Physical, chemical, and radiological characterization of the radioactive corrosion film have provided data for a safety analysis for transportation of the reactor pressure vessel/neutron shield tank as an LSA Type B package for burial.

In an effort to characterize the long-lived activation products generated in reactor pressure vessel and fuel assembly hardware, samples of stainless steel, inconel, and zircaloy materials have been obtained from a variety of components from a number of nuclear power stations. To date, these include: stainless steel, inconel, and zircaloy materials from Shippingport fuel assemblies; stainless steel, inconel, and zircaloy materials from each of three fuel assemblies: 1) a General Electric spent fuel assembly from Cooper Station; 2) a Westinghouse assembly from Point Beach Station; and 3) a Combustion Engineering assembly from Calvert Cliffs Station. Also, samples of the steel pressure vessel from the Gundremmigen KRB-A reactor have been analyzed. These measurements and assessments have shown that ^{63}Ni, ^{59}Ni, and ^{94}Nb sometimes greatly exceed the 10CFR61 Class C limit for some components of fuel assembly hardware, and thus would require disposal in a high level waste repository or some other approved alternative facility. These measurements are providing the basis for an assessment of the disposal options for these types of highly radioactive materials.

An associated task in this program is to provide a comparison of empirical versus predicted (calculated) radionuclide inventories in neutron-activated components to ascertain the accuracy of the predictive methods and identify any possible weak links in the calculation techniques. Results to date indicate that the calculational methods for predicting the concentrations of long-lived activation products (^{60}Co, $^{59,63}Ni$, ^{55}Fe, ^{94}Nb) in commercial fuel assembly hardware and reactor construction materials generally agree to within 10% to a factor of two near the fueled region of the assembly hardware, but may be an order of magnitude different near the end fittings. The discrepancies are attributed to insufficient neutronics data for use in the calculational methods. These studies have identified problem areas for certain radionuclide inventory calculations, but provide a degree of confidence in the ability to predict concentrations of other activation products.

The results of the Gundremmigen measurements indicated good agreement between measured versus calculated concentrations of ^{55}Fe, ^{63}Ni, ^{60}Co, and ^{94}Nb in the reactor pressure vessel. An assessment showed that the pressure vessel (not including internals) would qualify as Class A waste.

With the completion of the Shippingport Station decommissioning and the radiological analyses of the spent fuel assembly hardware, the project will focus on the radiological characterization of spent PWR and BWR control rod assemblies and in addressing current issues/problems relating to reactor decommissioning, such as the adequacy of dose-to-curie conversion techniques, and adequacy of radiochemical methods for determining 10CFR61 radionuclides, and assessing alternative ways of disposing of greater-than-Class C radioactive materials. These efforts will be reported on in future supplements to this report.

ACKNOWLEDGMENTS

The U.S. Nuclear Regulatory Commission (NRC) project manager for this work is Carl Feldman, and Donald Cool is the Branch Chief, Radiation and Health Effects Branch. The authors wish to express our appreciation to Carl Feldman for his expert guidance, suggestions, and support during the course of this work. We also acknowledge and appreciate the assistance of Keith Steyer and Charles Serpan of the NRC in support of this project.

CONTENTS

FIGURES

TABLES

1.0 INTRODUCTION

1.1 PROJECT PLAN AND OBJECTIVES

The U.S. Nuclear Regulatory Commission (NRC) has recently enacted rules setting forth technical, safety, and financial criteria for decommissioning of licensed nuclear facilities, including commercial nuclear power stations.[1] These rules have addressed six major issues, including decommissioning alternatives, timing, planning, financial assurance, residual radioactivity, and environmental review. Also, the rules governing disposal of low-level radioactive wastes in commercial shallow land burial facilities will be applicable to most of the wastes generated during reactor decommissioning.[2] The appropriate response to each of these issues by the licensee and the NRC depends greatly on an accurate and reliable assessment of the residual radiological conditions existing at the nuclear power stations at the time of decommissioning. Large volumes of data exist which describe the radionuclide concentrations associated with active waste streams generated at nuclear power stations. However, comparatively little information is available that documents the residual radionuclide concentrations, distributions, and inventories residing in contaminated piping, components, and materials of nuclear plant systems and in neutron-activated materials associated with the reactor pressure vessel and biological shield. Especially lacking is a detailed radiological characterization of the numerous types of wastes encountered during an actual reactor decommissioning and a characterization of the highly neutron-activated metal components associated with pressure vessel components and spent fuel assembly hardware.

This study has been implemented to provide the NRC and licensees with a more comprehensive and defensible data base and regulatory assessment of the radiological factors associated with reactor decommissioning and disposal of wastes generated during these activities. The objectives of this study are being accomplished during a two-phase sampling, measurement, and appraisal program utilizing 1) the decommissioning of Shippingport Atomic Power Station and 2) neutron-activated materials from commercial reactors. Radioactive materials obtained from Shippingport Station and from a number of commercial stations for comprehensive radionuclide and stable element analyses are being utilized to assess the following important aspects of reactor decommissioning and radioactive waste characterization:

- radiological safety and technology assessment from an actual reactor decommissioning (Shippingport)
- radiological characterization of intensely radioactive materials (greater than Class C) associated with the reactor pressure vessel and spent fuel assembly hardware from commercial nuclear power plants
- evaluation of the accuracy of computer codes for predicting radionuclide inventories in retired reactors and neutron-activated components

- assessment of waste disposal options associated with reactor decommissioning.

1.2 SCOPE OF STUDY

This study comprises two main research areas associated with reactor decommissioning: 1) providing a detailed radiological characterization and assessment from the actual complete decommissioning of Shippingport Atomic Power Station, and 2) conducting a detailed radiological assessment of the highly neutron-activated metal components associated with reactor internals and spent fuel assembly hardware.

1.2.1 Radiological Characterization from Shippingport Decommissioning

The complete dismantlement of Shippingport Atomic Power Station, which began in 1985, and the restoration of the site to unrestricted use in 1989 has provided a unique opportunity to conduct a detailed radiological assessment during an actual reactor decommissioning. Although this reactor station was a Department of Energy (DOE) facility and was not subject to the decommissioning and radioactive waste disposal rules provided by the NRC for commercial reactors, the technology, safety, and transportation methods associated with its decommissioning are very similar to that which a commercial licensee would utilize.

Shippingport Station was significantly smaller than most commercial reactors and it is recognized that there were some differences in design, materials, and operations. However, the similarities were such that an examination of the residual radioactivity associated with its decommissioning could provide valuable generic information for helping to assess the technology, safety, and costs of decommissioning commercial stations.

The residual radionuclide inventory remaining within nuclear power plants following permanent shutdown is primarily affected by the following parameters:

- composition and purity of construction materials
- general design of the primary and secondary systems
- core design
- operational parameters (water chemistry, corrosion control, fuel integrity, radwaste management, maintenance operations and housekeeping)
- criticality control
- reactor power level (megawatts)
- length of operation.

With regard to all of the above parameters, except reactor power level and later water chemistry, the Shippingport Station possessed many similarities to a modern, commercial pressurized water reactor (PWR) power station. It is quite probable that the inventory and distribution of residual radionuclides would scale-up in a generic way to larger light-water reactor stations that have experienced little or no fuel failures. Therefore, a sampling and analysis of the primary, secondary, and auxiliary systems during decommissioning provided a unique opportunity to develop information generically applicable to the eventual decommissioning of larger commercial PWR stations.

Table 1.1 gives a comparison of important parameters of the Shippingport Station primary system with that for the Reference PWR used in the conceptual decommissioning assessment by Smith et al. (1978).[3]

TABLE 1.1. Comparison of the Shippingport Primary System with the Primary System in a Reference PWR

Component	Reference PWR[3]	Shippingport
Power	1000 MWe	72 MWe
Pressure vessel size	44′ X 15′ diam.	33.2′ X 10.5′ dia.
Piping Systems	80 miles	20 miles
Fuel Cladding	Zircaloy	Zircaloy
Control Rods	Ag-In (ss clad)	Hafnium (cores 1 and 2)
Vessel Internals	Stainless and Inconel	Stainless and Inconel
Reactor Vessel	Carbon steel, stainless steel clad, 0.156" min.	Carbon steel, stainless steel clad, 0.125" min.
Heat Exchangers	Carbon steel, inconel and stainless steel clad, U tube type	Stainless tubes, U and straight tube types
Coolant Loops	4	4
Primary Piping	Stainless steel	Stainless steel
pH Control	LiOH, 0.2 to 2 ppm	LiOH (Core 1); NH_4OH (Cores II & III)
Oxygen Control	Hydrogen, 30 ml/kg	Hydrogen, 25 ml/kg
Reactivity Control	Boric acid, 0-2000 ppm	(a)

(a) Core I controlled with rods only; Core II used control rods and burnable poison inside the fuel rods; Core III was controlled by moveable fuel rods only. $K_2B_4O_7 \cdot 8H_2O$ was used only for defueling criticality control.

The similarity between the two primary systems was striking. The composition of the fuel cladding, reactor vessel internals, and primary loop materials were essentially identical. These materials supply the major and trace elements which are the parent elements of the radionuclides formed by neutron activation of the pressure vessel, vessel internals, and corrosion product impurities in the primary coolant. The important water chemistry parameters, e.g., pH and oxygen control, were also similar. The main difference, other than size, was the composition of the control rods. However, the control rods do not contribute significantly to the residual radionuclide inventory deposited throughout the primary and secondary systems.

The Shippingport primary loop contained all the components of a typical PWR, e.g., a pressurizer, steam generators, coolant pumps, the reactor vessel itself, and a chemical purification system. As shown in the above table, the materials of construction within the primary loop were, stainless steel, carbon steel, Zircaloy, and Inconel, and were very similar to those used in typical PWR primary systems. The coolant and purification system was also typical of other PWRs, being a combination of regenerative and non-regenerative heat exchangers with filters and ion exchange beds. Likewise, pH and corrosion controls were similar to commercial PWRs. Lithium hydroxide (and later NH_4OH) was utilized for pH control, and hydrogen and hydrazine (at starting only) were used to limit oxygen levels and thus minimize corrosion. Thus, the fact that the Shippingport Station was similar to a scaled-down version of a modern, commercial PWR would permit generic observations and conclusions regarding residual radioactivity considerations during dismantlement and decommissioning of PWRs in general.

To the extent possible, samples from the primary, secondary, and auxiliary systems at Shippingport were obtained for detailed radiochemical analyses. These measurements have provided the basis for estimating the radionuclide inventory and distribution within the various plant systems, and for assessing the waste disposal options under the assumption that the decommissioning materials were representative of commercial wastes which would come under NRC and U.S. Department of Transportation (DOT) regulations.

1.2.2 Radiological Characterization of Neutron-Activated Metals Associated with Pressure Vessel and Fuel Assembly Hardware

One of the most significant information gaps associated with commercial reactor decommissioning is a detailed characterization of the highly neutron-activated metal components associated with the reactor pressure vessel internals and the fuel assembly hardware. As shown in Table 1.2, it has been estimated that some of these materials will have concentrations of long-lived radionuclides (^{14}C, ^{59}Ni, ^{63}Ni, and ^{94}Nb) that will greatly exceed the Class C limit for disposal in low-level waste shallow land burial facilities.[4] Recently, the NRC has proposed that radioactive materials of this type, which are greater than Class C, be disposed of in geologic repositories or some other approved alternative facility.[5] It is, therefore, essential that a complete characterization of these types of materials and their radionuclide contents at the time of decommissioning be obtained in

TABLE 1.2. Ratio of Calculated Specific Activity to Maximum Allowable Specific Activity for Shallow Land Burial for Selected Components (adapted from Luksic et al., 1986, Ref. 4).

	m^3/MTU	^{14}C	^{59}Ni	^{94}Nb	^{63}Ni
Half-Life		5730 yr	8×10^4 yr	2×10^4 yr	100 yr
10 CFR 61 Class C Limit		80 Ci/m^3	220 Ci/m^3	0.2 Ci/m^3	7000 Ci/m^3
PWR Fuel Assembly (33,000 MWd/MTU)					
Total Fuel	0.00651	1.1	3.6	990	15
Assembly Hardware					
Grids/Springs/Etc. (SS-304 & Inconel-718)	0.00312	2.4	7.4	2100	32
End Fitting (SS-304)	0.00339	0.03	0.02	0.08	0.08
BWR(a) Assembly (28,000 MWd/MTU)					
Total Fuel	0.04526	0.15	0.09	9.8	0.43
Assembly Hardware and Channel					
Grid/Springs/Etc. (Zircaloy-4 and Inconel X-750)	0.00209	0.41	1.5	86	7.3
End Fittings (SS-304)	0.00461	0.33	0.20	0.94	0.95
Channel (Zircaloy-4)	0.03856	0.12	<0.01	6.8	<0.01

(a) BWR = boiling-water reactor.

order to minimize the volumes of these wastes that need to go to a high-level waste repository or alternative facility.

In order to accomplish this characterization, samples of stainless steel, Inconel and Zircaloy alloys used in pressure vessel components and spent fuel assembly hardware have been acquired for analyses. These measurements will empirically determine the concentrations of all intermediate and long-lived radionuclides of significance in these materials, including ^{14}C, ^{59}Ni, ^{63}Ni, ^{90}Sr, ^{93}Mo, ^{93}Zr, ^{93m}Nb, ^{94}Nb, ^{99}Tc, ^{129}I, ^{137}Cs, and Pu, Am and Cm isotopes. Concurrently with the empirical measurements, estimates of activation product concentrations in these materials are being independently calculated using existing codes (e.g. ORIGEN-II, ANISN, etc.) and materials compositions. These calculations allow a direct comparison with the measured radionuclide concentrations and provide an assessment of the accuracy of the calculational methods.

1.2.3 Waste Disposal Options Associated with Reactor Decommissioning

The recent rule governing disposal of low-level radioactive wastes in shallow land burial facilities (10CFR61) will have direct impact on the options available for disposal of decommissioning wastes. Previous studies[6,7] have indicated that essentially all primary, secondary, and auxiliary systems in a nuclear power plant would generally have residual radionuclide contamination levels sufficiently low to permit disposal as Class A waste. The Shippingport Station decommissioning provided an excellent

opportunity to test these previous observations. In addition, the pressure vessel together with the neutron shield tank, was prepared for packaging as a low specific activity (LSA) shipment. DOE decided to qualify this package as Type B to further demonstrate it's integrity. The radionuclide characterization and compliance procedures for DOT regulations associated with the shipment and disposal of the pressure vessel have provided important information for evaluating disposal options for commercial reactor pressure vessels.

1.3 BACKGROUND INFORMATION

During the late 1970's and early 1980's, Pacific Northwest Laboratory conducted a number of studies for the NRC to assess the technology, safety and costs associated with reactor decommissioning.[3,8-11] These studies were based on extremely limited radionuclide source terms for residual radioactivity within a retired nuclear power plant. To fill this data gap the NRC sponsored two research projects to provide a detailed database describing the residual radionuclide concentrations, distributions, and inventories within retired nuclear power stations.[6,7,12,13] These projects characterized the neutron activation products formed in reactor pressure vessels and their internal components, and the residual surface contamination spread to all other systems and areas of the station. Although these studies greatly strengthened the radionuclide source term information on residual radioactivity in nuclear power stations, several major data gaps were further identified. These consisted of a lack of detailed radiological characterization data during an actual reactor decommissioning, and a lack of information on the radionuclide contents of neutron activated metal components from within reactor pressure vessels.

This present study is conducting research to address these important areas of reactor decommissioning. The Shippingport Station decommissioning has provided a valuable opportunity to conduct a detailed radiological characterization during the dismantlement and decommissioning of a nuclear power station. In addition, specimens of spent fuel assembly hardware and other pressure vessel components are being analyzed to determine their radionuclide contents, waste classifications, disposal options, and the degree of accuracy of calculational methods for predicting the concentrations of neutron activation products in irradiated metal components. The results of this source term characterization work will provide for more accurate and reliable assessments of the technology, safety, and costs of reactor decommissioning.

2.0 RADIONUCLIDE CHARACTERIZATION OF SHIPPINGPORT STATION DECOMMISSIONING WASTES

Specimens of surface-contaminated and neutron-activated components from Shippingport Station were obtained for detailed radiochemical analyses. These materials have provided the basis for evaluating the radiological safety and waste disposal options associated with reactor decommissioning.

2.1 RESIDUAL RADIONUCLIDES ASSOCIATED WITH PRIMARY, SECONDARY, AND AUXILIARY SYSTEMS

During the dismantlement of the Shippingport Station, numerous components from the primary and secondary coolant loops and the auxiliary systems were made available for sampling and subsequent detailed radionuclide characterization for the 10CFR61 radionuclides. Specimens of primary coolant piping, primary coolant check valves, main steam piping, feedwater piping, coolant purification system piping, monitoring/instrumentation system piping, and fuel pool recirculation system piping were obtained for residual radionuclide characterization of contaminated surfaces. In addition, a 208-liter drum of concrete chips spilled from the surface of the fuel canal was obtained for assessing the radionuclide contamination of the concrete surface of the fuel pool.

2.1.1 Primary Coolant Piping

2.1.1.1 Radiological Analyses

The majority of the residual radioactive material residing within a retired nuclear plant (excluding the neutron-activated pressure vessel and internals) is located within the primary coolant loop attached to the surface corrosion film. Five excellent cores of the primary coolant piping were provided for analysis at PNL by the Shippingport Station Decommissioning Project Office for characterization of the contaminated corrosion layer in the primary system. These cores, shown in Figure 2.1, were 7 cm in diameter by 4 cm thick and contained a thin, black, radioactive corrosion product layer on the inside surface which was very hard and retentive. Cores were taken from the "A," "B," and "C" loop primary coolant piping, at the entrance to (cold side) and exit from (hot side) the reactor pressure vessel at the outer surface of the neutron shield tank (see Figure 2.2). The radioactive corrosion film was removed by immersing the contaminated side in hot 6N hydrochloric acid for several minutes and brushing the surface with a stiff nylon brush. The stripped corrosion film was then completely solubilized by heating in a mixture of hydrochloric and nitric acids. The acid solutions were used for direct gamma spectrometric and radiochemical analyses. One of the core specimens ("A" loop-hot side) was saved for special testing and was cut into four equal wedge-shaped pieces for conducting a series of special form tests for shipment of radioactive materials described in Section 2.1.3 of this report.

The primary coolant piping core specimens were analyzed for the long-lived radionuclides of a safety and waste disposal concern. The results are

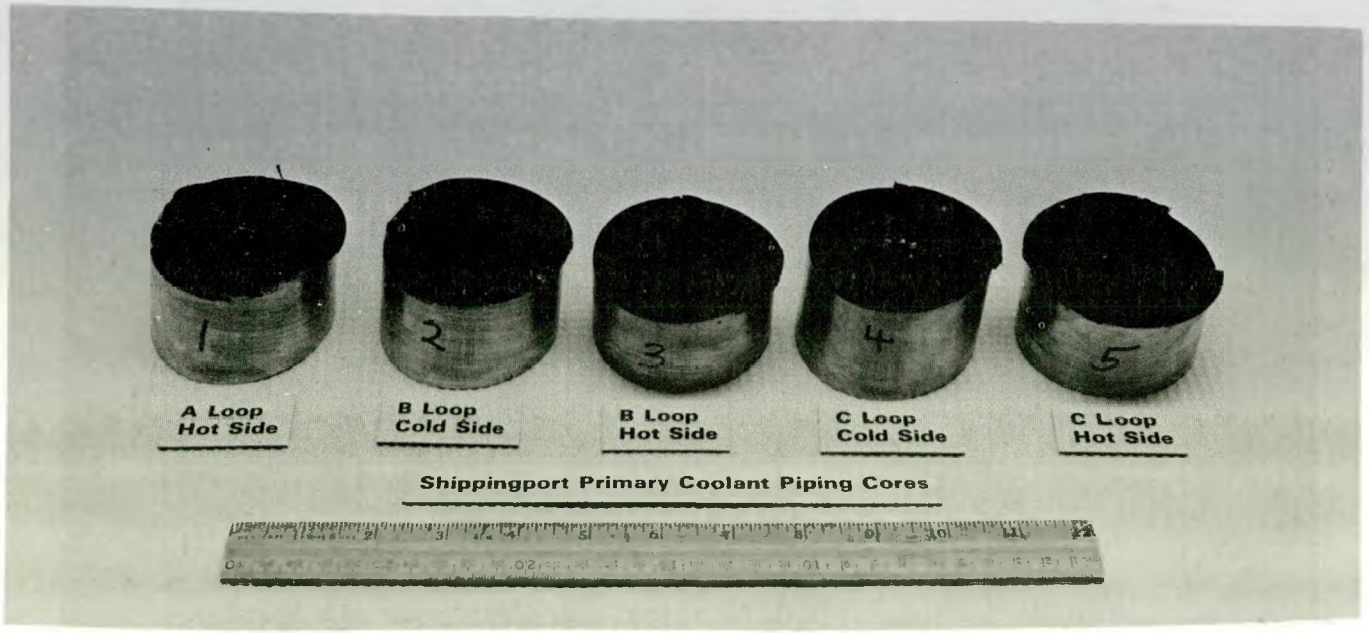

FIGURE 2.1. Shippingport Station Primary Coolant Piping Cores Showing Contaminated Inner Surface

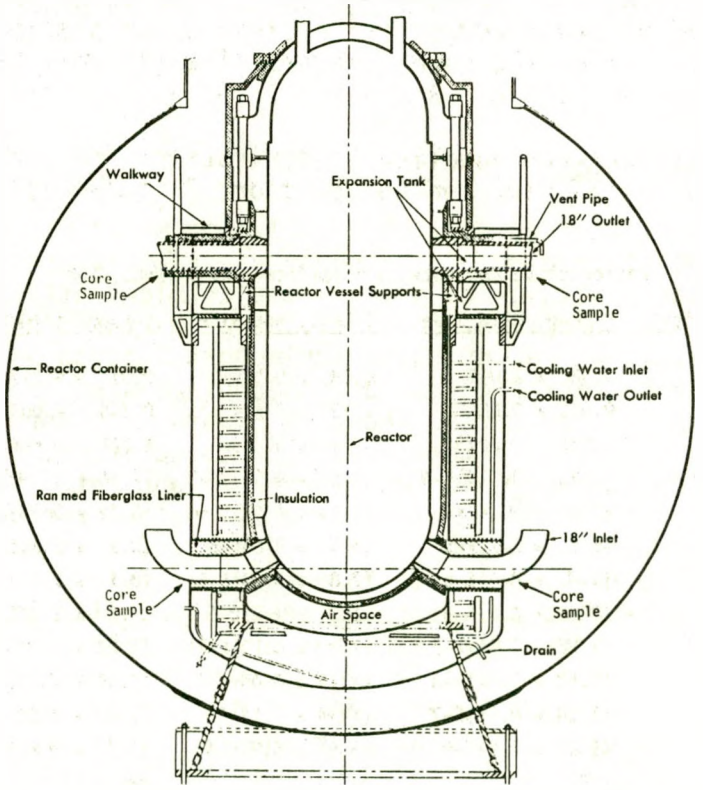

FIGURE 2.2. Shippingport Reactor Pressure Vessel Surrounded by the Neutron Shield Tank and Reactor Chamber. Sampling locations for cores from the primary coolant inlet (cold) and outlet (hot) piping are shown.

given in Table 2.1. It is immediately obvious that the residual radioactivity at Shippingport Station was somewhat atypical of that observed in a number of commercial nuclear power stations.[6,7] First, the gamma-ray spectra of the stripped corrosion layer resembled a pure ^{60}Co spectrum. A careful examination of the spectra could not identify any other gamma-emitting radionuclides. Although the samples contained ^{55}Fe and ^{63}Ni concentrations that were sometimes comparable to the ^{60}Co levels, these radionuclides emit only low-energy x-rays and beta particles and cannot be detected by direct gamma-ray spectrometry. The second unusual feature of the residual radioactivity was the almost complete absence of any fission products or transuranic radionuclides. Although trace amounts of Pu, Am, and Cm isotopes were detectible in the corrosion film samples, their concentrations were so low that their origin appears to have been from traces of tramp uranium on the outer surfaces of the fuel elements, and not due to leakage from failed fuel. These measurements confirmed the fact that no measurable fuel failures occurred at Shippingport Station during the entire operating history of the plant - a truly noteworthy operational record.

A comparison of the residual radionuclide concentrations associated with the contaminated surfaces of primary coolant piping at Shippingport Station with those observed at seven commercial nuclear power stations is shown in Figure 2.3. The data from the seven commercial units were taken from Reference 6 and 7. Shown in Figure 2.3 are the range and average concentrations

TABLE 2.1. Residual Radionuclide Concentrations Associated with the Corrosion Layer on Shippingport Primary Coolant Piping

		Radionuclide Concentration ($\mu Ci/cm^2$) as of Feb., 1987			
Radionuclide	Half-Life(yr)	B-Loop, Cold Side	B-Loop, Hot Side	C-Loop, Cold Side	C-Loop, Hot Side
^{60}Co	5.27	0.38 ± 0.011	0.88 ± 0.029	0.57 ± 0.017	0.88 ± 0.029
^{55}Fe	2.7	0.050 ± 0.0002	1.13 ± 0.034	0.100 ± 0.003	0.62 ± 0.019
^{63}Ni	100	0.035 ± 0.0018	0.53 ± 0.029	0.069 ± 0.006	0.74 ± 0.037
^{59}Ni	8.0×10^4	(2.25 ± 0.113)E-4	(4.04 ± 0.121)E-3	(4.40 ± 0.132)E-4	(3.20 ± 0.096)E-3
^{94}Nb	2.0×10^4	(2.40 ± 0.44)E-6	(1.13 ± 0.07)E-5	(6.09 ± 0.53)E-6	(7.85 ± 0.43)E-6
^{14}C	5730	(5.6 ± 7.7)E-5	(4.9 ± 8.8)E-5	(8.1 ± 7.8)E-5	(6.9 ± 6.1)E-5
^{99}Tc	2.13×10^5	(3.4 ± 2.4)E-6	(2.8 ± 0.24)E-5	(8.1 ± 2.2)E-6	(1.29) ± 0.27)E-5
^{3}H	12.33	(1.4 ± 1.6)E-6	(1.7 ± 1.6)E-6	(1.2 ± 1.3)E-6	(1.6 ± 1.8)E-6
$^{239\text{-}240}Pu$	2.44×10^4	(1.26 ± 0.06)E-7	(1.88 ± 0.10)E-7	(3.09 ± 0.04)E-6	(2.79 ± 0.09)E-7
^{238}Pu	87.8	(7.51 ± 0.43)E-8	(1.16 ± 0.08)E-7	(5.56 ± 0.18)E-7	(1.31 ± 0.07)E-7
^{241}Am	433	(1.10 ± 0.16)E-7	(1.36 ± 0.14)E-7	(1.16 ± 0.04)E-6	(1.67 ± 0.16)E-7
^{244}Cm	18.1	(9.0 ± 7.9)E-9	(5.9 ± 5.9)E-9	(8.7 ± 3.8)E-9	(5.8 ± 5.8)E-9
^{137}Cs	30.2	<3E-4	<5E-4	<4E-4	<5E-4
Dose Rate @ 1 cm					
w/beta shield (mR/h)		10	32	15	22
w/out beta shield (mRad/h)		230	1000	350	800

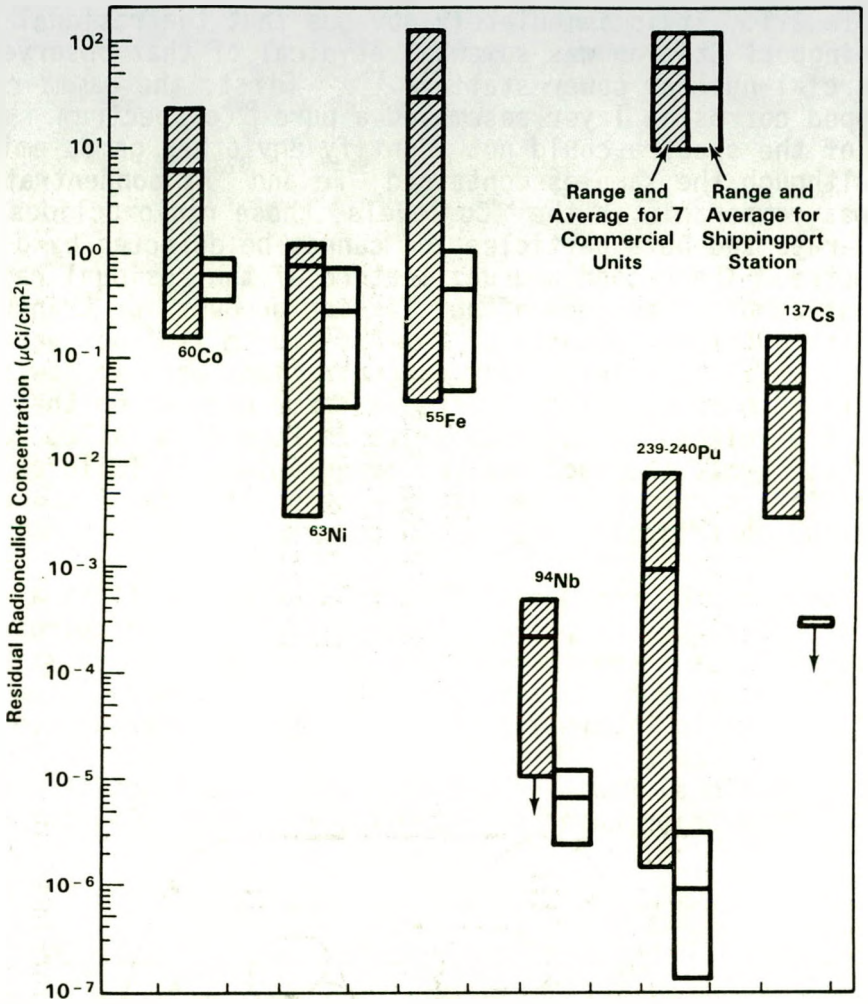

FIGURE 2.3. Comparison of Residual Radionuclide Concentrations on Primary Coolant Piping from Shippingport Station with Seven Commerical Stations

of ^{60}Co, ^{63}Ni, ^{55}Fe, ^{94}Nb, ^{137}Cs, and $^{239-240}Pu$ associated with the residual radioactivity at these stations. The average concentrations of the activation product radionuclides ^{60}Co, ^{63}Ni, ^{55}Fe, and ^{94}Nb are lower in the Shippingport samples by factors of about 10, 2.7, 60, and 40, respectively. The $^{239-240}Pu$ and ^{137}Cs are 1000 and greater than 200 times lower, respectively, than the average concentrations for the commercial units.

In addition to the surface contamination, the stainless steel cores from the primary coolant piping had also become slightly neutron activated, and ^{60}Co, ^{55}Fe, and $^{63,59}Ni$ were the main radionuclide constituents in the metal itself. Drill turnings were collected from six locations in each core sample (shown in Figure 2.4), dissolved in acid, and analyzed for gamma-emitting radionuclides, plus ^{55}Fe and ^{63}Ni. The ^{60}Co concentrations are given in Table 2.2, and averaged about 1000 pCi/g of steel for the B and C hoop "hot side" (outlet piping) and about 80 to 400 pCi/g of steel for the B and C loop

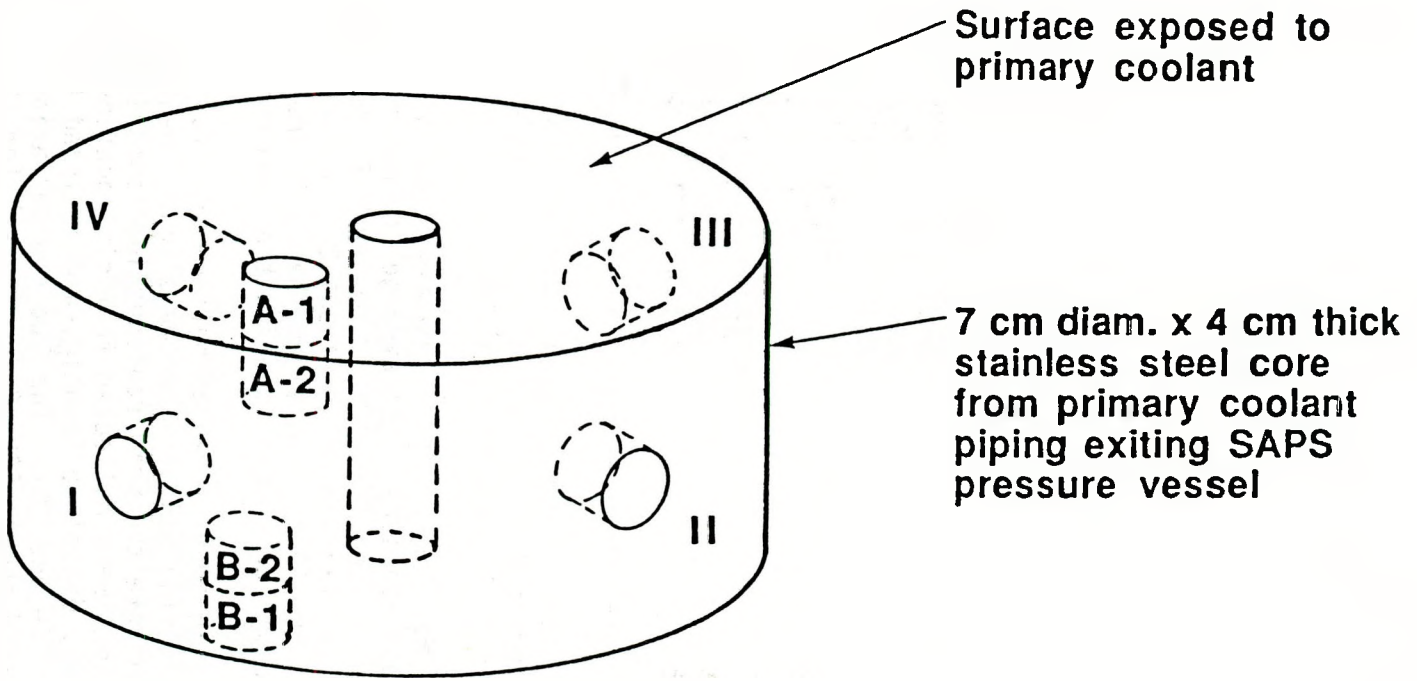

FIGURE 2.4. Sampling Locations for Obtaining Drill Turnings from Stainless Steel Primary Coolant Piping from Shippingport Station

TABLE 2.2. ^{60}Co Concentrations in Stainless Steel Primary Cooling Piping Exiting the Shippingport Reactor Pressure Vessel

Sample	Subsample (Drill Turnings) Location	^{60}Co Concentration (pCi/gm)[a]
B-Loop, Cold Side	I	128
	II	124
	III	119
	IV	59
	B-1	333
	B-2	431
	A-1	482
	A-2	150
B-Loop, Hot Side	I	965
	II	1,061
	III	962
	IV	1,111
	B-1	1,142
	B-2	1,109
	A-1	10,150[b]
	A-2	1,468
C-Loop, Cold Side	I	77.9
	II	82.9
	III	87.4
	IV	87.4
	B-1	206
	B-2	108
	A-1	793
	A-2	538
C-Loop, Hot Side	I	1,059
	II	975
	III	1,042
	IV	1,040
	B-1	1,237
	B-2	972
	A-1	6,428[b]
	A-2	6,733[b]

(a) Activity as of May, 1987.
(b) Drill turnings appear to be contaminated with surface contamination from the more radioactive corrosion film.

"cold side" (inlet piping) samples. Elemental analyses have provided stable Co, Fe, and Ni concentrations for calculating specific activities from which neutron fluences at these locations can be determined.

2.1.1.2 Physical and Chemical Analyses of the Radioactive Corrosion Layer

Also obtained from several of these cores were small strips of the thin lip of stainless steel around the outer circumference of the contaminated side of the cores. The lip segments were a remnant from the coring operation and were formed when the core prematurely broke free from the piping before the hole saw completely cut through the pipe. These lip segments can be seen still attached to the outer circumference of the cores in Figure 2.1. Pieces of these strips were mounted edgewise in epoxy resin and a cross-section was polished for examination by microphotography and scanning electron microscopy (SEM)/x-ray microprobe analysis for chemical composition and physical structure analyses.

Photomicrographic cross-sections of the contaminated corrosion layer on B-loop, hot (outlet) and cold (inlet) primary coolant piping are shown in Figure 2.5. The photomicrographs clearly show that the outer corrosion layer on the hot leg (outlet) piping was about three to four times thicker than that observed on the cold leg (inlet) piping. Both specimens showed a very thin oxide layer of a uniform thickness of about 1.5 to 2 μm attached directly to the base metal. Attached to this oxide layer was a granular layer of corrosion product particles which range in thickness from about 8 to 15 μm on the hot leg piping to about 3 to 5 μm on the cold leg piping. The corrosion product granules on the hot leg specimen were of a much coarser texture, with individual particles having diameters of up to 1 to 2 μm.

Figure 2.6 shows two SEM micrographs of the hot leg piping corrosion layer with specific regions selected for chemical analysis by energy dispersive x-ray fluorescence microprobe analysis (EDAX). These micrographs more clearly show the thin (1.5 to 2 μm) oxide layer attached to the base metal, with the thicker, granular outer layer of corrosion product particles. The chemical analyses for the probe locations are given in Table 2.3. As shown in Table 2.3, the analysis of the base metal (X1) was typical of AISI Type 304 stainless steel. The thin adherent oxide layer (X6) appeared to be a multimetal oxide, e.g., MXO_4, M_2O_3, or MO_2. The larger corrosion product metal oxide particles in the outer layer (X3, X4) were enriched in Al, Zr, and Ni, and depleted in Cr and Mn, relative to the base metal. The same analyses conducted on the cold leg piping specimen showed very similar results.

The inner oxide layer and the outer granular layer of corrosion product particles were very adherent to the base metal. Subsequent special form testing (49CFR173.469, Ref. 14) of another core specimen (A-loop, hot side) to determine the dispersability of the contaminated corrosion layer showed this layer to be highly resistant to detachment caused by impact, percussion, heating, and leaching with high-purity water and seawater (See Section 2.1.3). These tests were conducted to simulate the accidental release

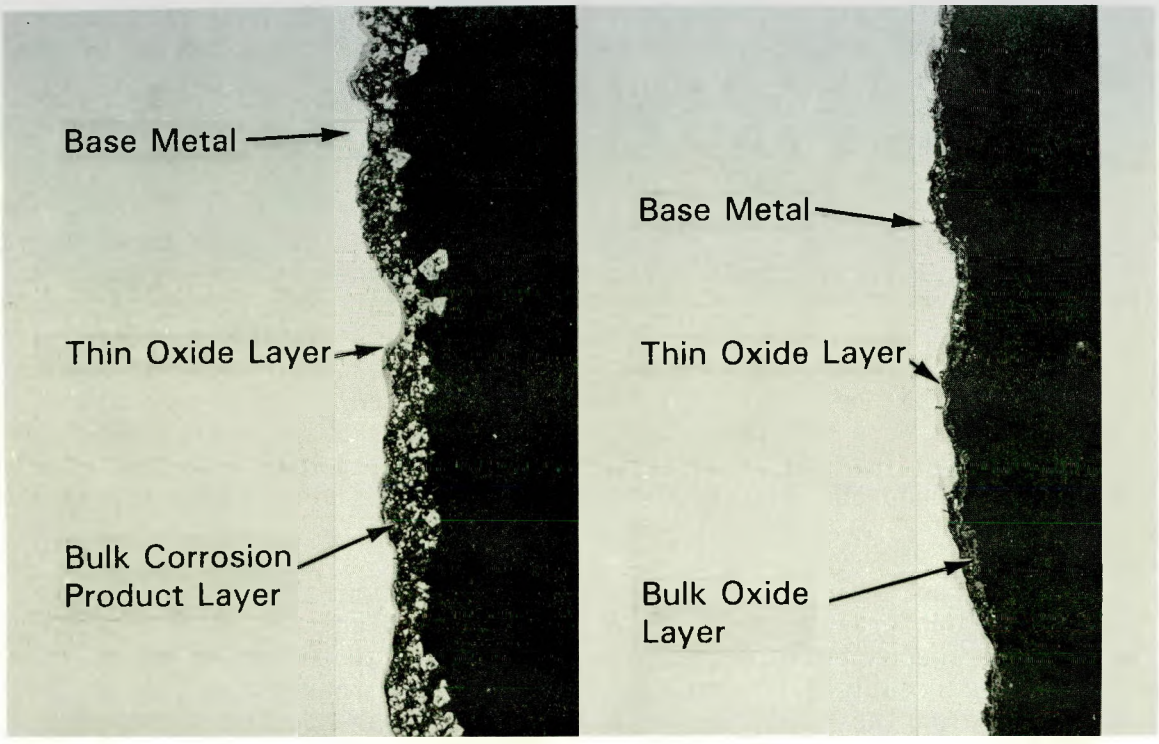

"B" Loop
Hot Leg (Outlet) Piping

"B" Loop
Cold Leg (Inlet) Piping

FIGURE 2.5. Photomicrographs of the Contaminated Surface of Primary Coolant Piping Cores from the "B" Loop at Shippingport Station

of radioactive material from the contaminated inside surfaces of the Shippingport reactor pressure vessel in the event of a hypothetical accident during transportation for disposal. The pressure vessel was prepared intact for an LSA shipment of a Type B container for burial at Hanford, Washington.[15]

Several other piping and component systems from the Shippingport primary coolant loop were obtained for residual radionuclide measurements. These have included four primary coolant check valves from the "A", "B", "C" and "D" loops. The radioactive corrosion film on the inside surfaces of these valves was scraped to bare metal from areas ranging from 100 to 900 cm^2 using razor blade type scrapers. The corrosion film surface was first dampened with a fine mist of distilled water to prevent airborne losses of the corrosion film during the scraping process.

In addition, samples of piping from the following systems were obtained for residual radionuclide measurements:

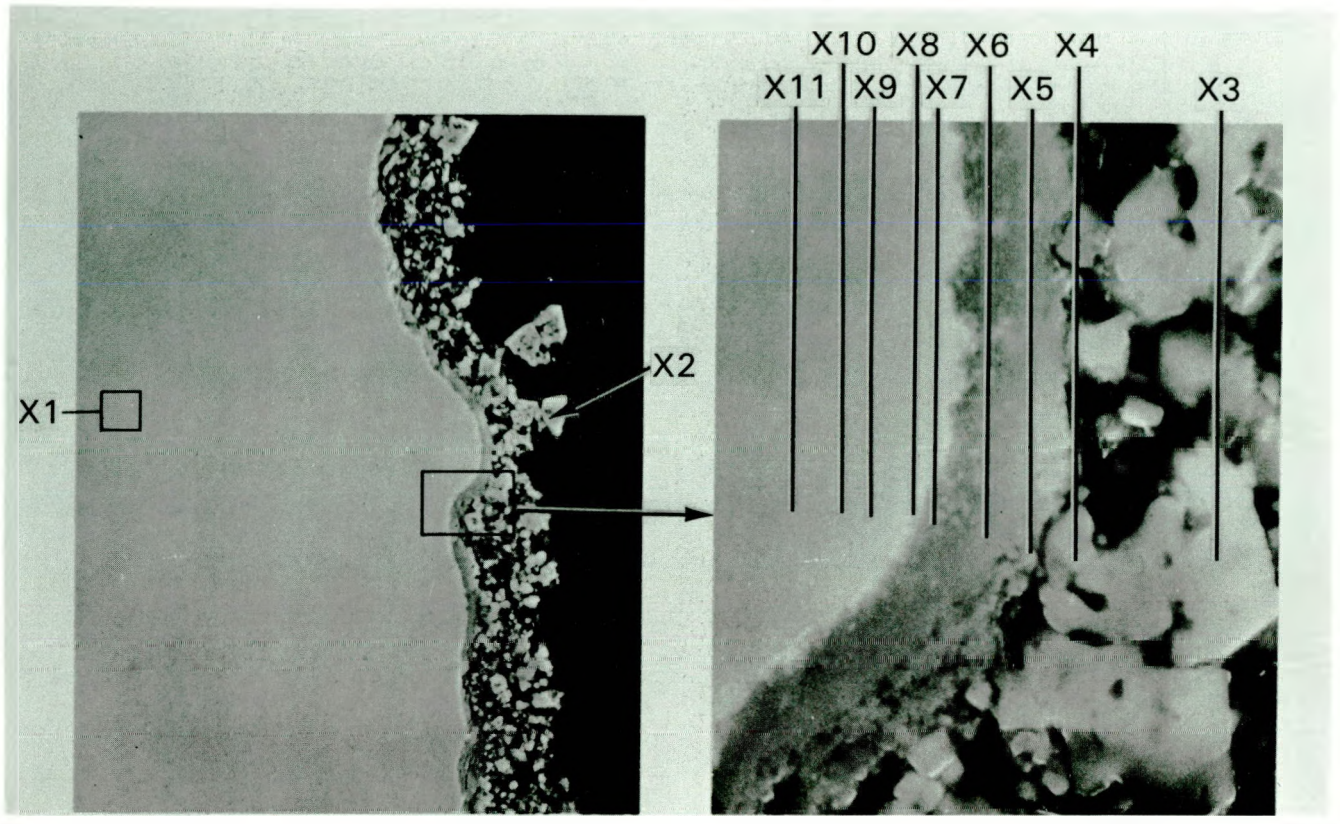

FIGURE 2.6. SEM Micrographs of Region of Shippingport Station Hot Leg Showing Probe Locations Selected for Chemical Analysis (EDAX). The chemical analysis for the probe locations are given in Table 2.3.

1. Sections of a 2.375 in. O.D. pipe from the primary coolant purification system which had been exposed to reduced temperature primary coolant.

2. Sections of 1.375 in. O.D. piping from the monitoring/ instrument system which had been exposed to reduced temperature primary coolant.

The scraping samples and piping specimens are presently undergoing radiochemical analyses for 10CFR61 radionuclides.

TABLE 2.3. Compositions in Weight % and (Atomic %) of the Shippingport Station Primary Coolant Piping Corrosion Film at Hot Leg (Specimen #3). Probe locations shown in Figure 4.4.

Element	Location X1	X2	X3	X4	X5	X6	X7	X8	X9	X10	X11
Al	0.7 (1.5)	1.2 (1.3)	1.6 (1.6)	2.2 (2.2)	1.4 (1.4)	0.8 (0.9)	0.8 (0.9)	1.1 (1.5)	0.7 (1.0)	1.1 (1.5)	0.7 (1.0)
Si	1.3 (2.5)	1.4 (1.4)	0.9 (0.9)	1.4 (1.4)	1.3 (1.3)	1.5 (1.5)	1.6 (1.8)	1.6 (2.1)	1.5 (2.1)	1.6 (2.3)	1.4 (2.1)
P	0 (0)	0 (0)	0 (0)	0 (0)	0 (0)	0 (0)	0 (0)	0 (0)	0 (0)	0 (0)	0 (0)
S	0 (0)	0 (0)	0 (0)	0 (0)	0 (0)	0 (0)	0 (0)	0 (0)	0.2 (0.3)	0 (0)	0 (0)
Cr	18.2 (18.9)	0.4 (0.2)	1.3 (0.7)	9.7 (5.0)	17.7 (9.3)	20.4 (10.9)	20.2 (12.1)	17.0 (11.6)	15.9 (12.1)	15.5 (11.8)	15.5 (12.1)
Mn	1.8 (1.8)	0 (0)	0.1 (0.1)	0.6 (0.3)	0.7 (0.3)	1.1 (0.6)	1.3 (0.7)	1.3 (0.8)	1.7 (1.2)	1.6 (1.1)	1.7 (1.3)
Fe	67.6 (65.3)	40.7 (20.4)	39.6 (18.8)	30.5 (14.5)	26.7 (13.0)	27.2 (13.6)	33.4 (18.7)	46.1 (29.3)	55.4 (39.2)	56.1 (39.6)	57.7 (41.9)
Ni	9.9 (9.1)	16.2 (7.7)	12.6 (5.7)	13.2 (6.0)	11.1 (5.2)	9.9 (4.7)	12.2 (6.5)	11.3 (6.8)	9.0 (6.1)	8.9 (6.0)	8.7 (6.0)
Zr	0 (0)	0.7 (0.2)	0.5 (0.1)	0 (0)	0 (0)	0.2 (0.1)	0 (0)	0 (0)	0 (0)	0 (0)	0 (0)
Mo	0 (0)	0 (0)	0 (0)	0 (0)	0.2 (0.5)	0 (0)	0.2 (0.1)	0 (0)	0 (0)	0 (0)	0 (0)
Cs	0.1 (0.05)	0 (0)	0.2 (0.04)	0 (0)	0.2 (0.04)	0 (0)	0 (0)	0 (0)	0.3 (0.1)	0 (0)	0.3 (0.1)
O[a]	0.3 (0.9)	39.3 (68.8)	43.3 (72.2)	42.5 (70.8)	40.8 (69.5)	38.9 (67.9)	30.3 (59.2)	21.6 (47.9)	15.3 (37.9)	15.3 (37.8)	14.0 (35.5)

(a) Residual Assumption.

2.1.2 Secondary Coolant Piping and Auxiliary System Components

Samples of piping from the 13-in. O.D. main steam line, the 6.625 in. O.D. feedwater piping, and the 6.50 in. O.D. fuel pool recirculation system piping were obtained for residual radionuclide analyses which are presently in progress. The corrosion film on the inner pipe surface was scraped from areas of 995 cm^2 and 280 cm^2 from the main steam piping specimen and the feedwater piping specimen, respectively. The fuel pool recirculation system piping has yet to be sampled.

Another important sample of opportunity obtained during the decommissioning was a drum of slightly contaminated surface concrete from the fuel canal. The top 0.6 cm of this concrete was mechanically spilled from the walls and floor of the fuel canal to remove surface-absorbed, non-smearable radionuclide contamination.

The entire 208-liter drum of concrete chips weighing 248 kg was directly assayed by gamma-ray spectrometry using a special barrel-counting system developed by PNL. This counting system consists of a collimated intrinsic germanium detector which scans the barrel, top to bottom, in eleven 7.6-cm vertical segments as the barrel rotates on a turntable at 30 rpm. This method in effect "homogenizes" the sample in the barrel during the counting period. The 208-liter barrel geometry has been calibrated by preparing standardized radionuclide mixtures in various density materials ranging from 0.1 to 1.4 g/cm^3. The density of the concrete chips was 1.2 g/cm^3.

The gamma ray spectrometry of the drum of concrete chips indicated that ^{60}Co was the only gamma-emitting radionuclide detectible, being present at an average concentration of 2.14 ± 0.03 $\mu Ci/kg$, or 2.14 nCi/g. This concentration of ^{60}Co was just slightly higher than the specific activity of 2 nCi/g considered in 49CFR173.389(e) to be radioactive for transportation purposes. An aliquot of the concrete chips is presently being radiochemically analyzed to determine the concentrations of alpha, beta, and low-energy photon emitting radionuclides, which are expected to be very low.

2.1.3 Radionuclide Characterization for DOT Requirements for Transportation of the Shippingport Station Pressure Vessel as a Type B, LSA Package

One of the important lessons learned from the Shippingport Station decommissioning that is directly applicable to the commercial nuclear power industry is the methodology for characterizing, preparing, packaging, and transporting the reactor pressure vessel for disposal. This information is contained in the "Safety Analysis Report for Packaging - Shippingport Reactor Pressure Vessel and Neutron Shield Tank Assembly."[16] One important aspect of the radionuclide characterization of the pressure vessel package is an assessment of the dispersivity, or conversely, the retentiveness of the radioactive corrosion film on the inside surfaces of the reactor pressure vessel and internal components under a variety of hypothetical accident conditions during transport to the disposal facility. This assessment is required under 49CFR173.467, "Tests for demonstrating the ability of Type B

and fissile radioactive materials packaging to withstand accident conditions in transportation"[14], which details a series of tests to determine the dispersivity of the inner radioactive corrosion film. These tests were conducted at PNL using specimens of the stainless steel primary coolant piping cores taken at the outlet of the Shippingport pressure vessel (see Section 2.1.1 of this report).

During the decommissioning of Shippingport Atomic Power Station, the pressure vessel, together with the neutron shield tank, was removed as an intact unit and shipped as an LSA package to the Hanford reservation in Washington for burial.[15] However, DOE also decided to qualify this package as Type B to further demonstrate it's integrity. The neutron shield tank surrounding the pressure vessel was filled with concrete, as was the pressure vessel, and the combination of the pressure vessel with its concrete-filled shield tank served as the actual shipping container. To ensure that no hazardous releases of dispersable radionuclides would occur in the event of an accident during transportation, the tests for special form radioactive materials described in 49CFR173.469 were conducted to demonstrate that the pressure vessel package would also comply with Type B packaging requirements. These tests included: 1) an impact test, 2) a percussion test, 3) a heat test, 4) a modified bend test, and 5) a leaching test.

2.1.3.1 Preparation of Test Specimens

A 7-cm diameter by 4-cm thick stainless steel core taken from the "A Loop - Hot Side" primary coolant piping section at the outlet of the Shippingport reactor pressure vessel was used to simulate the radioactively contaminated inner surfaces of the pressure vessel and internals. This specimen was cut into four wedge-shaped quarters. One-quarter sections, hereafter referred to as a specimen, were used in the impact test, the percussion test, and the heat test. The radionuclide contents and physical/chemical characteristics of the contaminated corrosion layer have been described in Section 2.1.1 of this report.

2.1.3.2 Impact Test - Room Temperature

The impact test at room temperature was conducted within the highbay of the 377 Building. A tape measure was used to measure a height of 9.1 m (30 feet) from the basement floor. A 24" x 54" x 1/4" (thick) aluminum plate was placed on the flat concrete floor to serve as the target. The test specimen was sealed in a thin plastic bag and dropped onto the target. The specimen was initially weighed and gamma counted to determine its original activity and weight. After the drop, the specimen was removed from the bag and recounted in the exact same geometry. The bag was also compacted into the same sample geometry and counted. "N" diode was used with the specimen centered 6 inches from the diode. The following results were obtained:

	wt.(gm)	Difference(gm)	dpm - ^{60}Co	Difference(dpm)
Before drop	280.07±0.02	--	$(1.186\pm0.006)\times10^{7}$	--
After drop	280.08±0.02	+0.01	$(1.207\pm0.006)\times10^{7}$	$+0.021\times10^{7}$

Activity in plastic containment bag 2.936 ± 10^{3}dpm

Fraction of total activity in plastic bag released from core specimen $\frac{2.936\times10^{3}}{1.186\times10^{7}} = 2.476\times10^{-4}$

A visual examination of the specimen after the drop test did not show any physical change in the contaminated surface, although several very small black specks (assumed to be corrosion particles) were observed inside the plastic containment bag.

No significant change in weight of the specimen before and after the impact test was observed. The gamma count of the specimen after the drop test was actually slightly higher than the initial count. This may be due to very slight geometry differences and/or spectrometer variability on the different counting dates. In actuality, the procedural uncertainty appears to be about ± 2% at most. The counting uncertainty is represented as three times the square root of the total counts (3σ).

The most reliable method of detecting very small releases of radioactive material from the specimen during this test was to count the plastic bag in which the specimen was contained. If any radioactive material was released from the specimen during the impact it would be contained inside the plastic bag. This examination showed that 2936 dpm of ^{60}Co was released from the specimen to the bag. This represents 2.476×10^{-4} of the total initial ^{60}Co activity on the specimen.

2.1.3.3 Percussion Test

The test specimen was initially gamma counted and weighed. The specimen was placed on a sheet of lead 12" x 12" x 1/4" (thick) laid on the lab floor. A guide tube was centered over the specimen about one inch above the contaminated surface. A 1.4 kg (3 lb) steel billet having the dimensions given in 49CFR173.469b, 2, II was dropped through the guide tube from a height of 1 m (3.3 ft) onto the contaminated surface of the specimen in a manner which would cause maximum damage. After the test, the striking end of the billet and the bottom end of the guide tube were wiped down several times with alcohol swabs and combined with a thin sheet of plastic which surrounded the specimen on the floor to catch any material impacted off the specimen. These wipes and plastic sheet were compacted and sealed in a plastic bag and gamma counted. The specimen was also recounted after weighing. The following results were obtained:

	wt.(gm)	Difference(gm)	dpm - ^{60}Co	Difference(dpm)
Before test	310.28±0.02g	--	$(1.436\pm0.006)\times10^{7}$	--
After test	310.22±0.02g	-0.06	$(1.431\pm0.006)\times10^{7}$	-0.005×10^{7}

Activity on wipes and plastic sheet 3.644×10^{3}dpm

Fraction of total activity in wipe and plastic sheet released from core specimen $\frac{3.644\times10^{3}}{1.436\times10^{7}} = 2.537\times10^{-4}$

After the percussion test, a visual imprint of the billet head was observed on the contaminated face of the specimen, but no flaking or obvious removal of the corrosion film was observed.

The weight of the specimen before and after the percussion test might indicate that 0.06 g. of material could have been removed. However, considering the uncertainty in the weighing this apparent loss is probably mostly due to experimental error. The gamma counting before and after the test indicated that no significant amount of radioactive material was lost from the specimen during the test, within the counting statistics. Again, the best way to measure the very small fraction of material lost during this test was to count the wipes of the billet face and the end of the guide tube, and the plastic floor-covering surrounding the specimen. This analysis showed that 3644 dpm of ^{60}Co was removed from the specimen by the impact test. This represents 2.537×10^{-4} of the total initial ^{60}Co activity of the specimen.

2.1.3.4 Heat Test

The specimen was weighted and gamma counted and placed in a porcelain dish. The temperature of the furnace was brought up to 800°C on the thermocouple temperature gauge. The temperature was also checked with a chromel/alumel thermocouple inserted into the front of the furnace, and showed a temperature of 830°C. A second porcelain dish was inverted and placed over the top of the dish containing the specimen (to serve as a cover) and the dishes were placed at the entrance to the furnace (temperature about 400-500°C) for several minutes to gradually warm the specimen. The dishes were then placed in the center of the furnace and the door closed. The temperature rapidly equilibrated within about 1 minute to 800°C and the sample was heated for 10 minutes at that temperature. The furnace was then shut off and the dishes brought to the front of the furnace for 20 minutes with the door of the furnace open to gradually cool the specimen. The dishes were placed in a fume hood and allowed to cool to room temperature. The specimen was reweighed and gamma counted. The inside surfaces of the porcelain dishes were wiped several times with alcohol swabs and the swabs were combined and sealed in a plastic bag and gamma counted. The following results were obtained:

	wt.(gm)	Difference(gm)	dpm - ^{60}Co	Difference(dpm)
Before heat	264.43±0.02	--	$(1.427\pm0.006)\times10^{7}$	--
After heat	264.40±0.02	-0.03	$(1.408\pm0.006)\times10^{7}$	-0.019×10^{7}

Activity in wipes of dishes 364 dpm

Fraction of total activity on wipes $\frac{364 \text{ dpm}}{1.427\times10^{7}} = 2.556\times10^{-5}$

Visual observation of the specimen after heating showed a dark, thin oxide surface on all surfaces of the specimen due to the heating. However, no significant measurable increase in weight due to oxidation was observed. The dark contaminated corrosion film surface looked the same as before the test.

The amount of ^{60}Co activity lost during the heating, as determined by gamma counting before and after the test, indicated a small loss (0.019 x 10^{7} dpm). However, this difference is so close to the counting and procedural uncertainty, that it should be considered an upper limit. Perhaps the most accurate method to determine any loss of radioactive material flaked off of the specimen during the heating would be to count the wipes of the porcelain dishes after the test. The wipes of the porcelain dishes indicated that only 364 dpm of ^{60}Co had been removed during the heating. This amounted to 2.55×10^{-5} of the total initial ^{60}Co activity of the specimen.

None of the major radionuclide constituents of the contaminated corrosion film (^{60}Co, ^{63}Ni, ^{55}Fe) would be expected to be volatilized at 800°C. The melting points of their oxides are as follows:

Metal Oxide	Melting Temperature - °C
CoO	1935
NiO	1990
Fe_2O_3	1538

2.1.3.5 Modified Bend Test

The test specimen was a remnant of the coring operation and consisted of a thin strip of stainless steel (2.5-mm wide x 20-mm long x 0.2-mm thick) removed from the outer perimeter of the core sample. This strip had an intact, undisturbed radioactive corrosion layer on the surface exposed to the primary coolant. The steel strip was initially gamma counted to determine its ^{60}Co activity. The strip was then placed in a thin polyethylene bag and bent 90°. The specimen was then removed and re-counted, along with the plastic contaminant bag, to determine if any corrosion film had flaked off during the bending. The following results were obtained:

	^{60}Co dpm	Difference(dpm)
Before bend	$(8.338 \pm 0.096)\times10^5$ dpm	--
After bend	$(8.035 \pm 0.094)\times10^5$ dpm	0.303×10^5
	Activity in plastic bag 5900 dpm	

The re-count after the bend test indicated that about 0.303×10^5 dpm of activity was removed from the specimen. However, much of this apparent loss may be due to the counting uncertainties associated with the measurements. The activity inside the containing bag accounted for 5.9×10^3 dpm. It is difficult to determine if the bending removed the activity or if it was removed by rubbing against the plastic containment bag during the bending. Also, slight differences in counting geometry and procedural uncertainty could account for a significant fraction of the observed loss. In any case, the maximum fractional loss incurred during this test would be

$$\frac{0.303 \times 10^5}{8.338 \times 10^5} = 0.036.$$

Because the amount of radioactive material removed from the test specimen during the modified bend test was greater then expected, the test was repeated using another specimen. Great care was taken during the repeat test not to rub the plastic containment bag against the contaminated surface during the bending. The results of the repeat test are as follows:

	^{60}Co dpm	Difference (dpm)
Before bend	$(9.042\pm0.099)\times10^5$	--
After bend	$(9.004\pm0.099)\times10^5$	-0.038×10^5
	Activity in plastic bag	<100 dpm
Fraction of total activity in plastic bag released from specimen		$\frac{<100}{9.042\times10^5} = <1.1\times10^{-4}$

The results of the repeat test indicated that no significant quantity of radioactive material was released from the test specimen during the modified bend test. It is felt that the repeat test was the more accurate of the two and should be used in any further assessments.

2.1.3.6 Leach Test

The four contaminated metal specimens utilized is the impact, percussion, heat, and bend test were subjected to the leach test specified in 49CFR173.469(4)(C). The specimens were each placed in 250-ml polypropylene jars and immersed for seven days in 200-ml of double-distilled, deionized water at ambient room temperature. The water had a pH of 6.0 and a conductivity of 1.25 micromho/cm at 20°C. The leaching test was commenced on 9/4/87 at 1530. On 9/11/87 at 0900 the specimens (in their jars) were placed

in a controlled temperature hot water bath set at 50 ± 1°C and maintained at this temperature for four hours. The samples were then removed from the bath, cooled to room temperature and 100-ml aliquots of the leachate water were removed and the radionuclide contents were measured by gamma-ray spectrometry. Table 2.4 summarizes the results of this leaching test.

Very low, but detectable, concentrations of ^{60}Co were observed in the water leachate. The fraction of total activity leached from the metal core specimens ranged from 2.00×10^{-4} for the sample previously used in the impact test, to 2.34×10^{-2} for the small specimen used in the modified bend test. It appears that the heat test allowed some of the radioactive material in the corrosion layer to become slightly more soluble compared to the specimens from the impact and percussion tests. The reason for the relatively higher solubility of the radioactive material from the modified bend test specimen is unclear. This may be an artifact of the way the specimen was produced during the core sampling, i.e. the thin lip of stainless steel containing the corrosion layer may have been significantly heated during the coring operation, or some physical alteration of the corrosion layer could have taken place which enhanced the leachability of the radionuclides.

Following the first phase leaching test, the core specimens were then placed in 250-ml polypropylene jars containing a wad of water-saturated tissue paper to provide a saturated humidity environment inside the jar when capped. The specimens were then stored for seven days in the jars having a nominal still-air humidity of greater than 90% at 30°C. After seven days the specimens were placed in 250-ml polypropylene jars and immersed in 200 ml of double-distilled deionized water having a pH of 6.0 and a conductivity of 1.25 micromho/cm at 20°C. The jars were then placed in the constant temperature water bath set at 50 ± 1°C for four hours. The jars were then removed, cooled to room temperature and 100-ml aliquots of the water leachate were analyzed for radionuclide content. Table 2.5 summarizes the results of this test.

In each case, significantly less ^{60}Co was leached from the specimens during the second phase of the leaching test compared to the first phase.

TABLE 2.4. ^{60}Co Activity of Water from First Leaching Test [49CFR173,467(C)(i-iii)]

Sample	Previous Test	Initial ^{60}Co Activity on Core Specimen(dpm)	^{60}Co Activity in 200 ml water(dpm)	Fraction of ^{60}Co Activity Leached
1	Impact	$(1.207 \pm 0.006) \times 10^{7}$	$(2.41 \pm 0.09) \times 10^{3}$	2.00×10^{-4}
2	Percussion	$(1.431 \pm 0.006) \times 10^{7}$	$(3.27 \pm 0.10) \times 10^{3}$	2.28×10^{-4}
3	Heat	$(1.408 \pm 0.006) \times 10^{7}$	$(1.67 \pm 0.03) \times 10^{4}$	1.19 ± 10^{-3}
5	Bend	$(8.035 \pm 0.094) \times 10^{5}$	$(1.88 \pm 0.01) \times 10^{4}$	2.34×10^{-2}

TABLE 2.5. ^{60}Co Activity of Water After the Second Phase of the Leach Test [49CFR173.469(c)(iv-vi)]

Sample	Previous Test	Initial ^{60}Co Activity on Core Specimen(dpm)	^{60}Co Activity in 200 ml water(dpm)	Fraction of ^{60}Co Activity Leached
1	Impact	$(1.207\pm0.006)\times10^{7}$	$(8.88\pm0.34)\times10^{2}$	7.36×10^{-5}
2	Percussion	$(1.431\pm0.006)\times10^{7}$	$(1.44\pm0.05)\times10^{3}$	1.01×10^{-4}
3	Heat	$(1.406\pm0.006)\times10^{7}$	$(4.55\pm0.12)\times10^{3}$	3.23×10^{-4}
5	Bend	$(7.847\pm0.094)\times10^{5}$	$(2.43\pm0.03)\times10^{2}$	3.10×10^{-4}

2.1.3.7 Leach Testing Using Seawater

Following the leach testing with the high purity water, the metal core specimen used in the impact test was then immersed in seawater for seven days. This test was conducted, in addition to the requirements specified in 49CFR173.469, to determine the amount of radioactive material that would be leached from the contaminated metal surface for the accident scenario where the pressure vessel would break open and become immersed in seawater. The seawater was obtained from Sequim Bay, Washington and had a nominal salinity of 32.0‰ and a pH of 8.0. The following results were obtained for this test:

Initial ^{60}Co on specimen - $(1.207\pm0.006)\times10^{7}$dpm

^{60}Co in 200 ml of seawater - 7.95×10^{2}dpm

Fraction of ^{60}Co leached - 6.59×10^{-5}

The seawater leached about 3 times less ^{60}Co than the initial high purity water leaching. However, since this metal core specimen had already been previously leached with high purity water it might be reasonable to conclude that the leachability of the high purity water and the seawater were not greatly different, and in each case very small. Obviously, the increased concentrations of chloride ion did not accelerate the leaching by the seawater.

2.1.3.8 Summary and Conclusions of Special Form Testing

The special form testing described in Section 2.1.3 indicated that the radionuclides associated with the corrosion layer on the primary coolant outlet piping from the SAPS pressure vessel were both very tightly bound to the underlying metal and very insoluble in both high-purity water and seawater. These results are summarized in Table 2.6.

The data obtained during this testing helped provide an assessment of the shipping requirements of the Shippingport pressure vessel package.

TABLE 2.6. Summary of Radioactive Material Releases from Test Specimens During Special Form Testing (49CFR173.469)

Test	Fraction of Radioactivity Released During Test
1. Impact	2.48×10^{-4}
2. Percussion	2.54×10^{-4}
3. Heat	2.56×10^{-5}
4. Modified Bend	$<1.1 \times 10^{-4}$
5. Leaching (1st phase, high-purity water)	
-Impact specimen	2.00×10^{-4}
-Percussion specimen	2.28×10^{-4}
-Heat specimen	1.19×10^{-3}
-Modified bend specimen	2.34×10^{-2}
6. Leaching (2nd phase, high-purity water)	
-Impact specimen	7.36×10^{-5}
-Percussion specimen	1.01×10^{-4}
-Heat specimen	3.23×10^{-4}
-Modified bend specimen	3.10×10^{-4}
7. Leaching (1st phase, seawater)	
-Impact specimen	6.59×10^{-5}

This assessment has been made in Ref. 16, and indicated that any releases of dispersable radionuclides to the environment in the case of a hypothetical accident were within regulatory tolerances.

2.2 NEUTRON-ACTIVATED SHIPPINGPORT CORE-3 FUEL ASSEMBLY HARDWARE

Two sets of neutron-activated metal specimens were obtained from the Shippingport Core-3 fuel assembly hardware. These samples have been received at PNL and will be radiochemically analyzed to determine radionuclide classification and to evaluate the accuracy of computer codes for predicting neutron activation product concentrations by comparisons with empirical measurements. The first was a set of three SII-3 stainless steel grid bolt specimens and one SII-3 stainless steel grid bolt locknut. These specimens were collected from a moveable seed module element. Core-3 at Shippingport had no control rods. Power levels were controlled by moving seed modules up and further into concentric blanket element modules. Because of their movement it was difficult to accurately position the location of the grid bolts and locknut in the cores neutron flux. However, sophisticated computer codes have accurately characterized the neutron fluence levels in various areas of interest in the fuel modules. The closest estimates obtainable by this method were fluence levels experienced by fuel rods located directly adjacent to the seed modules. The actual fluence experienced by the grid bolts and nut was less than that of the adjacent fuel rods, but difficult to determine, so the upper bound of neutron fluence experienced by the grid bolt is that of adjacent fuel rod 7Q6 or 7Q7. These calculated fluences were as follows:

Sample No.	Sample Type	Estimated Neutron Fluence
M9971	SS Grid Bolt	5.46 E20 n/cm^2
M9972	SS Grid Bolt	6.52 E20 n/cm^2
M9973	SS Grid Bolt	5.38 E20 n/cm^2
M9974	SS Lock Nut	5.38 E20 n/cm^2

The second set of neutron-activated metal specimens from the Shippingport Core 3 were samples of Type 348 stainless steel, Inconel-X750, and Zircaloy-4 removed from various locations from three different types of fuel assemblies: 1) a blanket rod, 2) a reflector rod, and 3) a seed rod. The activated metal specimens from each rod included one piece of Inconel-X750 plenum spring, one piece of Type 348 stainless steel support sleeve, and two pieces of Zircaloy-4 cladding from the midplane and upper end of the rod.

These samples will be extremely valuable for characterizing the long-lived radionuclides produced in fuel assembly hardware and adjacent pressure vessel components, and for assessing the accuracy of predictive neutron activation codes.

2.3 CLASSIFICATION OF SHIPPINGPORT DECOMMISSIONING WASTES WITH RESPECT TO 10CFR61

Although the decommissioning wastes generated at Shippingport Station were not subject to the regulations governing shallow land disposal of commercial low-level wastes (10CFR61), an assessment of the radionuclide contamination associated with the various decommissioning wastes was of interest. Based upon the comprehensive radiochemical analyses of the corrosion film associated with the primary coolant piping (Table 2.1), and assuming that the average concentration and observed range were representative of the contamination level of all plant systems exposed to primary coolant, e.g., steam generators, pressurizer, coolant pumps, primary purification systems, etc., it was possible to classify the waste with respect to the regulations in 10CFR61. Previous related studies have shown that for commercial power reactor stations having 5 to 50 times higher residual radioactivity levels in the primary systems, all components (excluding the pressure vessel) could be disposed of as Class A low-level waste (the least restrictive classification) in shallow land burial facilities. All radioactively contaminated concrete spilled from the fuel pool walls would also be Class A waste. It therefore becomes obvious that all primary systems removed during the decommissioning was well below Class A radionuclide concentrations and therefore eligible for disposal as Class A waste if it were to be disposed of in a commercial facility. These results confirm that for well-maintained power reactors, the residual radionuclide levels associated with the most contaminated systems outside of the pressure vessel can be readily disposed as Class A waste during commercial reactor decommissioning.

An important consideration for future assessment is the quantities of decommissioning wastes that could have been disposed of as below-regulatory-concern (BRC) types of waste. The Electric Power Research Institute (EPRI) is presently conducting extensive research to characterize a number of waste

streams, including dry active waste (DAW), from commercial nuclear power stations for consideration as BRC material if the total radionuclide concentration is below a certain level which is yet to be determined. The impact on disposal of nuclear power station decommissioning wastes could be substantial, since a large fraction of the total volume of decommissioning waste is only very slightly radioactively contaminated.

3.0 RADIONUCLIDE CHARACTERIZATION OF SPENT FUEL ASSEMBLY HARDWARE FROM COMMERCIAL NUCLEAR POWER STATIONS

Because little information currently exists describing measurements of long-lived radionuclides in activated metal components from within reactor pressure vessels, it is imperative that empirical analyses of such components be conducted. These measurements will be utilized to assess the radionuclide concentrations, waste classification, and disposal options associated with reactor decommissioning activated-metal wastes.

A number of well-characterized spent fuel assemblies from commercial nuclear power stations have become available at PNL for obtaining samples of the various metals of construction. These specimens are being radiochemically analyzed for the long-lived activation products of waste disposal concern to determine their 10CFR61 waste classification. The empirical measurements will then be compared with calculated activation product concentrations using existing codes (e.g., ORIGEN, ANISN, etc.) to determine the accuracy with which calculated estimates can be made. This comparison will lend confidence to calculational methods and/or identify shortcomings in these methods.

3.1 SAMPLE DESCRIPTION

Three high-burnup commercial fuel assemblies are currently being characterized. The materials in Table 3.1 have been obtained for analysis.

These fuel assemblies are representative (both in their irradiation history and material composition) of the type of spent fuel assembly hardware that must be accommodated by the federal waste management system and many utilities.

TABLE 3.1. Spent Fuel Assembly Hardware Samples

Assembly Type	Reactor Station	Materials Sampled
General Electric (7 X 7)	Cooper	Stainless steel bottom end fittings and upper tie plate, Inconel expansion springs, Zircaloy grid spacers
Combustion Engineering (14 X 14)	Calvert Cliffs	Stainless steel bottom end fittings and flow/hold-down plates, Zircaloy and Inconel grid spacers, Inconel hold-down springs
Westinghouse (14 X 14)	Point Beach	Stainless steel bottom and upper end fittings, Inconel hold-down springs, Zircaloy guide tube and grid spacers

Tables 3.2, 3.3 and 3.4 list important information for each fuel assembly. Their irradiation histories were obtained from information supplied by the utilities to the Department of Energy in the annual spent fuel data survey, RW-859.

Metal specimens were taken from each grid spacer in each of the fuel assemblies, and from both the bottom and top end fittings (see Figures 3.1, 3.2 and 3.3). The main casting of the bottom and top end fittings was manufactured of stainless steel. The top end fitting, however, had several additional pieces that were composed of various grades of Inconel. Samples were obtained to represent each of the materials of construction, in each possible location, as well as each of the main components.

Thirty-eight samples of activated metal were obtained from the three spent fuel assemblies by mechanical means (i.e. by cutting and snipping). The sample sizes were on the order of 0.1 to 5 g. These were latter subsamples, as described in Section 3.2. The remaining sample was retained in the event that further analysis would be required. The sample locations are shown in Figures 3.1, 3.2 and 3.3. These locations were selected to represent all the different materials available on each fuel assembly in as many different regions as practicable. Samples were taken from each grid spacer to provide as much data as possible regarding the shape of the neutron flux. The grid spacer sample also provided a good indication of the variance in the elemental composition, in particular for the trace elements.

TABLE 3.2. Westinghouse 14 x 14 Fuel Assembly Irradiation History (Peach Bottom, 400.7 kg U, 3.192 $^{w}/_{o}$ ^{235}U)

Cycle #	End of Cycle	Burnup @ EOC [MWD/MTU]
4 (out)	1 OCT 76	0
5	10 OCT 77	6,147
6	20 SEP 78	16,784
7	5 OCT 79	26,195
8	26 NOV 80	29,621
9	8 OCT 81	32,729

TABLE 3.3. Combustion Engineering 14 x 14 Fuel Assembly Irradiation History (Calvert Cliffs, 388.6 kg U, 3.068 $^{w}/_{o}$ ^{235}U)

Cycle #	End of Cycle	Burnup @ EOC [MWD/MTU]
1 (out)	1 JAN 77	0
2	23 JAN 78	9,466
3	21 APR 79	20,895
4	18 OCT 80	32,317
5	17 APR 82	41,781

TABLE 3.4. General Electric 8 x 8 Fuel Assembly Irradiation History (Cooper Nuclear Station, 190.4 kg U, 2.506 $^{W}/_{o}$ ^{235}U)

Cycle #	End of Cycle	Burnup @ EOC [MWD/MTU]
Begin Commercial Operation	JUL 74	0
1	SEP 76	13,046
2	SEP 77	18,910
3	APR 78	22,098
4 (out)	APR 79	22,098
5 (out)	MAR 80	22,098
6	APR 81	24,974
7	MAY 82	27,480

3.2 LABORATORY ANALYSES

3.2.1 Radiochemical Measurements

The 0.1- to 5-gram specimens of neutron activated stainless steel, Inconel, and Zircaloy, cut from the fuel assemblies were transferred from the original hot cell to a sample-preparation hot cell where the metal specimens were initially surface-decontaminated by acid etching. This cleaning consisted of immersing each specimen in hot (80-90°C) 6N hydrochloric acid for 60 seconds, followed by rinsing with fresh 6N hydrochloric acid. This etching was repeated three times, and was followed by a final acid etching by immersing each specimen for 60 seconds in hot (80-90°) 8N nitric acid. The specimens were then immediately rinsed with distilled water, dried on a paper towel, and placed in clean polyethylene vials. The vials were then transported to a radiochemistry laboratory for final decontamination of the metal specimens prior to initiating the radiochemical analyses.

The final acid etching was conducted in a clean, shielded laboratory fume hood and consisted of repeating the immersion and rinsing steps conducted in the hot cell. This repeated etching and rinsing was necessary to completely remove traces of fission product and transuranic radionuclide contamination picked up during the cutting operations in the original hot cell, as well as removing remnants of contaminated corrosion films formed on the metal surface during its exposure to the reactor primary coolant.

Following the cleaning operation, the metal specimens were initially weighed and then partially dissolved in high-purity acid (Ultrex) for radiochemical analyses. The stainless steel samples were immersed in hot (80-90°), 6N Ultrex hydrochloric acid for 10-20 minutes. The samples were then rinsed with doubly-distilled-deionized water, dried, and re-weighed to determine the amount of metal dissolved in the acid solution. The acid was then diluted with high-purity water to give a final stock solution of exactly 100 ml in 3N HCl, and the samples stored in cleaned polyethylene bottles. Aliquots of this solution were then taken for gamma spectrometric analysis

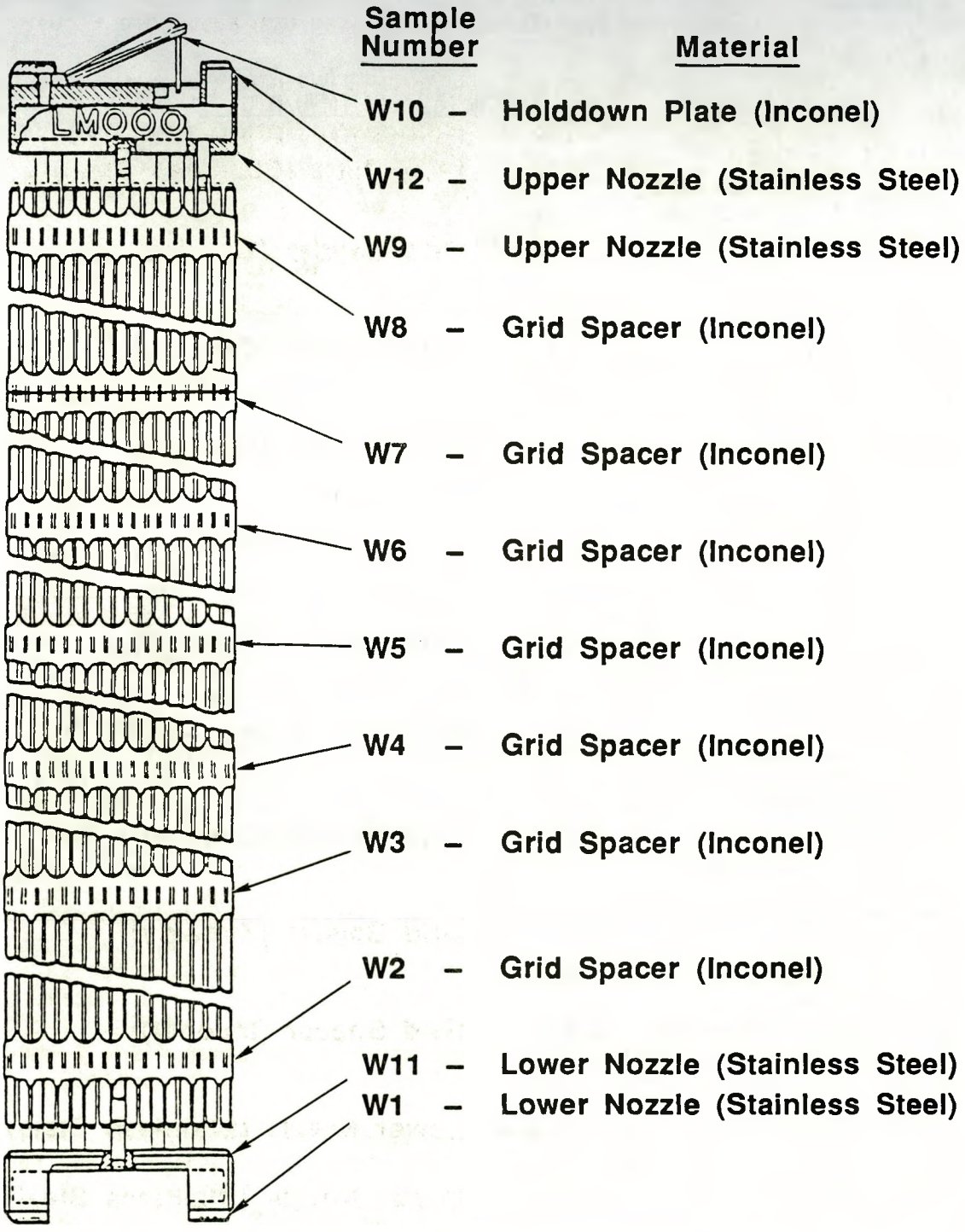

FIGURE 3.1. Sample Locations for Westinghouse 14 x 14 Fuel Assembly

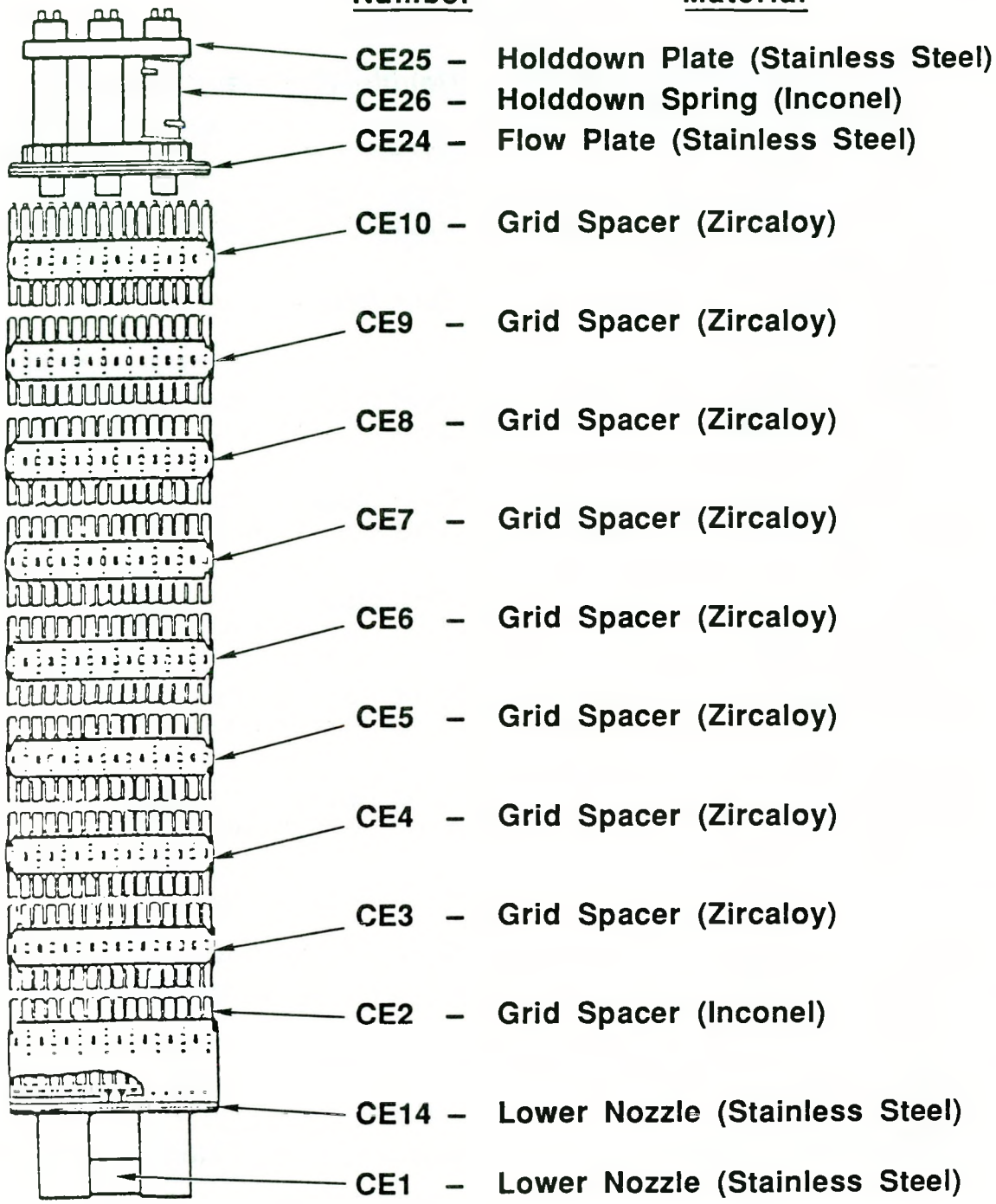

FIGURE 3.2. Sample Locations for Combustion Engineering 14 x 14 Fuel Assembly

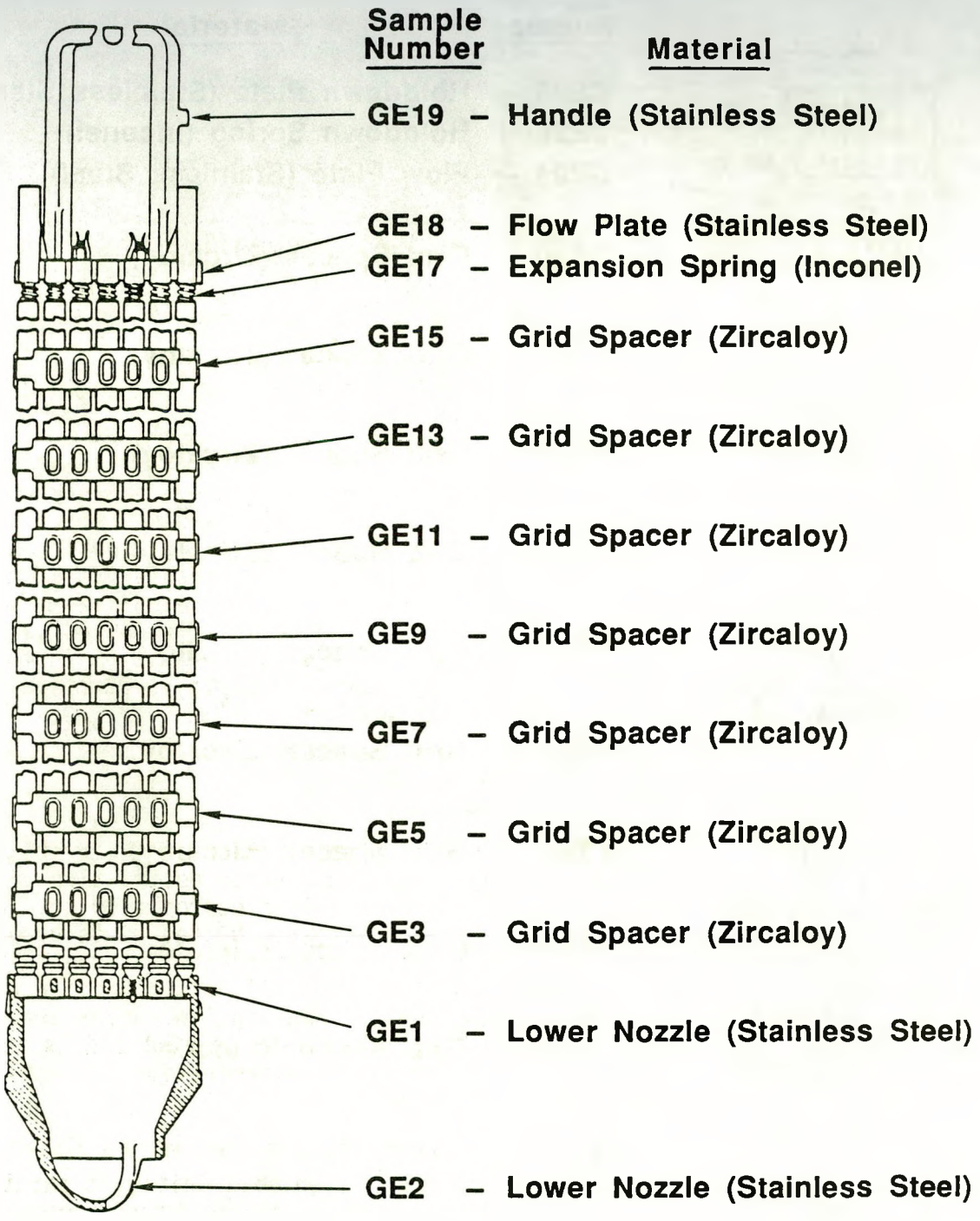

FIGURE 3.3. Sample Locations for General Electric 7 x 7 Fuel Assembly

and destructive radiochemical analyses. The partial dissolution of the Inconel specimens was identical to that for the stainless steel, except that several drops of hydrofluoric acid were added during the acid leaching to aid in the dissolution of niobium constituents, and for preservation of these solutions during storage. The Zircaloy specimens were partially dissolved as described for the Inconel samples, except that a total of 3 to 5 ml of hydrofluoric acid was gradually added during the acid leaching to aid in the sample dissolution and preservation of the zirconium solutions. The HCl/HF acid dissolution of the Inconel and Zircaloy specimens was conducted in cleaned teflon beakers to avoid etching of glass containers by the HF.

The following radiochemical analyses were performed on aliquots of the stock solutions as described below for measurement of ^{54}Mn, ^{55}Fe, ^{60}Co, ^{59}Ni, ^{63}Ni, ^{94}Nb, and ^{125}Sb. Eventually, ^{14}C, ^{90}Sr, ^{99}Tc, ^{129}I, ^{237}Np, $^{238,239,240}Pu$, $^{242,244}Cm$ and ^{241}Am will also be determined.

3.2.1.1 Gamma Spectrometric Analyses

Appropriate aliquots of the stock solutions were taken, diluted to appropriate levels, and 10 ml volumes placed in a standard calibrated counting geometry. The samples were then counted from 10 to 100 minutes on a Ge(Li) or IG gamma ray spectrometer to measure all detectible gamma emitting radionuclides. Cobalt-60 was detectable in all samples, with ^{54}Mn being measurable in most specimens. Niobium-94 was detectible in Inconel samples containing niobium additives, and ^{125}Sb was a major gamma-emitter in the Zircaloy samples. The ^{125}Sb (2.73y) was produced by an (n,γ) reaction on ^{124}Sn to form ^{125}Sn, (9.65d) followed by beta decay to ^{125}Sb. Zircaloy typically contains percent levels of tin.

3.2.1.2 Nickel-59 and Nickel-63

The nickel separation entails initial precipitation of the hydroxide and additional purification using dimethyloglyoxime. After destruction of the nickel dimethylglyoxime precipitate, the nickel is electroplated onto a stainless steel disc from a basic sulfate solution. Nickel-59 is quantified using a thin window intrinsic germanium diode via the cobalt x-ray emitted during decay. Nickel-63 is determined using a NaI(Tl) anticoincidence shielded windowless beta proportional counter. Absorption curves are determined for all samples to confirm the ^{63}Ni. Nickel-65 is utilized as an internal tracer for quality assurance and yield determination.

3.2.1.3 Iron-55

The analytical procedure utilized for ^{55}Fe entails initial separation by precipitation as the hydroxide in the presence of stable iron carrier and a ^{59}Fe yield tracer. The hydroxide is then dissolved with strong hydrochloric acid and the solution passed through an anion exchange column, where the iron chloride complex is retained. Iron is eluted from the exchange media using strong nitric acid. This solution is evaporated to dryness, the residue dissolved in acid, and the iron electroplated from an oxalate-sulfate media onto a copper disc. The ^{55}Fe is quantified using a thin window intrinsic

germanium diode via the Mn x-ray. Analytical yields are determined simultaneously using a ^{59}Fe gamma-ray.

3.2.1.4 Niobium-94

When ^{94}Nb concentrations are too low to measure by direct gamma spectrometry, the niobium is radiochemically separated from other radionuclides by precipitation of niobic oxide from an acid medium after dissolution of the metal sample. Both niobium carrier and ^{95}Nb tracer were added during the separation. Niobium-94 was measured by gamma-ray spectrometric techniques and radiochemical yield determined by tracing with ^{95}Nb.

3.2.1.5 Carbon-14

Carbon-14 is separated by either acid distillation in the case of inorganic carbonates or by oxidation at high temperature in the case of organic carbon compounds or carbides. The distilled carbon dioxide is trapped in either instance in a caustic solution. Analytical yields are determined gravimetrically using a barium carbonate precipitate. Carbon-14 is quantified using a windowless beta proportional counter, and beta absorption curves are determined on all samples to confirm the ^{14}C measurement.

3.2.1.6 Strontium-89 and Strontium-90

Strontium isotopes are separated by consecutive precipitation of the basic carbonate followed by precipitation in fuming nitric acid. After an ingrowth period, the ^{90}Sr is then calculated for the ^{90}Y daughter measurements. Strontium-89 is determined by difference. A measurement of total strontium (^{90}Sr and ^{89}Sr) is made immediately after separation via fuming nitric acid. The ^{90}Sr determined after ^{90}Y ingrowth is subtracted from the total strontium measurement to give ^{89}Sr. The yield for the ^{90}Y separation after ingrowth is determined gravimetrically.

3.2.1.7 Technetium-99

The ^{99}Tc separation procedure entails initial purification using repeated coprecipitation with iron hydroxide followed by coprecipitation with rhenium using tetraphenyl arsonium chloride reagent. Technetium-99 is quantified using a thin window beta proportional detector. Absorption curves are determined for all samples to confirm the presence of ^{99}Tc. Technetium-95 is used for quality assurance and determination of analytical yield during the separation and purification procedure.

3.2.1.8 Iodine-129

Iodine-129 is initially separated onto anion exchange resin. Elution is achieved by oxidation. The element is then further purified by solvent extraction using carbon tetrachloride and hydroxylamine-hydrochloride. The iodine is then back-extracted into a water/sulfite solution. The iodide is then co-precipitated with palladious chloride. Iodine-129 is quantified using a thin window intrinsic germanium detector through measurement of the

xenon x-ray. Iodine-131 is utilized for quality assurance as a yield tracer during the purification procedure.

3.2.1.9 Neptunium-237

Neptunium-237 is separated from the sample onto anion exchange resin from a strong nitric acid solution. The anion exchange column is then washed with strong hydrochloric acid containing ammonium iodide. The neptunium is then eluted using hydrochloric-hydrofluoric acid, evaporated to dryness with nitric acid and subsequently electroplated from a weak sulfuric acid solution. The separated and purified ^{237}Np is determined using an alpha energy spectrometer. Neptunium-239 is utilized during the separation procedure for yield tracer and quality assurance purposes.

3.2.1.10 Plutonium-238 and Plutonium-239/240

Plutonium isotopes are separated by anion exchange from a strong nitric acid solution. The resin is eluted using hydrochloric acid-ammonium iodide solution. The plutonium is then electroplated from a weak sulfuric acid solution onto a stainless steel disc. Plutonium-242 is used for quality assurance purposes as a yield tracer and plutonium isotopes determined via alpha energy spectrometry. Plutonium-242 is used as a yield tracer for two reasons. First, the alpha emission energy for ^{242}Pu is lower than for ^{238}Pu and $^{239-240}Pu$; thus there is no potential for interference in the analytical peaks of interest. Secondly, the half-life is longer than the other possible tracer ^{236}Pu. Use of ^{242}Pu thus reduces recalibration requirements and decay corrections. This also makes the quality assurance process easier to maintain.

3.2.1.11 Americium-241, Curium-242, and Curium-244

Because of their very similar chemistries, americium and curium isotopes are separated and purified in one procedure. The isotopes are co-precipitated with iron hydroxide and then dissolved in strong nitric acid. Plutonium and neptunium are removed from the analytical solution by filtering through anion resin. The americium and curium in the filtrate are then co-precipitated at pH 3.0 using 1 mg of calcium carrier and oxalic acid. The americium and curium isotopes are then electroplated from the dissolved oxalate precipitate in a weak sulfuric acid solution onto a stainless steel disc. Americium-243 is used for analytical yield determination and isotopic concentrations determined using alpha energy spectrometry.

3.2.2 Stable Element Measurements

Elemental analyses of the 3N hydrochloric acid stock solution of activated metals was accomplished by inductively coupled argon plasma atomic emission spectrometry (ICAP/AES). Appropriate dilutions (10 or 100-fold) of the original stock solutions and reagent blanks were analyzed in a shielded ICAP system.

The ICP is an argon plasma formed by the interaction of an RF field and an inert argon gas stream. This spatially stable plasma is reported to reach a temperature as high as 10,000 °K. This high temperature and inert argon atmosphere minimize chemical interferences such as refractory oxide formations with aluminum and rare earths which are encountered in flame emission methods. The argon carrier gas nebulizes the liquid sample into the spray chamber. It also transports the smaller sample droplets into the center of the plasma. The high temperature in the plasma desolvates the droplets and dissociates the sample material into individual atoms and ions which are excited to emit light at wavelengths characteristic of the elements in the sample. The atomic emission spectrometer (AES) sorts the various wavelengths and measures the intensity of specific spectral lines. The photomultiplier tubes convert the emitted light to an electrical signal which is proportional to the intensity of the spectral lines. The digitized signals are converted by the computer into mg/L units which are printed directly on the input/output terminal.

Three ICP/AES systems are used for various analysis. A Jarrell-Ash Model 95-965 direct reader spectrometer with the capability of determining up to 40 elements simultaneously has the source stand isolated in a hood, and thus allows the analysis of samples containing low levels of radioactivity. An ARL Model 35000 vacuum system for the simultaneous determination of 37 elements is also utilized. A third ARL Model 35800 instrument has the source mounted inside a lead-shielded glovebox. This ICP/AES is used for the analysis of samples containing high levels of radioactive isotopes.

In ICP/AES analyses, spectral interferences from the major elements in the samples (e.g., Fe, Cr, and Ni in stainless steel) is a potential source of error in the determination of trace elements. Correction on the trace elements are performed by analyzing different concentrations of single element standards of the major constituents in the sample at the time of sample analysis and these values are used for spectral corrections of the trace elements.

A fourth plasma system was used to measure niobium at extremely low concentrations in highly diluted samples. This instrument, a VG Plasmaquad inductively coupled plasma mass spectrometer (ICP/MS) is capable of measuring part-per-billion concentrations of niobium, as well as many other elements.

TABLE 3.5. Radionuclide Concentrations in Westinghouse Spent Fuel Assembly Hardware Materials (Point Beach Station)

Sample No.	Material	Location	Concentration (Ci/g metal)[a]						
			^{54}Mn[b]	^{55}Fe	^{59}Ni	^{63}Ni	^{60}Co	^{94}Nb	^{93m}Nb[c]
W-10	Inconel	holddown spring @ top end	(5.73±3.08)E-5	(1.84±0.02)E-3	(1.18±0.01)E-5	(2.70±0.03)E-3	(7.34±0.07)E-4	(7.39±1.17)E-7	(5.48±0.55)E-5
W-12	SS	upper end fitting (top)	(1.79±0.48)E-4	(3.67±0.04)E-3	(1.66±0.01)E-6	(3.51±0.04)E-4	(1.63±0.02)E-3	(4.09±0.69)E-10	(7.36±0.74)E-8
W-9	SS	upper end fitting casting (bottom)	(6.39±3.89)E-4	(2.87±0.02)E-2	(1.31±0.01)E-5	(3.05±0.04)E-3	(1.30±0.01)E-2	(1.79±0.37)E-9	(2.39±0.24)E-7
W-8	Inconel	spacer grid #7	<3.5E-4	(1.29±0.01)E-2	(7.52±0.01)E-5	(1.96±0.02)E-2	(1.31±0.01)E-2	(6.98±1.17)E-6	(6.06±0.61)E-4
W-7	Inconel	spacer grid #6	(5.50±1.14)E-3	(5.31±0.05)E-2	(2.55±0.03)E-4	(6.51±0.04)E-2	(4.07±0.04)E-2	--	--
W-6	Inconel	spacer grid #5	(8.52±0.21)E-3	(5.53±0.05)E-2	(3.50±0.04)E-4	(8.49±0.08)E-2	(7.47±0.07)E-2	--	--
W-5	Inconel	spacer grid #4	(3.76±2.33)E-3	(6.27±0.05)E-2	(3.27±0.04)E-4	(8.80±0.08)E-2	(8.82±0.09)E-2	(1.20±0.32)E-4	(2.81±0.28)E-2
W-4	Inconel	spacer grid #3	(3.90±2.36)E-3	(6.45±0.05)E-2	(2.76±0.03)E-4	(7.99±0.08)E-2	(8.01±0.08)E-2	--	--
W-3	Inconel	spacer grid #2	(3.52±1.68)E-3	(6.92±0.05)E-2	(3.35±0.03)E-4	(8.89±0.08)E-2	(8.03±0.08)E-2	--	--
W-2	Inconel	spacer grid #1	<1.1E-3	(3.14±0.02)E-2	(1.35±0.01)E-4	(3.74±0.04)E-2	(3.05±0.03)E-2	(4.14±0.77)E-5	(8.45±0.85)E-3
W-11	SS	bottom end fitting (top)	(3.52±0.33)E-3	(4.75±0.04)E-2	(1.48±0.01)E-5	(3.75±0.04)E-3	(1.28±0.01)E-2	(6.40±0.81)E-9	(8.07±0.81)E-7
W-1	SS	bottom end fitting (bottom)	(2.26±0.69)E-3	(4.21±0.04)E-2	(1.00±0.01)E-5	(2.86±0.03)E-3	(1.83±0.02)E-2	(2.07±0.36)E-8	(2.67±0.27)E-6

(a) Decay corrected to discharge date of 10/8/81.
(b) Parent element is Fe. ^{54}Mn is produced by the fast neutron reaction $^{54}Fe(n,p)^{54}Mn$.
(c) Parent element is Nb. ^{93m}Nb is predominantly produced by the reaction $^{93}Nb(n,n')^{93m}Nb$.

TABLE 3.6. Radionuclide Concentrations in Combustion Engineering Spent Fuel Assembly Hardware Materials (Calvert Cliffs Station)

Sample No.	Material	Location	Concentration (Ci/g metal)[a]							
			^{54}Mn[b]	^{55}Fe	^{59}Ni	^{63}Ni	^{60}Co	^{94}Nb	^{93m}Nb[c]	^{125}Sb[d]
CE-25	SS	upper holddown plate	(2.92±0.15)E-4	(3.25±0.08)E-3	(1.09±0.02)E-6	(1.64±0.03)E-4	(6.53±0.13)E-4	(4.77±0.81)E-10	(7.70±0.77)E-8	(1.99±0.82)E-6
CE-26	Inconell	upper holddown spring	(4.27±2.37)E-5	(1.71±0.03)E-3	(1.38±0.03)E-5	(4.00±0.08)E-3	(8.79±0.18)E-4	(2.85±0.50)E-7	(3.18±0.32)E-5	(3.70±1.38)E-6
CE-24	SS	upper flow plate	(7.70±1.35)E-4	(3.29±0.08)E-2	(7.12±0.18)E-6	(1.63±0.03)E-3	(7.98±0.33)E-3	(4.35±0.73)E-9	(9.20±0.92)E-7	<7.4E-6
CE-10	Zircaloy	top spacer grid	(6.77±0.89)E-6	(2.83±0.06)E-4	(2.40±0.24)E-9	(6.97±1.10)E-7	(1.32±0.3)E-4	--	--	(1.36±0.14)E-4
CE-9	Zircaloy	spacer grid #7	(1.79±0.06)E-4	(1.17±0.02)E-3	(1.75±0.10)E-8	(5.94±0.49)E-6	(9.03±0.18)E-5	(1.68±0.26)E-8	(1.95±0.20)E-5	(2.46±0.25)E-3
CE-8	Zircaloy	spacer grid #6	(1.80±0.07)E-4	(1.77±0.04)E-3	(1.35±0.12)E-8	(4.50±0.50)E-6	(1.04±0.03)E-4	--	--	(2.49±0.25)E-3
CE-7	Zircaloy	spacer grid #5	(2.02±0.10)E-4	(1.81±0.04)E-3	(3.89±0.18)E-8	(8.80±0.70)E-6	(1.40±0.03)E-4	--	--	(2.68±0.27)E-3
CE-6	Zircaloy	spacer grid #4	(2.06±0.08)E-4	(1.45±0.03)E-3	(1.23±0.10)E-8	(3.59±0.43)E-6	(1.09±0.03)E-4	--	--	(2.29±0.23)E-3
CE-5	Zircaloy	spacer grid #3	(2.65±0.14)E-4	(3.63±0.06)E-3	(3.54±0.22)E-8	(8.38±1.17)E-6	(1.67±0.04)E-4	(2.97±0.58)E-8	(3.64±0.36)E-5	(3.50±0.24)E-3
CE-4	Zircaloy	spacer grid #2	(2.19±0.11)E-4	(2.17±0.06)E-3	(1.77±0.21)E-8	(3.00±0.69)E-6	(1.19±0.03)E-4	--	--	(1.68±0.17)E-3
CE-3	Zircaloy	spacer grid #2	(1.54±0.05)E-4	(1.16±0.02)E-3	(1.08±0.14)E-8	(2.23±0.32)E-6	(8.65±0.19)E-5	(2.09±0.45)E-8	(1.63±0.16)E-5	(1.56±0.16)E-3
CE-2	Inconel	bottom spacer grid	(9.70±0.75)E-4	(1.04±0.03)E-2	(1.63±0.05)E-4	(4.50±0.14)E-2	(4.23±1.07)E-2	(2.26±0.39)E-5	(4.46±0.45)E-3	<4.6E-5
CD-14	SS	bottom retention plate	(8.69±0.12)E-3	(1.18±0.05)E-1	(5.54±0.17)E-5	(1.59±0.05)E-2	(6.18±0.49)E-2	(1.59±0.27)E-8	(2.17±0.22)E-6	<7.0E-5
CE-1	SS	bottom end fitting near axial middle	(2.98±0.48)E-3	(1.03±0.03)E-1	(2.28±0.68)E-5	(6.34±1.83)E-3	(3.10±0.46)E-2	(4.68±0.81)E-9	(1.21±0.12)E-6	<2.9E-5

(a) Decay corrected to discharge data of 4/17/82.
(b) Parent element is iron (Fe). ^{54}Mn is formed by the fast neutron reaction $^{54}Fe(n,p)^{54}Mn$.
(c) Parent element is Nb. ^{93m}Nb is predominantly produced by the reaction $^{93}Nb(n,n)^{93m}Nb$.
(d) Parent element of ^{125}Sb is Sn. ^{125}Sb is formed by the thermal neutron reaction $^{124}Sn(n,\gamma)^{125}Sn$ followed by beta decay to ^{125}Sb.

TABLE 3.7. Radionuclide Concentrations in General Electric Spent Fuel Assembly Hardware Materials (Cooper Station)

Sample	Material	Location	Concentration--Ci/g metal[a]							
			^{54}Mn	^{55}Fe	^{59}Ni	^{63}Ni	^{60}Co	^{94}Nb	^{93m}Nb[c]	^{125}Sb[d]
GE-19	SS	Tab on handle	(1.10±0.30)E-4	(1.43±0.08)E-2	(3.68±0.55)E-6	(8.01±0.95)E-4	(5.95±0.06)E-4	(7.61±1.26)E-10	(2.49±0.26)E-7	(4.23±1.34)E-6
GE-18	SS	Upper tie plate	(1.15±0.32)E-4	(8.79±0.30)E-3	(5.00±0.68)E-6	(8.86±0.90)E-4	(5.41±0.05)E-4	(3.89±0.63)E-9	(9.04±0.95)E-7	<1.9E-6
GE-17	Inconel	Expansion spring (at top of fuel pin)	<9.5E-5	(2.42±0.08)E-3	(4.73±0.68)E-5	(9.48±1.04)E-3	(1.88±0.01)E-3	(5.95±0.99)E-7	(3.98±0.42)E-5	(1.44±0.37)E-5
GE-15	Zircaloy	Spacer grid #7	(3.53±0.95)E-5	(8.41±0.53)E-4	(2.77±0.34)E-7	(3.10±0.27)E-5	(2.42±0.01)E-4	(5.09±1.13)E-9	(2.36±0.25)E-5	(4.16±0.02)E-3
GE-13	Zircaloy	Spacer grid #6	(1.58±0.53)E-4	(2.59±0.08)E-3	(1.07±0.16)E-6	(1.07±0.12)E-4	(1.68±0.01)E-3	--	--	(1.41±0.01)E-3
GE-11	Zircaloy	Spacer grid #5	(1.49±0.49)E-4	(1.87±0.03)E-3	(8.56±1.31)E-7	(8.10±0.19)E-5	(9.20±0.87)E-3	--	--	(1.02±0.01)E-3
GE-9	Zircaloy	Spacer grid #4	(2.14±0.73)E-4	(3.31±0.15)E-3	(9.41±1.31)E-7	(1.39±0.10)E-4	(1.68±0.02)E-3	--	--	(1.81±0.02)E-3
GE-7	Zircaloy	Spacer grid #3	(1.61±0.33)E-4	(3.52±0.21)E-3	(1.35±0.16)E-6	(1.91±0.20)E-4	(7.32±0.07)E-4	(9.14±4.28)E-9	--	(1.72±0.02)E-3
GE-5	Zircaloy	Spacer grid #2	(2.02±0.27)E-4	(2.46±0.08)E-3	(5.45±0.81)E-7	(7.06±1.52)E-5	(4.68±0.02)E-4	--	--	(1.33±0.01)E-3
GE-3	Zircaloy	Spacer grid #1 (starting @ bottom)	(1.01±0.20)E-4	(2.55±0.06)E-3	(2.16±0.28)E-7	(2.63±0.31)E-5	(2.28±0.03)E-4	(9.86±1.89)E-9	(1.50±0.16)E-5	(1.22±0.02)E-3
GE-1	SS	Bottom end fitting (near top of casting)	<4.3E-3	(1.35±0.07)E-1	(8.15±1.13)E-5	(7.54±0.76)E-3	(6.24±0.07)E-2	(7.97±1.35)E-8	(6.86±0.72)E-6	<1.7E-4
GE-2	SS	Bottom end fitting (near nozzle end)	<5.8E-4	(1.27±0.09)E-2	(1.14±0.13)E-5	(1.28±0.13)E-3	(7.03±0.07)E-3	(6.04±0.99)E-9	(4.84±0.51)E-7	<2.3E-5

(a) Decay corrected to discharge date of 5/1/82.
(b) Parent element is Fe. ^{54}Mn is produced by the fast neutron reaction $^{54}Fe(n,p)^{54}Mn$.
(c) Parent element is Nb. ^{93m}Nb is produced by the reaction $^{93}Nb(n,n')^{93m}Nb$.
(d) Parent element is Sn. ^{125}Sb is produced by the reaction $^{124}Sn(n,\gamma)^{125}Sn$, followed by beta decay to ^{125}Sb.

TABLE 3.8. Elemental Concentrations in Westinghouse Spent Fuel Assembly Hardware Materials (Point Beach Station)

Sample No.	Material	Location	Concentration--Weight Percent							
			Mn	Fe	Cr	Ni	Co	Nb	Cu	Mo
W-10	Inconel	holddown spring @ top end	0.0629±0.004	17.2±0.5	17.6±0.5	50.8±1.5	0.0709±0.009	4.50±0.05	0.062±0.006	2.86±0.08
W-12	SS	upper end fitting (top)	1.52±0.05	67.5±2.0	18.3±0.5	8.27±0.25	0.150±0.015	0.0033±0.0007	0.10±0.010	0.41±0.01
W-9	SS	upper end fitting casting (bottom)	1.44±0.04	65.0±2.0	18.0±0.5	9.10±0.25	0.149±0.015	0.0024±0.0024	0.095±0.009	0.23±0.01
W-8	Inconel	spacer grid #7	0.133±0.008	16.0±0.5	16.6±0.5	53.0±1.6	0.148±0.015	4.40±0.05	0.18±0.02	2.79±0.08
W-7	Inconel	spacer grid #6	0.133±0.008	15.2±0.5	15.7±0.5	46.5±1.4	0.089±0.009	--	0.18±0.02	2.66±0.08
W-6	Inconel	spacer grid #5	0.069±0.002	16.0±0.5	17.0±0.5	48.0±1.4	0.115±0.012	--	0.078±0.008	2.83±0.08
W-5	Inconel	spacer grid #4	0.073±0.002	17.0±0.5	17.8±0.5	50.8±1.5	0.131±0.013	4.60±0.05	0.085±0.008	2.98±0.08
W-4	Inconel	spacer grid #3	0.062±0.002	16.2±0.5	16.2±0.5	47.1±1.4	0.119±0.012	--	0.075±0.008	2.65±0.08
W-3	Inconel	spacer grid #2	0.068±0.006	16.5±0.5	17.4±0.5	49.2±1.5	0.130±0.017	--	0.091±0.009	2.87±0.08
W-2	Inconel	spacer grid #1	0.113±0.006	15.8±0.5	17.4±0.5	49.3±1.5	0.111±0.011	4.60±0.05	0.172±0.017	2.67±0.08
W-11	SS	bottom end fitting (top)	1.71±0.05	65.5±2.0	18.7±0.5	9.36±0.25	0.115±0.035	0.03±0.03	0.094±0.009	0.23±0.01
W-1	SS	bottom end fitting (bottom)	1.54±0.05	65.0±2.0	17.6±0.5	7.96±0.24	0.147±0.015	0.0156±0.0022	0.125±0.013	0.25±0.01

TABLE 3.9. Elemental Concentrations in Combustion Engineering Spent Fuel Assembly Hardware Materials (Calvert Cliff Station)

Sample No.	Type	Location	Concentration--Weight Percent								
			Mn	Fe	Cr	Ni	Co	Nb	Sn	Mo	Zr
CE-25	SS	upper holddown plate		69.7±2.1	21.2±0.8	9.72±0.39	0.0513±0.004	<0.0015	<0.018		
CE-26	Inconel	upper holddown spring		8.00±0.33	15.5±0.6	72.9±2.2	0.0316±0.003	2.25±0.03	0.27±0.09		
CE-24	SS	upper flow plate		60.5±1.8	16.2±0.7	8.52±0.33	0.0927±0.008	<0.0015	<0.018		
CE-10	Zircaloy	top spacer grid		0.212±0.009	0.11±0.01	<0.005	<0.0027	--	2.2±0.2		91.8±2.9
CE-9	Zircaloy	spacer grid #7		0.213±0.008	0.11±0.01	<0.005	<0.0027	0.0156±0.0009	2.3±0.2		89.0±2.8
CE-8	Zircaloy	spacer grid #6		0.211±0.006	0.11±0.01	<0.005	<0.0027	--	2.4±0.2		91.7±2.7
CE-7	Zircaloy	spacer grid #5		0.229±0.011	0.11±0.01	<0.005	<0.0027	--	2.6±0.3		92.0±2.8
CE-6	Zircaloy	spacer grid #4		0.220±0.018	0.11±0.01	<0.005	<0.0027	--	3.0±0.5		92.5±3.0
CE-5	Zircaloy	spacer grid #3		0.200±0.020	0.13±0.01	<0.005	<0.0027	0.0259±0.0017	3.9±1.0		115±3.5
CE-4	Zircaloy	spacer grid #2		0.260±0.028	0.10±0.004	<0.005	<0.0027	--	3.4±1.0		106±3.9
CE-3	Zircaloy	spacer grid #1		0.182±0.017	0.078±0.023	<0.005	<0.0027	0.0147±0.0009	2.0±0.4		73.5±2.5
CE-2	Inconel	bottom spacer grid	0.093±0.009	2.49±0.07	13.8±0.4	36.6±1.1	0.114±0.029	2.25±0.03	--	14.5±0.4	--
CE-14	SS	bottom retention plate	1.08±0.03	60.8±1.8	18.2±0.5	9.60±0.3	0.128±0.010	<0.0091	--	0.032±0.005	--
CE-1	SS	bottom end fitting near axial middle	1.10±0.03	67.1±2.0	18.8±0.5	9.84±2.95	0.148±0.022	<0.02	--	0.050±	--

TABLE 3.10. Elemental Concentrations in General Electric Spent Fuel Assembly Hardware Materials (Cooper Station)

Sample	Material	Location	Concentration--Weight Percent									
			Mn	Fe	Cr	Ni	Co	Nb	Sn	Cu	Mo	Zr
GE-19	SS	Tab on handle	0.58±0.02	68.3±2.1	19.3±0.1	8.38±0.25	0.026±0.004	0.001±0.00067	<0.22	0.013±0.002	<0.007	<0.004
GE-18	SS	Upper tie plate (at base where fuel pin touches)	0.56±0.02	67.6±2.0	19.0±0.1	8.26±0.25	0.025±0.005	0.00074±0.00016	<0.21	0.009±0.002	<0.006	<0.003
GE-17	Inconel	Expansion spring (at top of fuel pin)	0.070±0.003	6.04±0.18	13.2±0.4	68.2±2.0	0.050±0.008	0.81±0.01	<0.26	0.027±0.003	0.049±0.007	0.094±0.009
GE-15	Zircaloy	Spacer grid No. 7	0.011±0.005	0.47±0.01	0.14±0.02	0.072±0.011	<0.006	0.0051±0.0032	1.09±0.18	<0.004	0.072±0.011	93.1±2.8
GE-13	Zircaloy	Spacer grid No. 6	0.02±0.006	0.43±0.02	0.14±0.02	0.083±0.012	<0.007	--	1.13±0.20	<0.005	0.083±0.012	96.5±2.9
GE-11	Zircaloy	Spacer grid No. 5	0.013±0.005	0.45±0.01	0.10±0.02	0.066±0.010	<0.006	--	0.86±0.17	<0.004	<0.02	72.3±2.2
GE-9	Zircaloy	Spacer grid No. 4	0.02±0.005	0.62±0.02	0.14±0.02	0.088±0.013	<0.007	--	1.09±0.20	<0.005	0.03±0.02	94.9±2.8
GE-7	Zircaloy	Spacer grid No. 3	0.009±0.005	0.47±0.02	0.13±0.02	0.040±0.009	<0.006	0.020±0.003	1.10±0.20	<0.005	<0.02	95.6±2.9
GE-5	Zircaloy	Spacer grid No. 2	0.01±0.005	0.55±0.02	0.13±0.02	0.043±0.009	<0.007	--	1.06±0.20	<0.004	<0.02	94.3±2.8
GE-3	Zircaloy	Spacer grid No. 1 (starting at bottom)	0.008±0.004	0.56±0.02	0.12±0.01	0.030±0 010	<0.007	0.018±0.003	1.10±0.22	<0.003	0.02±0.02	92.4±2.8
GE-1	SS	Bottom end fitting (near top of casting)	1.01±0.03	69.9±2.0	17.5±0.5	8.68±0.26	0.21±0.02	0.037±0.011	<0.3	0.28±0.01	0.37±0.03	0.006±0.003
GE-2	SS	Bottom end fitting (near nozzle end)	1.03±0.03	69.1±2.0	17.4±0.5	8.75±0.26	0.207±0.02	0.018±0.003	<0.2	0.29±0.01	0.87±0.04	<0.003

discharge was ^{60}Co, with much smaller amounts of ^{54}Mn being present. The Inconel components contained about the same concentrations of stable cobalt as the stainless steel in each assembly, and therefore the ^{60}Co levels were also comparable. Following radiochemical separations, the concentrations of ^{55}Fe, ^{59}Ni, ^{63}Ni, ^{93m}Nb, and ^{94}Nb were readily detectable in the stainless steel and Inconel.

The Inconel contained percent levels of stable niobium, and ^{94}Nb could often be detected directly by gamma-ray spectrometry in the presence of the relatively large amounts of ^{60}Co. However, because ^{94}Nb is an important long-lived activation product specified on 10CFR61, selected samples of stainless steel, Inconel, and Zircaloy from each fuel assembly were subjected to special radiochemical and elemental analyses (see Sections 3.2.1 and 3.2.2) to improve the accuracy and precision of the initial measurements.

The improved ^{94}Nb measurements are given in Tables 3.5, 3.6, and 3.7. The highest ^{94}Nb concentrations were associated with the Inconel specimens, particularly the spacer grids from the fueled region of the Westinghouse assembly. These specimens contained up to 1.2E-4 Ci/g of ^{94}Nb in the Inconel, a reflection of the nominal 4% niobium content of this alloy. The stable niobium was measured in diluted aliquots of the acid-digest solutions of the activated metal specimens by extremely sensitive inductively coupled plasma mass spectrometry.

The radiochemically separated niobium was also counted on an intrinsic germanium (IG) detector set up at 0.2 keV/channel to measure ^{93m}Nb, which was present in surprisingly high concentrations. To our knowledge, these are the first measurements of this radionuclide in activated metal components. This radionuclide is produced in the metal specimens primarily by the reaction $^{93}Nb\ (n,n')\ ^{93m}Nb$. The ^{93m}Nb decays by emission of a 30-keV gamma-ray which is essentially all converted. The predominant external radiation emitted by ^{93m}Nb is, therefore, due to the 16.5-keV Nb x-rays. Previously calculated concentrations of ^{93m}Nb and ^{94}Nb in the neutron activated stainless steel shroud from a reference BWR estimated that the $^{93m}Nb/^{94}Nb$ ratio would be 0.09.[8] For the 13 specimens of stainless steel components from the Westinghouse, Combustion Engineering, and General Electric spent fuel assemblies the average $^{93m}Nb/^{94}Nb$ ratio was 158±74. Thus, the actual measured ^{93m}Nb in neutron-activated stainless steel is some 1800 times higher than predicted by calculations. Although this new finding will probably not affect the waste classification or disposal requirements for activated metals, an environmental dose assessment should be conducted to insure that ^{93m}Nb will not be an environmental problem.

The ^{63}Ni and ^{59}Ni concentrations were highest in the Inconel and stainless steel components, where the stable nickel concentrations were usually in the range of 36-72% and 7-9%, respectively. The Westinghouse fuel assembly, which contained Inconel spacer grids (~50% Ni) in the fueled region of the assembly, had the highest observed ^{63}Ni and ^{59}Ni concentrations, averaging (6.63±2.75)E-2 and (2.50±1.06)E-4 Ci/g metal, respectively. The ^{63}Ni concentrations were very similar in magnitude to the observed ^{60}Co concentrations in the spacer grids. The ^{63}Ni and ^{59}Ni concentrations in the Zircaloy spacer

girds in the Combustion Engineering and General Electric fuel assemblies were several orders of magnitude lower compared to the Westinghouse assembly.

The ^{55}Fe concentrations were very similar in magnitude to the ^{60}Co concentrations in all materials from each fuel assembly. Iron was a significant constituent of the Inconel components (2.5-17%), and ranged from 61-69% in the stainless steel specimens sampled from all assemblies. However, both the iron and cobalt concentrations in the Zircaloy were very low, resulting in relatively low concentrations of ^{55}Fe and ^{60}Co compared to the Inconel and stainless steel components.

The ^{54}Mn was produced by the fast neutron reaction ^{54}Fe (n,p) ^{54}Mn, and its production is a reflection of the iron content of the parent materials and the fast neutron flux. Generally, the ^{54}Mn concentrations in the various materials were near or slightly below the ^{60}Co concentrations at the time of discharge of the fuel assemblies. Because ^{54}Mn has a relatively short half-life (0.854 yr), it will become a minor constituent in the activated metal specimens after a few years.

Antimony-125 was a major constituent of the Zircaloy-4 spacer grids used in the Combustion Engineering and General Electric fuel assemblies. The ^{125}Sb is produced from tin by the reaction ^{124}Sn (n,τ) ^{125}Sn followed by beta decay of the ^{125}Sn to ^{125}Sb. Zircaloy-4 contains about 1-3 tin. Since the ^{125}Sb half-life is only 2.73 years it will decay relatively fast compared to ^{60}Co.

3.4 RADIONUCLIDE SCALING FACTORS FOR ACTIVATED METAL COMPONENTS

This study has provided one of the few opportunities to systematically measure the long-lived 10CFR61 radionuclides produced in activated metal components from within reactor pressure vessels. Because many of these radionuclides are very difficult to measure, it is desirable to determine if useful correlations exist between the difficult-to-measure radionuclides (^{55}Fe, ^{59}Ni, ^{63}Ni, ^{93m}Nb and ^{94}Nb) and ^{60}Co which is easily measured by gamma-ray spectrometry. If appropriate correlations exist, then scaling factors (relative to ^{60}Co) could be used to estimate their concentrations by multiplying the easily measured ^{60}Co concentrations by the empirically determined scaling factors. Table 3.11 presents the empirical scaling factors determined for stainless steel, Inconel, and Zircaloy components from the three fuel assemblies. In general, the activity correlations are quite good, indicating that the use of scaling factors for estimating radionuclide concentrations of the long-lived, difficult-to-measure 10CFR61 radionuclides in activated metals may be entirely appropriate. The $^{55}Fe/^{60}Co$, $^{59}Ni/^{60}Co$, and $^{63}Ni/^{60}Co$ scaling factors for the fuel assembly hardware components were particularly good. The scaling factors for the BRW assembly hardware generally had larger uncertainties compared to the PWR assemblies. Although the variability of the $^{94}Nb/^{60}Co$ and $^{93m}Nb/^{60}Co$ scaling factors were generally somewhat higher than the other scaling factors, they still appear to be useful for estimating the ^{94}Nb and ^{93m}Nb concentrations in activated metal components.

TABLE 3.11. Activity Scaling Factors for Activition Products in Spent Fuel Assembly Hardware Materials

	Average Activity Scaling Factors[a]						
	Westinghouse		Combustion Engineering			General Electric	
Ratio	Stainless Steel	Inconel	Stainless Steel	Inconel	Zircaloy	Stainless Steel	Zircaloy
$^{54}Mn/^{60}Co$	(1.39±0.096)E-1	(7.70±3.90)E-2	(2.14±1.60)E-1	(3.94±1.31)E-2	(1.54±0.62)E0	(2.62±1.37)E0	(4.02±3.17)E0
$^{55}Fe/^{60}Co$	(2.62±0.73)E0	(1.13±0.64)E0	(3.91±0.83)E0	(1.10±1.19)E0	(1.39±0.57)E1	(1.10±1.09)E1	(4.07±3.63)E0
$^{59}Ni/^{60}Co$	(9.30±2.60)E-4	(6.07±4.16)E-3	(1.03±0.44)E-3	(9.68±8.51)E-3	(1.52±0.77)E-4	(4.59±3.82)E-3	(9.11±5.55)E-4
$^{63}Ni/^{60}Co$	(2.25±0.56)E-1	(1.53±0.89)E0	(2.24±0.29)E-1	(2.78±2.50)E0	(3.89±2.06)E-2	(8.23±7.86)E-1	(1.15±0.79)E-1
$^{94}Nb/^{60}Co$	(5.05±4.43)E-7	(1.07±0.39)E-3	(4.16±2.70)E-7	(4.16±1.30)E-4	(2.02±0.34)E-2	(2.76±3.25)E-6	(1.45±2.48)E-3
$^{93m}Nb/^{60}Co$	(6.82±5.50)E-5	(1.79±1.39)E-1	(7.59±4.70)E-5	(6.81±4.51)E-2	(2.07±0.17)E-1	(5.67±7.52)E-4	(8.17±2.24)E-2
$^{59}Ni/^{63}Ni$	(4.12±0.52)E-3	(3.85±0.29)E-3	(4.53±1.47)E-3	(3.54±0.12)E-3	(4.02±1.02)E-3	(7.49±2.87)E-3	(8.47±1.44)E-3
$^{93m}Nb/^{94}Nb$	(1.43±0.25)E2	(1.50±0.81)E2	(1.92±0.54)E2	(1.55±0.60)E2	(1.06±0.24)E3	(1.81±1.19)E2	(5.83±15.2)E2

(a) Activity at time of discharge.

Note: ± values are 1 σ.

The $^{59}Ni/^{63}Ni$ was also sufficiently constant that a generic scaling factor for all activated metal components from all assemblies would seem reasonable. An overall $^{59}Ni/^{63}Ni$ scaling factor of 0.00524 ± 0.00227 was obtained for all samples listed in Tables 3.5, 3.6 and 3.7.

3.5 CLASSIFICATION OF SPENT FUEL ASSEMBLY HARDWARE WITH RESPECT TO 10CFR61

The licensing requirements for shallow land disposal of radioactive waste, 10CFR61, specifies three classes of waste, A, B and C that are permissible for disposal in commercial low-level waste disposal facilities.[2] Recently, the rule has been amended to require that all waste greater than Class C be disposed of in a high-level waste repository or some other approved alternative facility.[5] It is therefore critical to carefully assess the radionuclide concentrations in spent fuel assembly hardware and other highly activated internal components of reactor pressure vessels in an effort to seek ways to minimize the volume of greater-than-Class C waste destined for repository (or alternative facility) burial.

The three long-lived radionuclides which control the waste classification of highly activated metals are ^{63}Ni, ^{59}Ni and ^{94}Nb. However, since the ^{59}Ni limit will never be exceeded without first exceeding the ^{63}Ni limit, the classification controlling radionuclides are ^{63}Ni and ^{94}Nb.

Table 3.12 compares the average concentrations of ^{63}Ni, ^{59}Ni, and ^{94}Nb (in units of Ci/m^3) in various components of spent fuel assembly hardware with the 10CFR61 Class C limit, and Table 3.13 gives the ratio of the measured concentrations to the Class C limit. Any materials exceeding the Class C limits for these radionuclides will need to be disposed of in a high level waste repository or approved alternative facility. As shown in Tables 3.12 and 3.13, the ^{63}Ni, ^{59}Ni, and ^{94}Nb concentrations often exceeded the Class C limit for various components of the spent fuel assembly hardware. The Inconel-718 spacer grids on the Westinghouse assembly and the Inconel-625 bottom spacer grid on the Combustion Engineering assembly were the components which exceeded the Class C limit the most. For example, the Inconel-718 spacer grids on the Westinghouse assembly exceeded the Class C limits for ^{63}Ni and ^{94}Nb by average factors of 86 and 2390, respectively. The Inconel-718 and Inconel-625 contained about 4.5% and 2.3% Nb, respectively, and about 50% and 73% Ni, respectively. Thus, from a radiological waste disposal standpoint, these alloys have the highest concentrations of parent elements which produce the activation products exceeding the Class C limit.

The stainless steel end fittings and hold down flow plates in all cases except the bottom end fittings on the General Electric assembly only exceeded the Class C limit for ^{63}Ni. Stainless steel contains about 8 to 9.3% nickel. The ^{94}Nb concentrations in the stainless steel end fittings and hold-down/flow plates were often close to the Class C limit and did slightly exceed the limit for the General Electric bottom end fitting.

The Zircaloy-4 spacer grids in the Combustion Engineering and General Electric did not exceed the Class C limits for ^{63}Ni, ^{59}Ni, or ^{94}Nb, although they come close to the ^{94}Nb limit. From a radiological standpoint, nuclear

TABLE 3.12. Average Concentrations of 10CFR61 Radionuclides in Spent Fuel Assembly Hardware Components

		Average Concentration (Ci/m^3)		
	Material	^{63}Ni	^{59}Ni	^{94}Nb
Westinghouse				
Upper end fittings	SS-304	1.34E4	5.83E1	8.69E-3
Bottom end fittings	SS-304	2.61E4	9.80E1	1.07E-1
Spacer grids	Inconel-718	5.63E5	2.13E3	4.77E2
Upper holddown spring	Inconel-718	2.30E4	1.00E2	6.28E-0
Combustion Engineering				
Upper holddown & flow plates	SS-304	7.09E2	3.24E1	1.90E-2
Bottom end fitting & retention plate	SS-304	8.78E4	3.09E2	8.13E-2
Spacer grids	Zircaloy-4	3.02E1	1.21E-1	1.46E-1
Upper holddown spring	Inconel-625	3.40E4	1.17E2	2.42E1
Bottom spacer grid	Inconel-625	3.83E5	1.39E3	1.92E2
General Electric				
Upper handle & tie plate	SS-304	6.66E3	3.43E1	1.84E-2
Upper expansion spring	Inconel-X750	8.06E4	4.01E2	5.06E-0
Spacer grids	Zircaloy-4	3.45E2	4.87E0	6.83E-2
Bottom end fitting	SS-304	3.48E4	3.67E2	3.39E-1
10CFR61 Class C Limit		7.0E3	2.2E2	2.0E-1

TABLE 3.13. Ratio of Measured Radionuclide Concentrations in Spent Fuel Assembly Hardware to Their 10CFR61 Class C Limit

		Ratio: Measured Concentration/Class C Limit		
	Material	^{63}Ni	^{59}Ni	^{94}Nb
Westinghouse				
Upper end fittings	SS-304	1.91	0.27	0.043
Bottom end fittings	SS-304	3.73	0.45	0.54
Spacer grids	Inconel-718	80.4	9.68	2390
Upper holddown spring	Inconel-718	3.29	0.45	31.4
Combustion Engineering				
Upper holddown & flow plates	SS-304	0.10	0.15	0.095
Bottom end fitting & retention plate	SS-304	12.5	1.40	0.41
Spacer grids	Zircaloy-4	0.0043	5.5E-4	0.73
Upper holddown spring	Inconel-625	4.9	0.53	121
Bottom spacer grid	Inconel-625	54.7	6.3	960
General Electric				
Upper handle & tie plate	SS-304	0.95	0.16	0.092
Upper expansion spring	Inconel-X750	11.5	1.8	25.3
Spacer grids	Zircaloy-4	0.049	0.022	0.34
Bottom end fitting	SS-304	4.97	1.67	1.7

grade Zircaloy-4 is a very desirable material because it contains very low concentrations of the parent elements which produce the long-lived radionuclides of concern.

For future waste disposal considerations, it would be expeditious for fuel assembly vendors to consider alternate materials to replace the Inconel alloys which are high in nickel and niobium concentrations. Although these alloys are used in limited volumes in fuel assembly construction, they have a significant impact on the future radioactive waste disposal options.

4.0 RADIONUCLIDE CHARACTERIZATION OF GUNDREMMIGEN REACTOR PRESSURE VESSEL STEEL

During the past year it was possible to obtain two specimens of the steel reactor pressure vessel from the decommissioned Gundremmigen KRB-A reactor. The purpose of acquiring these specimens was twofold: 1) to provide real measurements of the concentrations of neutron activation products in a decommissioned reactor pressure vessel, and to provide a comparison with 10CFR61 waste classification levels, and 2) to compare calculated estimates of the activation product concentrations in the pressure vessel with the empirical measurements to determine the accuracy of the calculational methods. This information is of vital importance in reactor decommissioning because it provides an assessment of disposal options and transportation requirements for decommissioned reactor pressure vessels, and provides confidence (or identifies shortcomings) in calculational methods for estimating radionuclide inventories.

The Boiling Water Reactor KRB-A had a nominal thermal power of 801 MW (250 MW electrical). The reactor was put in operation in November 1966 and, until the last shutdown on January 13, 1977, generated a total of about 16 TWh of electrical power, with an average availability of 75%.

After decommissioning, 15 cores (trepans) of the reactor pressure vessel were taken at different axial and azimuthal positions within the 90 to 135 degree octane of the reactor. The axial and azimuthal positions of the trepans named A,B,C,D,E,F,G,K,L,M,N,P,Q,R,T are shown in Figures 4.1 and 4.2.

The two specimens received at PNL were cut from trepan G (115°). Vessel steel from the 0.41T and 0.67T depths (e.g. 41% and 67%, respectively, through the vessel wall referenced to the steel/cladding interface) were cut from a slab of trepan G (see Figure 4.3). The weights of the 0.41T and 0.67T pieces were 7.8793 g. and 9.4835 g., respectively. Each piece was cut into thirds and subjected to the radionuclide and elemental analyses described in Sections 3.2.1 and 3.2.2.

The only long-lived gamma-emitting radionuclide present in the samples was ^{60}Co (see Table 4.1). The most abundant radionuclide was ^{55}Fe, which was almost a factor of ten higher in concentration than ^{60}Co. The ^{63}Ni concentrations averaged about 26 times lower than ^{60}Co, and the ^{94}Nb concentrations were below the limit of detection.

Also shown in Table 4.1 is the ratio of the measured radionuclide concentrations to the 10CFR61 Class A limit for disposal in a low level waste shallow land burial facility. It is obvious that these concentrations are well below the Class A limit and the entire pressure vessel (not including internal components) could be disposed of as Class A waste. This is consistent with the classification measurements for the Shippingport reactor pressure vessel. Thus, it appears that disposal of commercial station pressure vessels will not pose a serious problem from a radiological standpoint in future reactor decommissioning.

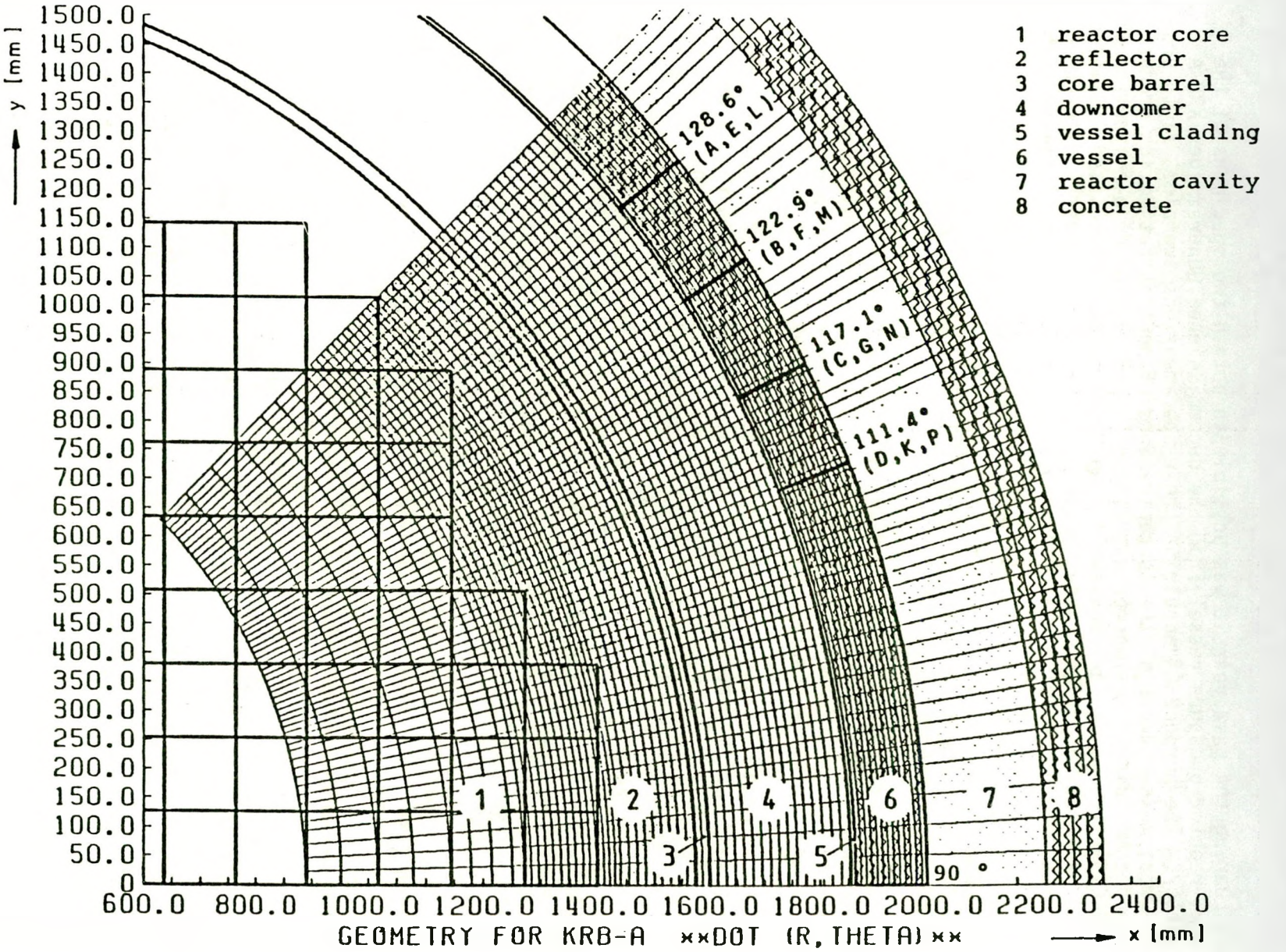

FIGURE 4.1. (R-O)-Geometry for KRB/A Reactor with Trepan Positions (from Prillinger, 1986)

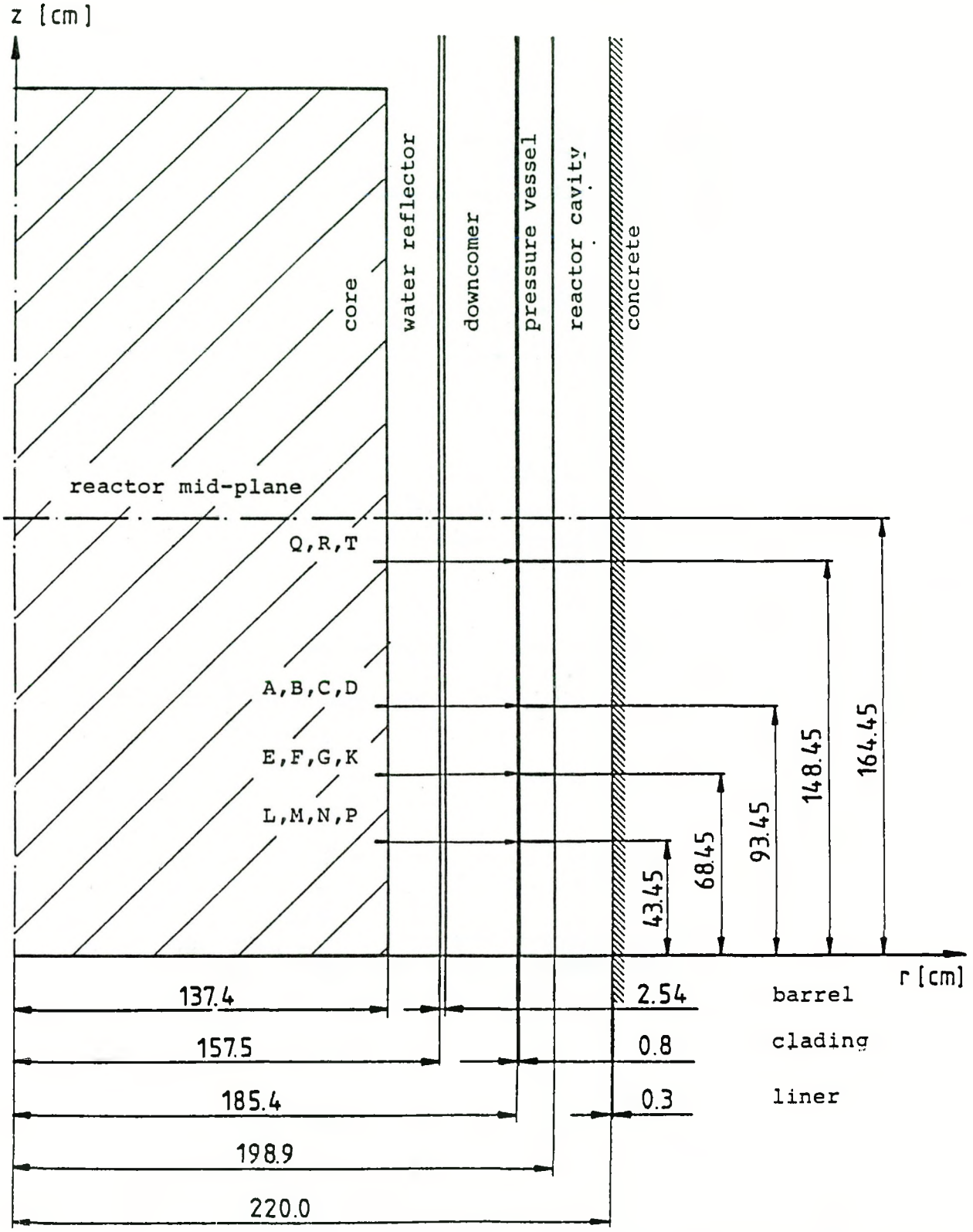

FIGURE 4.2. (R-Z)-Geometry for KRB/A Reactor with Trepan Positions (from Prillinger, 1986)

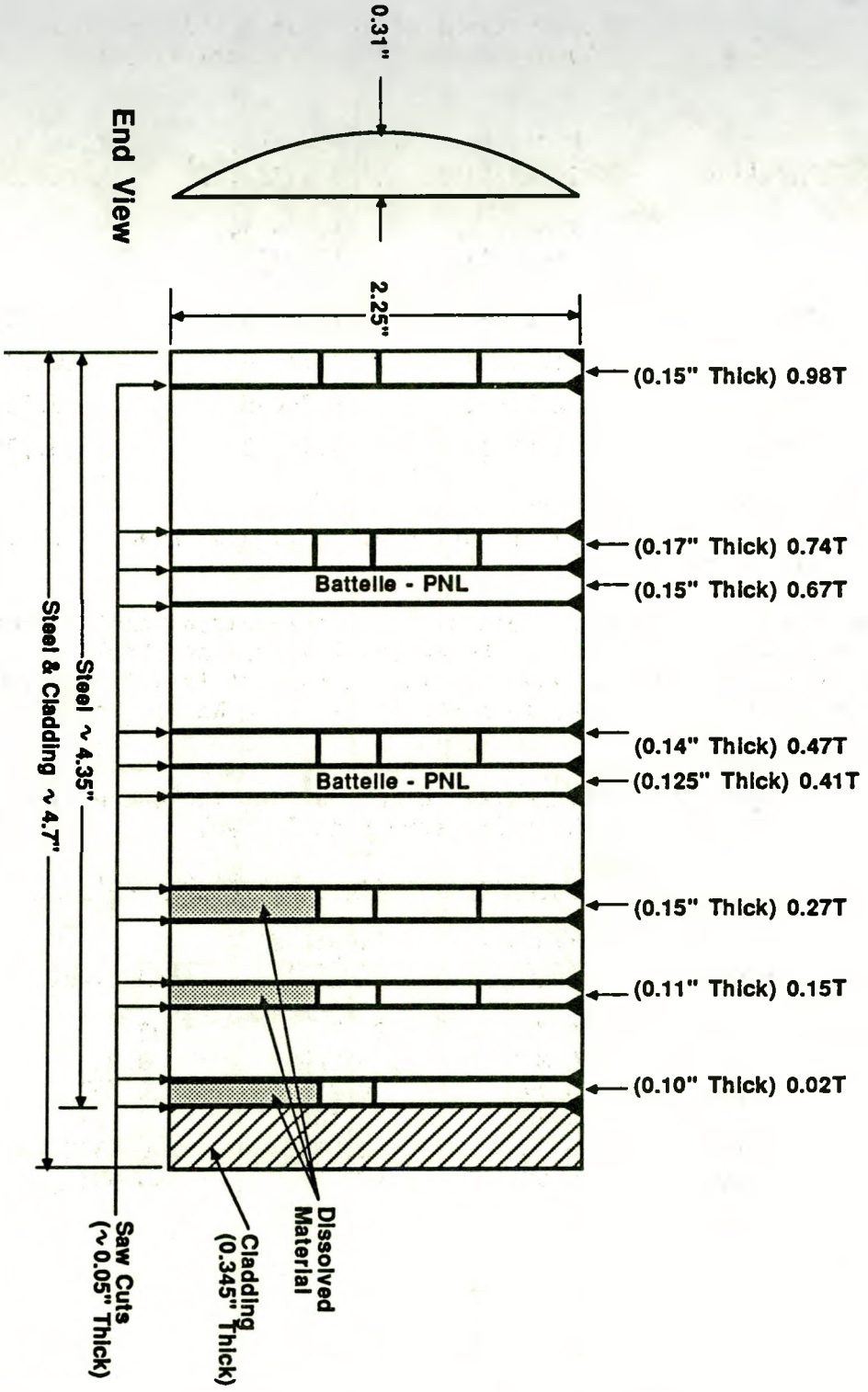

FIGURE 4.3. Gundremmigen KRB-A Reactor Pressure Vessel Core (Trepan G, 115°) Sampling Locations for Radionuclide and Elemental Analyses at PNL

TABLE 4.1. Concentrations of Neutron Activation Products in Gundremmigen KRB-A Pressure Vessel Steel

Radionuclide	Radiochemically Measured Concentration (Ci/g steel)[a]		Ratio: Meas. Conc./ Class A Limit
	Sample #3 (0.41T)	Sample #4 (0.67T)	
^{60}Co	2.53E-6	1.32E-6	0.028
^{63}Ni	1.14E-7	4.37E-8	0.025
^{55}Fe	2.91E-5	9.25E-6	0.32
^{94}Nb	<2.8E-12	<3.1E-12	<0.00012

(a) Concentrations decay corrected to time of reactor shutdown (January 13, 1977)

The elemental concentrations of the Gundremmigen reactor pressure vessel steel are shown in Table 4.2. The material is carbon steel and contains less than one percent of Ni, Mn and Cr. The Co content is slightly lower than that observed for U. S. stainless steels, and the Nb was undetectable at less than 0.001 percent.

TABLE 4.2. Elemental Concentrations in Gundremmigen KRB-A Pressure Vessel Steel

Element	Concentration - Weight Percent		
	Sample #3 (0.41T)	Sample #4 (0.67T)	Avg. Conc.
Fe	92.7	92.7	92.7
Ni	0.813	0.829	0.821
Mn	0.749	0.757	0.753
Cr	0.409	0.406	0.408
Co	0.0339	0.0338	0.0339
Nb	<0.001	<0.001	<0.001

5.0 COMPARISON OF CALCULATED VERSUS MEASURED RADIONUCLIDE CONCENTRATIONS

This project has provided the opportunity to conduct calculated estimates of the concentrations of neutron activation products in various types of reactor pressure vessel and fuel assembly hardware components, and to compare the calculated values with carefully measured radionuclide concentrations. The empirical measurements involved both radionuclide and stable element analyses in order to obtain specific activities of the radionuclides of interest so that material compositional differences would not obviate the comparisons. Comparisons of calculated versus measured neutron activation product concentrations were made for the three fuel assembly hardware components described in Section 3 and for the Gundremmigen KRB-B reactor pressure vessel steel. These comparisons provide a measure of the degree of accuracy of the calculational methods and identify any shortcomings in the predictive methods, such as insufficient cross section information, neutron flux and energy spectrum measurements, etc. It should be stressed that the calculations were conducted completely independently of the measurements, except that the actual elemental concentrations were supplied for the calculations. Thus, this exercise was a true blind comparison.

5.1 SPENT FUEL ASSEMBLY HARDWARE

5.1.1 Measured Specific Activities

The specific activities of the long-lived activation products in the components described in Section 3 are given in Tables 5.1, 5.2 and 5.3. The specific activities were reported in units of Ci/g of parent element by dividing the radionuclide concentrations in units of Ci/g of metal by the elemental concentration in units of g element/g metal. This normalizes the induced activities so that geometrical variations in the radionuclide concentrations can be observed. The sampling locations for the three fuel assemblies are shown in Figures 3.1, 3.2 and 3.3. The highest specific activities observed in each fuel assembly hardware were in the materials adjacent to the fueled region of the assemblies. The activities drop off rapidly at each end of the assemblies. The highest specific activity is due to ^{60}Co, generally followed by ^{55}Fe, ^{63}Ni and ^{93m}Nb. The ^{54}Mn specific activity in the Zircaloy spacer girds in the General Electric assembly were relatively high due to the relatively higher fast neutron flux.

5.1.2 Calculated Specific Activities

The calculated radionuclide concentrations were performed by a nuclear engineering group at PNL and details of the method have been published elsewhere.[17] Briefly, The process of calculating the radionuclide concentrations in the activated metal is two-fold. The first step is to calculate a core average inventory based on the irradiation history of the activated metal. This is performed using the ORIGEN2 code. Since the results of the ORIGEN2 calculation are valid for an average over the cores' fueled region only, adjustments need to be made if the results are to be applicable to metals that are activated outside the fueled region (this is more fully explained below). These adjustment factors were calculated using the

TABLE 5.1. Specific Activities of Long-Lived Radionuclides in Westinghouse Spent Fuel Assembly Hardware Materials (Point Beach Station)

Sample No.	Material	Location	Concentration (Ci/g of parent element)[a]						
			^{54}Mn[b]	^{55}Fe	^{59}Ni	^{63}Ni	^{60}Co	^{94}Nb	^{93m}Nb[c]
W-10	Inconel	holddown spring @ top end	(3.33±1.79)E-4	(1.07±0.03)E-2	(2.32±0.07)E-5	(5.30±0.16)E-3	(1.04±0.13)E0	(1.64±0.26)E-5	(1.22±0.12)E-3
W-12	SS	upper end fitting (top)	(2.65±0.71)E-4	(5.43±0.16)E-3	(2.01±0.06)E-5	(4.25±0.13)E-3	(1.09±0.11)E0	(1.24±0.26)E-5	(2.21±0.47)E-3
W-9	SS	upper end fitting casting (bottom)	(9.83±5.98)E-4	(4.41±0.13)E-2	(1.44±0.04)E-4	(3.35±0.10)E-2	(8.72±0.87)E0	(7.20±7.20)E-5	(9.9±9.9)E-3
W-8	Inconel	spacer grid #7	<2.2E-3	(8.06±0.24)E-2	(1.42±0.04)E-4	(3.70±0.11)E-2	(8.85±0.89)E0	(1.59±0.27)E-4	(1.37±0.14)E-2
W-7	Inconel	spacer grid #6	(3.62±0.75)E-2	(3.49±0.10)E-1	(5.48±0.16)E-4	(1.40±0.04)E-1	(4.57±0.46)E1	--	--
W-6	Inconel	spacer grid #5	(5.33±0.13)E-2	(3.46±0.10)E-1	(7.29±0.22)E-4	(1.77±0.05)E-1	(6.49±0.65)E1	--	--
W-5	Inconel	spacer grid #4	(2.21±0.62)E-2	(3.69±0.10)E-1	(6.44±0.19)E-4	(1.73±0.05)E-1	(6.73±0.67)E1	(2.61±0.70)E-3	(6.12±0.61)E-1
W-4	Inconel	spacer grid #3	(2.41±1.46)E-2	(3.98±0.11)E-1	(5.86±0.18)E-4	(1.70±0.05)E-1	(6.73±0.67)E1	--	--
W-3	Inconel	spacer grid #2	(2.13±1.02)E-2	(4.19±0.12)E-1	(6.81±0.20)E-4	(1.81±0.05)E-1	(6.18±0.62)E1	--	--
W-2	Inconel	spacer grid #1	<6.9E-3	(1.99±0.06)E-1	(2.74±0.08)E-4	(7.59±0.22)E-2	(2.75±0.28)E1	(9.01±1.67)E-4	(1.83±0.18)E-1
W-11	SS	bottom end fitting (top)	(5.37±0.50)E-3	(7.25±0.22)E-2	(1.58±0.05)E-4	(4.01±0.12)E-2	(1.11±0.34)E1	(2.20±2.20)E-5	(2.7±2.7)E-3
W-1	SS	bottom end fitting (bottom)	(3.48±1.06)E-3	(6.48±0.19)E-2	(1.26±0.04)E-4	(3.59±0.11)E-2	(1.24±0.12)E1	(1.32±0.23)E-4	(1.72±0.24)E-2

(a) Decay corrected to discharge date of 10/8/81.
(b) Parent element is iron (Fe). ^{54}Mn is formed by the fast neutron reaction $^{54}Fe(n,p)^{54}Mn$.
(c) Parent element is Nb. ^{93m}Nb is predominantly produced by the reaction $^{93}Nb(n,n')^{93m}Nb$.

TABLE 5.2. Specific Activities of Long-Lived Radionuclides in Combustion Engineering Spent Fuel Assembly Hardware Materials (Calvert Cliff Station)

Sample No.	Material	Location	Concentration (Ci/g of parent element)[a]						
			^{54}Mn[b]	^{55}Fe	^{59}Ni	^{63}Ni	^{60}Co	^{94}Nb	^{93m}Nb[c]
CE-25	SS	upper holddown plate	(4.19±0.22)E-4	(4.66±0.14)E-3	(1.12±0.02)E-5	(1.68±0.07)E-3	(1.27±0.09)E0	>3.2E-5	<5.1E-3
CE-26	Inconel	upper holddown spring	(5.34±3.40)E-4	(2.14±0.09)E-2	(1.89±0.05)E-5	(5.49±0.16)E-3	(2.78±0.26)E0	(1.27±0.22)E-5	(1.42±0.14)E-3
CE-24	SS	upper flow plate	(1.27±0.23)E-3	(5.44±0.16)E-2	(8.36±0.32)E-5	(1.91±0.06)E-2	(8.61±0.74)E0	>2.9E-4	>6.1E-2
CE-10	Zircaloy	top spacer grid	(3.19±0.42(E-3	(1.33±0.06)E-1	>4.8E-5	>1.4E-2	>4.9E0	--	--
CE-9	Zircaloy	spacer grid #7	(8.40±0.28)E-2	(5.49±0.21)E-1	>3.5E-4	>1.2E-1	>3.3E0	(1.09±0.17)E-4	(1.24±0.04)E-1
CE-8	Zircaloy	spacer grid #6	(8.53±0.33)E-2	(8.39±0.33)E-1	>2.7E-4	>9.0E-2	>3.9E0	--	--
CE-7	Zircaloy	spacer grid #5	(8.82±0.44)E-2	(7.90±0.32)E-1	>7.8E-4	>1.8E-1	>5.2E0	--	--
CE-6	Zircaloy	spacer grid #4	(9.36±0.36)E-2	(6.59±0.26)E-1	>2.5E-4	>7.2E-2	>4.0E0	--	--
CE-5	Zircaloy	spacer grid #3	(1.33±0.07)E-1	(1.82±0.07)E0	>7.1E-4	>1.7E-1	>6.2E0	(1.19±0.23)E-4	(1.40±0.09)E-1
CE-4	Zricaloy	spacer grid #2	(8.42±0.42)E-2	(8.35±0.33)E-1	>3.5E-4	>6.0E-2	>4.4E0	--	--
CE-3	Zricaloy	spacer grid #1	(8.46±0.27)E-2	(6.37±0.25)E-1	>2.2E-4	>4.5E-2	>3.2E0	(1.42±0.30)E-4	(1.11±0.68)E-1
CE-2	Inconel	bottom spacer grid	(3.90±3.02)E-2	(4.18±0.24)E-1	(4.45±0.13)E-4	(1.35±0.04)E-1	(3.71±0.94)E1	(1.00±0.17)E-3	(1.98±0.19)E-1
CE-14	SS	bottom retention plate	(1.43±0.19)E-2	(2.97±0.08)E-1	(5.77±0.17)E-4	(1.66±0.05)E-1	(4.83±0.38)E1	>1.8E-4	>2.4E-2
CE-1	SS	bottom end fitting near axial middle	(4.44±0.72)E-3	(1.52±0.06)E-1	(2.32±0.07)E-4	(6.44±0.19)E-2	(2.09±0.31)E1	>2.3E-5	>2.8E-3

(a) Decay corrected to discharge data of 4/17/82.
(b) Parent element is iron (Fe). ^{54}Mn is formed by the fast neutron reaction $^{54}Fe(n,p)^{54}Mn$.
(c) Parent element is Nb. ^{93m}Nb is predominantly produced by the reaction $^{93}Nb(n,N')^{93m}Nb$.

TABLE 5.3. Specific Activities of Long-Lived Radionuclides in General Electric Spent Fuel Assembly Hardware Materials (Cooper Station)

Sample	Material	Location	Concentration--Ci/g of parent element)[a]							
			^{54}Mn[b]	^{55}Fe	^{59}Ni	^{63}Ni	^{60}Co	^{94}Nb	^{93m}Nb[c]	^{125}Sb[d]
GE-19	SS	Tab on handle	(1.61±0.44)E-4	(2.08±0.11)E-2	(4.39±0.66)E-5	(9.55±1.13)E-3	(2.39±0.36)E0	(7.61±5.09)E-5	(2.49±1.66)E-2	--
GE-18	SS	Upper tie plate	(1.70±0.47)E-4	(1.30±0.05)E-2	(6.04±0.82)E-5	(1.07±0.11)E-2	(2.16±0.43)E0	(5.27±1.13)E-4	(1.23±0.27)E-1	--
GE-17	Inconel	Expansion spring	<1.6E-3	(4.00±0.14)E-2	(6.94±0.99)E-5	(1.39±0.15)E-2	(3.77±0.60)E0	(7.34±1.21)E-5	(4.92±0.49)E-3	<5.5E-3
GE-15	Zircaloy	Spacer grid #7	(7.51±2.02)E-3	(1.79±0.04)E-1	(3.85±0.59)E-4	(4.31±0.66)E-2	<3.4E0	(1.00±0.63)E-4	(4.62±2.90)E-1	(3.81±0.63)E-1
GE-13	Zircaloy	Spacer grid #6	(3.67±1.23)E-2	(6.03±0.28)E-1	(1.29±0.19)E-3	(1.29±0.19)E-1	<1.8E1	--	--	(1.24±0.22)E-1
GE-11	Zircaloy	Spacer grid #5	(3.31±1.04)E-2	(4.16±0.09)E-1	(1.30±0.20)E-3	(1.23±0.19)E-1	<1.3E1	--	--	(1.18±0.24)E-1
GE-9	Zircaloy	Spacer grid #4	(3.45±1.18)E-2	(5.34±0.17)E-1	(1.07±0.16)E-3	(1.58±0.23)E-1	<2.4E1	--	--	(1.65±0.30)E-1
GE-7	Zircaloy	Spacer grid #3	(3.43±0.70)E-2	(7.50±0.32)E-1	(3.38±0.71)E-3	(4.78±1.08)E-1	<1.0E1	(4.59±2.16)E-5	--	(1.56±0.28)E-1
GE-5	Zircaloy	Spacer grid #2	(3.67±0.49)E-2	(4.48±0.16)E-1	(1.27±0.27)E-3	(1.64±0.34)E-1	<6.7E0	--	--	(1.26±0.24)E-1
GE-3	Zircaloy	Spacer grid #1	(1.80±0.36)E-2	(4.55±0.16)E-1	(7.20±2.38)E-4	(8.77±2.89)E-2	<3.3E0	(5.45±1.04)E-5	(8.32±1.39)E-2	(1.11±0.22)E-1
GE-1	SS	Bottom end fitting	<6.2E-3	(1.92±0.10)E-1	(9.39±1.30)E-4	(8.69±0.87)E-2	(2.97±0.30)E1	(2.15±0.64)E-4	(1.85±0.55)E-2	<5.8E-2
GE-2	SS	Bottom end fitting	<8.4E-4	(1.83±0.12)E-2	(1.30±0.15)E-4	(1.46±0.15)E-2	(3.50±0.35)E0	(3.35±0.56)E-5	(2.69±0.45)E-3	<1.1E-2

(a) Decay corrected to discharge date from reactor--5/1/82.
(b) Parent element is iron (Fe). ^{54}Mn is formed by the fast neutron reaction $^{54}Fe(n,p)^{54}Mn$.
(c) Parent element is Nb. ^{93m}Nb is produced mainly by the reaction $^{93}Nb(n,n')^{93m}Nb$.
(d) Parent element of ^{125}Sb is Sn. ^{125}Sb is formed by the thermal neutron reaction $^{124}Sn(n,\gamma)^{125}Sn$ followed by ^{125}Sn beta decay to ^{125}Sb.

one-dimensional neutronics code, ANISN. The factors are then applied to the ORIGEN2 results to obtain the calculated radionuclide concentrations for the regions outside of the fueled sections of the assemblies.

The ORIGEN2 computer code is a widely used tool for estimating the radionuclide inventory of irradiated materials. The code is an extremely useful tool due to capabilities in tracking a large number of isotopes through specified irradiations and decays. It accounts for depletion and creation of isotopes through time. The code requires the user to describe the materials to be irradiated, the irradiation history it is subjected to, and specify the data library that supplies the basic neutronics data with which the code performs its calculations. These libraries are supplied to the user by the Radiation Shielding Information Center (RSIC) with the code. The list of available libraries consists of many reactor types, including a nominal and high burnup library for PWRs and a nominal burnup library for BWRs. These libraries have in them, in addition to half-lives and decay data, one-group cross-sections.

For the ORIGEN2 calculations, the standard PWR libraries were used. The irradiation histories specified in Tables 3.2, 3.3, and 3.4 and appropriate decay times were modeled. For each of the radionuclides of interest, the irradiation of one gram of the parent element was modeled. ORIGEN2 outputs a table of radionuclides resulting from the irradiation of the gram of material, in units of curies. An example is the irradiation of one gram of cobalt, and the resultant number of curies of ^{60}Co. ORIGEN2 calculates the production of ^{60}Co due to activation of the initial elemental cobalt, and accounts for the depletion of the initial ^{59}Co due to its transformation to ^{60}Co, as well as the decay of the ^{60}Co after its creation. The curies of ^{60}Co after irradiation per initial gram of elemental cobalt can then be compared with the sample data, and is independent of the amount of cobalt initially in each sample, which varies from sample to sample. ORIGEN2 calculations were done for each of the PNL fuel assemblies.

The cross-sections in the ORIGEN2 libraries were generated using detailed reactor core models and are applicable for use in estimating activation in neutron fluxes that resemble those in the fueled region of a reactor core. However, when the neutron flux varies significantly from that used in the reactor model, either a new one-group cross-section needs to be developed or an adjustment must be made to the ORIGEN2 results. A number of cross-section sets are available for a variety of reactor types, but all are applicable only to the fueled region of the specified reactor core. Much of the hardware that is of interest in this study is in the region of the end fittings, which are outside the cores active fuel region.

The neutron spectrum in the end fitting region is changed substantially from the fueled region. No fissions are occurring in this region, so as the fast neutrons are thermalized (slowed down in energy), the average neutron energy decreases, and the energy spectrum shifts downward. From Figure 5.1, it can be seen that the ^{59}Co (n,τ) cross-section generally increases with decreasing neutron energy. Therefore, it would be expected that the one-group cross-section in the end fitting region would increase compared to its

value in the core region. This change must be calculated accurately to estimate the amount of 1/v absorbing elements.

The one-group cross-sections used in the data libraries, are developed from rigorous multi-group calculations for the individual reactor models. In the multi-group calculations, the neutron spectrum is divided into many groups and the calculations are performed on a group basis. The interaction between the groups is taken into account within the calculation. The multi-group method is necessary for many problems, such as in the reactor core, because the cross-sections (which are a measure of the probability of reaction occurring) vary considerably with neutron energy.

As an example, the continuous cross-section for the activation of natural cobalt to ^{60}Co [^{59}Co (n,τ) ^{60}Co], see Figure 5.1(a), has a value of ~37 barns for thermal neutrons (0.0253eV). For fission neutrons, which are in the range of 1-10 MeV, the cross-section is less than 0.01 barns, almost four orders of magnitude less. For neutrons with energies just over 100 eV, the cross-section has a resonance of nearly 1000 barns. It should be apparent that in order to correctly estimate the total $^{59}Co(n,\tau)$ reaction rate over the entire neutron spectrum, i.e., the total ^{60}Co production rate, the energy dependence of the neutrons must be taken into account. One approach is to perform a multi-group calculation (other techniques exist as well). The continuous cross-section is divided into a finite number of groups, and a single value for the cross-section is determined for each group. The specific energy group divisions are in part based on how the cross sections vary with neutron energy. Figure 5.1(b) illustrates an arbitrary 11-group structure for the ^{59}Co (n,τ) cross-section. With an adequate number of groups, that is, if divided into small enough ranges of energy, the average value of the cross-section within an energy group is a reasonable representation of the continuous cross-section value.

Another consideration is that the neutron energy distribution affects the choice of the energy group structure for determination of the cross-section values. For example, if <u>all</u> the neutrons are above 1.0 MeV (fast spectrum), then a single value representing the cross-section would be determined by the continuous cross-section above 1.0 MeV. Alternately, if all the neutrons were less than 1.0 eV (thermal spectrum), the single value representing the cross-section would be determined by the continuous cross section below 1.0 eV. This would result in a significantly different value. This single value is referred to as the one-group cross-section. Figure 5.1(c) illustrates what the one-group cross-sections might look like for the two examples given. In most applications however, the neutrons have a wide range of energies, and the one-group cross-sections would not vary as much as in the two examples given. However, the cross-sections must still be appropriately weighted in order to account for differences in the neutron spectrum, which affect the one-group cross-section.

To calculate a one-group cross-section, it is first necessary to perform a multi-group calculation. A neutronic model is developed that represents the reactor core of interest and an appropriate multi-group cross-section

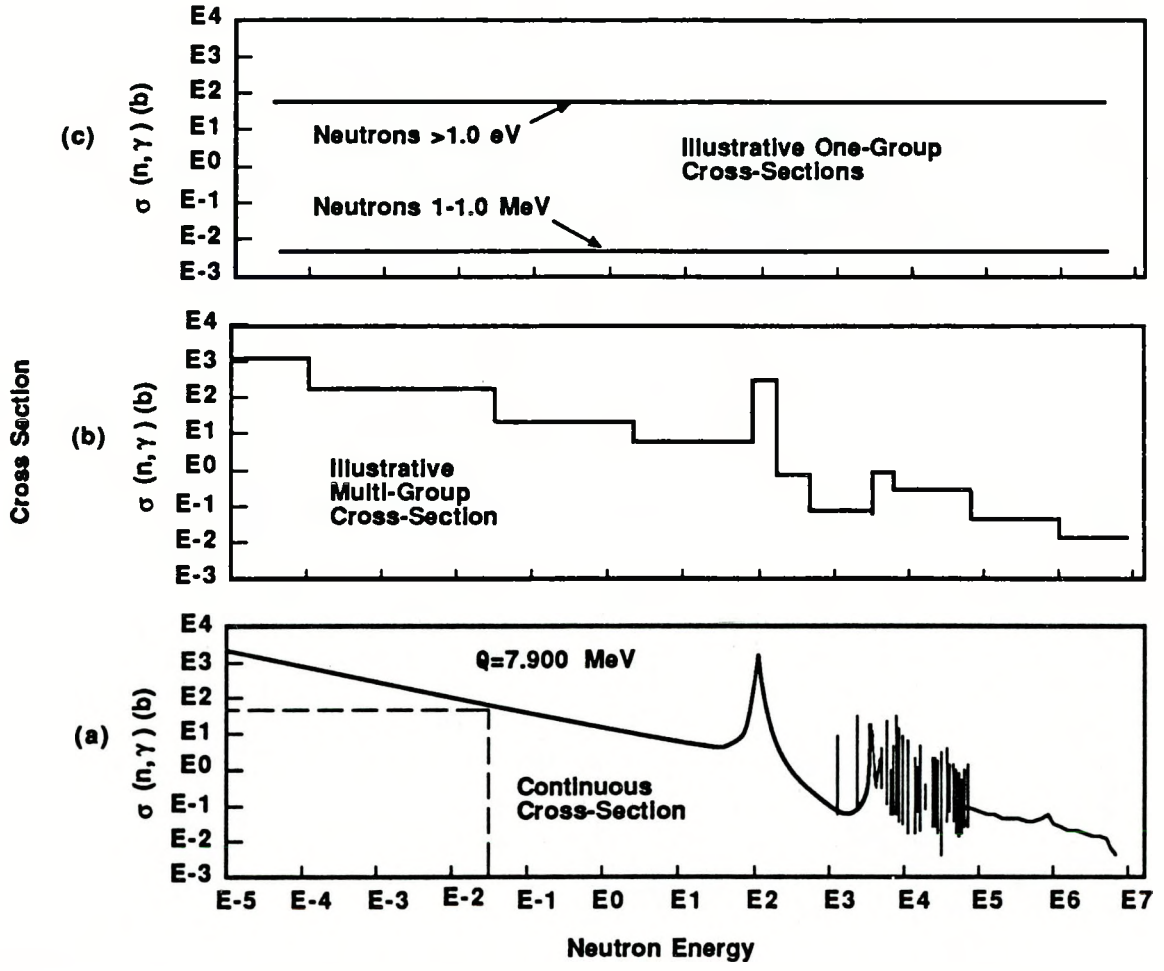

FIGURE 5.1. Cross-Section Versus Neutron Energy for the Reaction $^{59}Co(n,\tau)\ ^{60}Co$

library is selected. Once a group structure is defined, all the cross-sections used in that calculation must have the same energy group structure. Then the multi-group calculation is performed, and the multi-group reaction rate and flux can be summed up over all energy groups, to provide the total reaction rate and total flux. The total flux can then be divided into the total reaction rate, resulting in a one-group cross-section. By definition, the resultant one-group cross-section is the number, which when multiplied by the total flux, gives the correct total reaction rate. This one-group cross-section can now be used in subsequent calculations to multiply by the total flux, in order to estimate the total reaction rate, if the neutron spectrum does not change significantly. However, as discussed before, the spectrum does change upon leaving the fueled region, and in fact, changes within the fueled region itself. The changes with the fuel region are not significant from an activation perspective, but are significant outside the core.

The purpose of the neutronics calculations is to estimate the relative change of a variety of one-group cross-sections in PWRs. It is of interest

to determine how the cross-sections changed in the various regions of a fuel assembly and whether these changes were significant. It was also of interest to identify whether or not all the cross-sections changed in a similar, predictable manner. Three PWR models were generated in order to also determine whether the one-group cross-sections changed for various fuel designs. A representative model was generated for each of the major PWR vendors: Westinghouse, Babcock & Wilcox, and Combustion Engineering. Each reactor was modeled from almost the bottom of the reactor to the top. The greatest amount of detail was provided in the regions that comprised the fuel assembly. For a more detailed discussion of the neutronics calculations see Reference 17.

At this time, calculations were only performed for PWR reactors. It is anticipated that BWR calculations will be done sometime in the future. These fuel assemblies are representative of the type of spent fuel that must be accommodated by the federal waste management system and many utilities, both in their irradiation history and material composition. Other fuel types, such as Combustion Engineering 16x16, Westinghouse 15x15, and others, are neutronically similar to those sampled. In fact, there is little difference, neutronically, between the three reactor vendors. The main difference lies in the structural makeup of the core. After accounting for material differences, the factors developed in this study should be applicable to the other fuel types. This is because it is the fuel that determines the neutron flux and spectrum, and the structural material in the fueled region has little significant effect on it. The presence of the parent isotope, (i.e., ^{59}Co) has little effect on the reaction rate per unit mass of the isotope, within the ranges that exist in reactors. However, the absolute amount of the parent isotope does affect the amount of radionuclide (i.e., ^{60}Co) that is produced. In the region outside the fueled region, (i.e., end fittings), the lack of fuel results in the structural material having a greater effect on the neutron flux.

5.1.3 Comparison of Calculated Versus Measured Specific Activities

Figures 5.2 through 5.6 and Figures 5.7 through 5.11 show a comparison of the calculated versus measured long-lived neutron activation products in the Westinghouse and Combustion Engineering fuel assembly hardware, respectively. The radionuclides for which direct comparisons were made included ^{60}Co, ^{55}Fe, ^{63}Ni, ^{59}Ni, and ^{94}Nb.

Figures 5.2 and 5.7 show the comparison for ^{60}Co in the Westinghouse and Combustion Engineering assemblies. The agreement between measured and predicted ^{60}Co for the Westinghouse assembly is quite good. For the fueled region of the assembly the calculated values average about 1.3±0.2 times higher than the measured specific activities. Even at the end fittings where the one group neutron cross section for ^{59}Co varies by up to 5-fold over a distance of only a few centimeters, the predicted values were in fairly good agreement. For the Combustion Engineering assembly (see Figure 5.7), the ^{60}Co comparisons could not be made for the fueled region because the Zircaloy spacer grids contained such low elemental cobalt concentrations that specific activities could not be measured. At the stainless steel bottom end

Westinghouse Fuel Assembly, 14x14

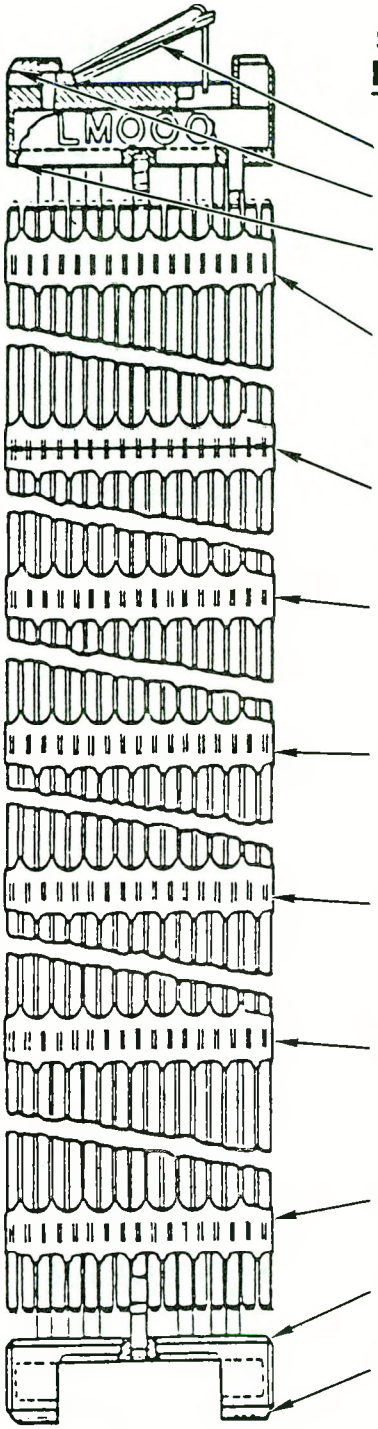

Predicted Ci/g-Co	Sample Number	Measured Ci/g-Co	Ratio: Predicted / Measured
8.78E-1	W10	(1.04±0.13)E0	0.844
1.02E0	W12	(1.09±0.11)E0	0.936
3.04E0	W9	(8.72±0.87)E0	0.349
9.99E0	W8	(8.85±0.89)E0	1.13
6.65E1	W7	(4.57±0.46)E1	1.46
8.47E1	W6	(6.49±0.65)E1	1.31
1.01E2	W5	(6.73±0.67)E1	1.50
1.00E2	W4	(6.73±0.67)E1	1.49
9.03E1	W3	(6.18±0.62)E1	1.46
2.57E1	W2	(2.75±0.28)E1	0.935
2.70E1	W11	(1.11±0.34)E1	2.43
1.74E1	W1	(1.24±0.12)E1	1.40

FIGURE 5.2. ^{60}Co Specific Activities in Spent Fuel Assembly Hardware

Westinghouse Fuel Assembly, 14x14

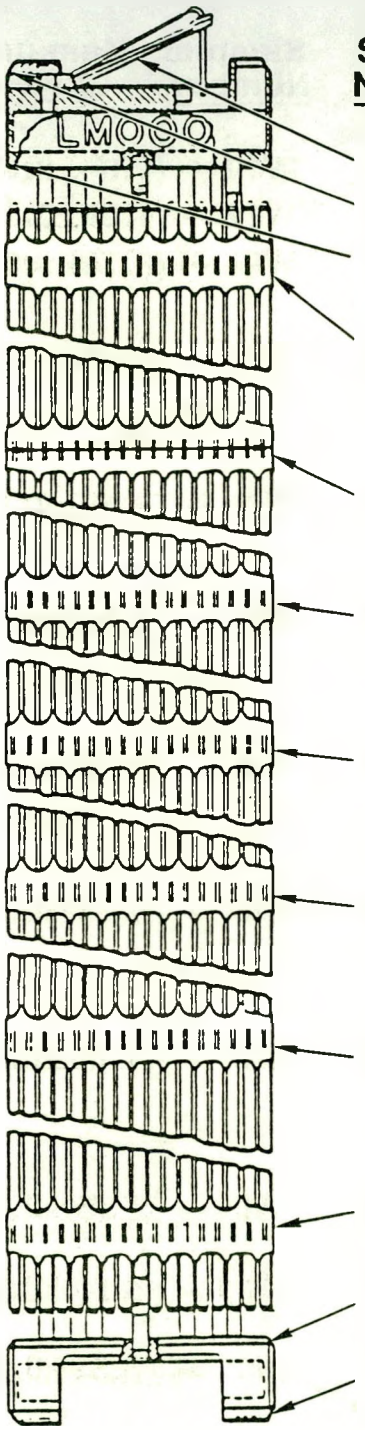

Predicted Ci/g-Fe	Sample Number	Measured Ci/g-Fe	Ratio: Predicted / Measured
4.63E-3	W10	(1.07±0.03)E-2	0.433
5.37E-3	W12	(5.43±0.16)E-3	0.989
1.54E-2	W9	(4.41±0.13)E-2	0.349
5.32E-2	W8	(8.06±0.24)E-2	0.660
2.75E-1	W7	(3.49±0.10)E-1	0.777
3.87E-1	W6	(3.46±0.10)E-1	1.12
4.18E-1	W5	(3.69±0.10)E-1	1.13
4.15E-1	W4	(3.98±0.11)E-1	1.04
3.75E-1	W3	(4.19±0.12)E-1	0.895
1.05E-1	W2	(1.99±0.06)E-1	0.533
1.39E-1	W11	(7.25±0.22)E-2	1.92
9.54E-2	W1	(6.48±0.19)E-2	1.47

FIGURE 5.3. ^{55}Fe Specific Activities in Spent Fuel Assembly Hardware

Westinghouse Fuel Assembly, 14x14

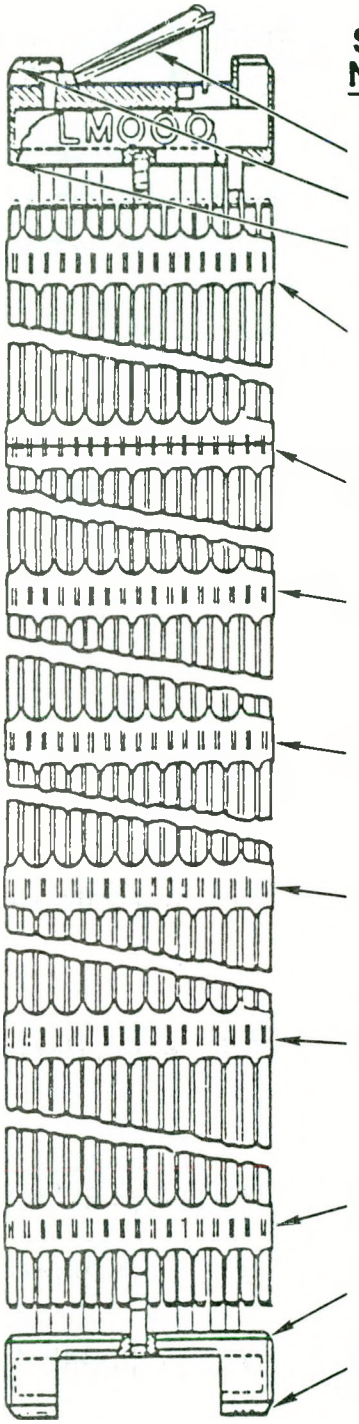

Predicted Ci/g-Ni	Sample Number	Measured Ci/g-Ni	Ratio: Predicted / Measured
2.93E-4	W10	(5.30±0.06)E-3	0.0553
3.38E-4	W12	(4.25±0.13)E-3	0.0795
1.19E-3	W9	(3.35±0.10)E-2	0.0355
3.19E-3	W8	(3.70±0.11)E-2	0.0862
5.57E-2	W7	(1.40±0.04)E-1	0.398
7.76E-2	W6	(1.77±0.05)E-1	0.438
8.39E-2	W5	(1.73±0.05)E-1	0.485
8.33E-2	W4	(1.70±0.05)E-1	0.490
7.53E-2	W3	(1.81±0.05)E-1	0.416
2.18E-2	W2	(7.59±0.22)E-2	0.287
9.64E-3	W11	(4.01±0.12)E-2	0.240
4.28E-3	W1	(3.59±0.11)E-2	0.119

FIGURE 5.4. ^{63}Ni Specific Activities in Spent Fuel Assembly Hardware

Westinghouse Fuel Assembly, 14x14

Predicted Ci/g-Ni	Sample Number	Measured Ci/g-Ni	Ratio: Predicted / Measured
2.16E-6	W10	(2.32±0.07)E-5	0.0931
2.50E-6	W12	(2.01±0.00)E-5	0.124
8.77E-6	W9	(1.44±0.04)E-4	0.0609
2.36E-5	W8	(1.42±0.04)E-4	0.166
4.12E-4	W7	(5.48±0.16)E-4	0.752
5.74E-4	W6	(7.29±0.22)E-4	0.787
6.21E-4	W5	(6.44±0.19)E-4	0.964
6.16E-4	W4	(5.86±0.18)E-4	1.05
5.57E-4	W3	(6.81±0.20)E-4	0.818
1.62E-4	W2	(2.74±0.08)E-4	0.591
7.13E-5	W11	(1.58±0.05)E-4	0.451
3.17E-5	W1	(1.26±0.04)E-4	0.252

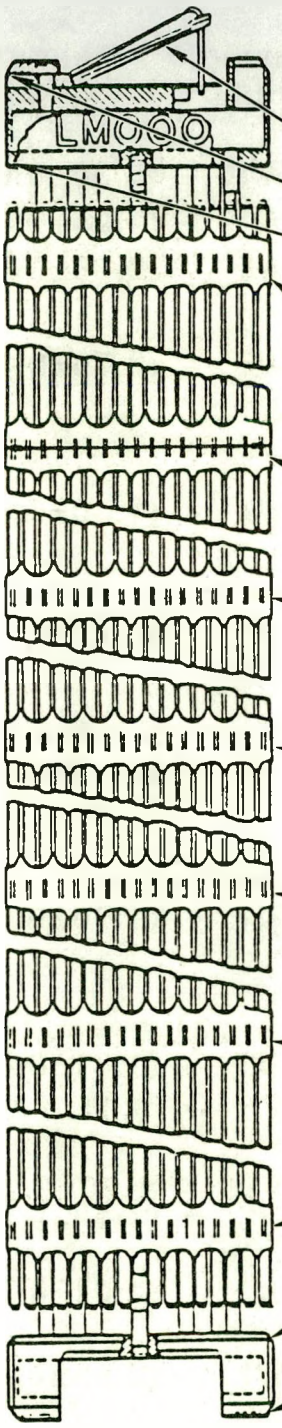

FIGURE 5.5. ^{59}Ni Specific Activities in Spent Fuel Assembly Hardware

Westinghouse Fuel Assembly, 14x14

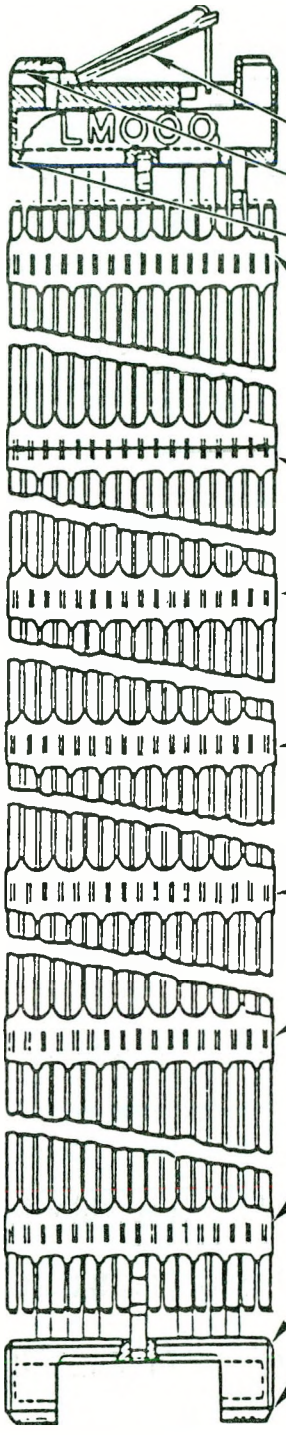

Predicted Ci/g-Nb	Sample Number	Measured Ci/g-Nb	Ratio: Predicted Measured
1.11E-5	W10	(1.64±0.26)E-5	0.677
1.29E-5	W12	(1.24±0.26)E-5	1.04
4.19E-5	W9	(7.20±7.20)E-5	0.58
1.43E-4	W8	(1.59±0.27)E-4	0.899
1.37E-3	W7	–	
1.91E-3	W6	–	
2.06E-3	W5	(2.61±0.70)E-3	0.789
2.00E-3	W4	–	
1.85E-3	W3	–	
5.28E-4	W2	(9.01±1.67)E-4	0.586
3.57E-4	W11	(2.20±2.20)E-5	16
1.96E-4	W1	(1.32±0.23)E-4	1.48

FIGURE 5.6. ^{94}Nb Specific Activities in Spent Fuel Assembly Hardware

Combustion Engineering 14x14 Fuel Assembly, Calvert Cliffs Nuclear Power Plant

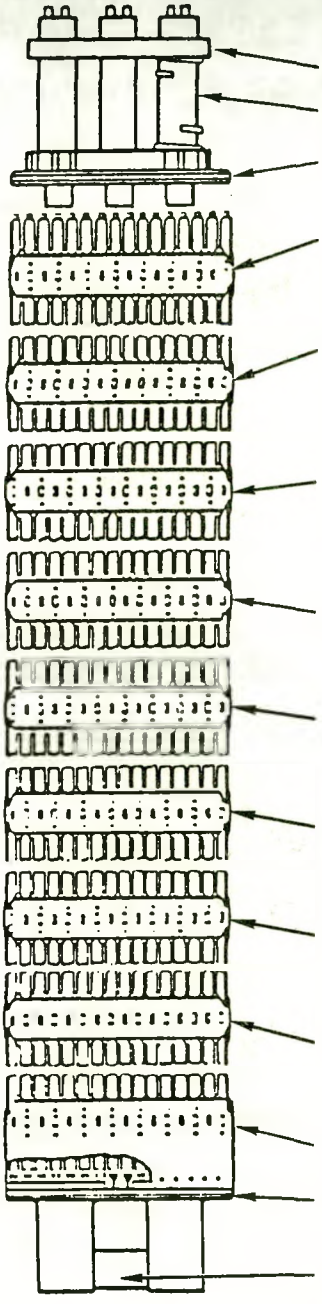

Predicted Ci/g-Co	Sample Number	Measured Ci/g-Co	Ratio: Predicted Measured
8.78E-2	CE25	(1.27±0.09)E0	0.0691
3.47E-1	CE26	(2.78±0.26)E0	0.125
8.80E-1	CE24	(8.61±0.74)E0	0.102
5.62E0	CE10	>4.9E0	<1.1
4.97E1	CE9	>3.3E0	<15
8.86E1	CE8	>3.9E0	<23
1.13E2	CE7	>5.2E0	<22
1.20E2	CE6	>4.0E0	<30
1.43E2	CE5	>6.2E0	<23
1.28E2	CE4	>4.4E0	<29
8.88E1	CE3	>3.2E0	<28
3.86E1	CE2	(3.71±0.94)E1	1.04
3.36E1	CE14	(4.83±0.38)E1	0.696
1.96E1	CE1	(2.09±0.31)E1	0.938

FIGURE 5.7. ^{60}Co Specific Activities in Spent Fuel Assembly Hardware

Combustion Engineering 14x14 Fuel Assembly, Calvert Cliffs Nuclear Power Plant

Predicted Ci/g-Fe	Sample Number	Measured Ci/g-Fe	Ratio: Predicted Measured
4.50E-4	CE25	(4.66±0.14)E-3	0.0966
1.90E-3	CE26	(2.14±0.09)E-2	0.0888
4.55E-3	CE24	(5.44±0.16)E-2	0.0836
3.03E-2	CE10	(1.33±0.06)E-1	0.228
1.99E-1	CE9	(5.49±0.21)E-1	0.362
3.65E-1	CE8	(8.39±0.33)E-1	0.435
4.63E-1	CE7	(7.90±0.32)E-1	0.586
4.97E-1	CE6	(6.59±0.26)E-1	0.754
5.98E-1	CE5	(1.82±0.07)E0	0.329
7.49E-1	CE4	(8.35±0.33)E-1	0.897
3.71E-1	CE3	(6.37±0.25)E-1	0.582
1.70E-1	CE2	(4.18±0.24)E-1	0.407
1.79E-1	CE14	(2.97±0.08)E-1	0.603
1.18E-1	CE1	(1.52±0.06)E-1	0.776

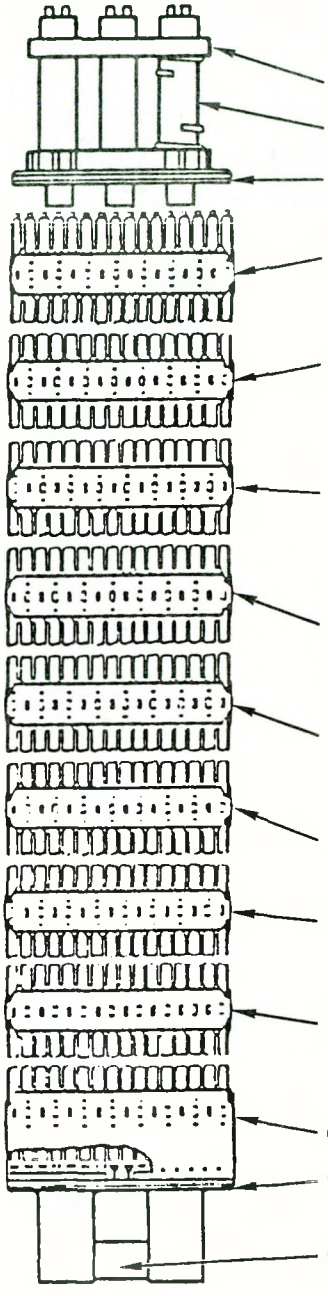

FIGURE 5.8. ^{55}Fe Specific Activities in Spent Fuel Assembly Hardware

Combustion Engineering 14x14 Fuel Assembly, Calvert Cliffs Nuclear Power Plant

Predicted Ci/g-Ni	Sample Number	Measured Ci/g-Ni	Ratio: Predicted / Measured
3.75E-5	CE25	(1.68±0.14)E-3	0.0223
1.07E-4	CE26	(5.49±0.09)E-3	0.0195
3.44E-4	CE24	(1.91±0.16)E-2	0.0180
1.77E-3	CE10	>1.4E-2	<0.13
4.14E-2	CE9	>1.2E-1	<0.35
6.97E-2	CE8	>9.0E-2	<0.77
8.87E-2	CE7	>1.8E-1	<0.49
9.46E-2	CE6	>7.2E-2	<1.3
1.09E-1	CE5	>1.7E-1	<0.64
9.81E-2	CE4	>6.0E-2	<1.6
7.02E-2	CE3	>4.5E-2	<1.6
2.84E-2	CE2	(1.35±0.04)E-1	0.210
1.36E-2	CE14	(1.66±0.05)E-1	0.0819
4.39E-3	CE1	(6.44±0.19)E-2	0.068

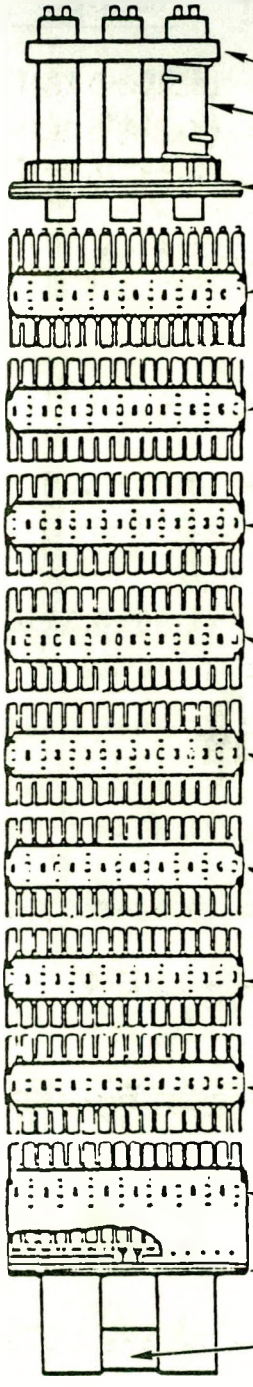

FIGURE 5.9. ^{63}Ni Specific Activities in Spent Fuel Assembly Hardware

Combustion Engineering 14x14 Fuel Assembly, Calvert Cliffs Nuclear Power Plant

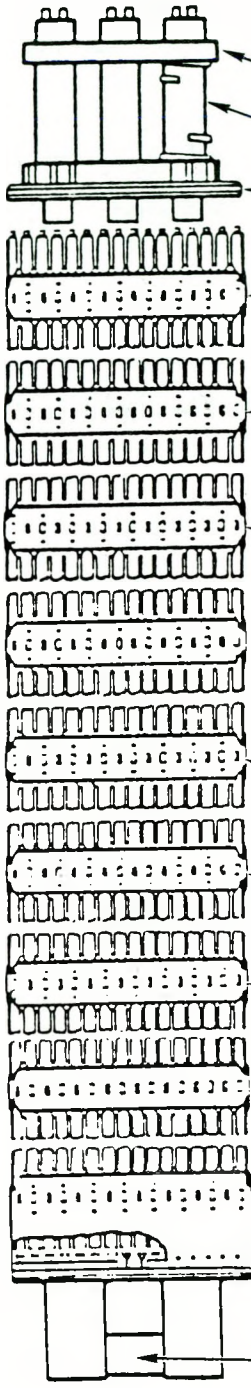

Predicted Ci/g-Ni	Sample Number	Measured Ci/g-Ni	Ratio: Predicted / Measured
2.36E-7	CE25	(1.12±0.02)E-5	0.0211
6.75E-7	CE26	(1.89±0.05)E-5	0.0357
2.17E-6	CE24	(8.36±0.32)E-5	0.0260
1.11E-5	CE10	>4.8E-5	<0.23
2.61E-4	CE9	>3.5E-4	<0.75
4.38E-4	CE8	>2.7E-4	<1.6
5.59E-4	CE7	>7.8E-4	<0.72
5.96E-4	CE6	>2.5E-4	<2.4
6.88E-4	CE5	>7.1E-4	<0.97
6.18E-4	CE4	>3.5E-4	<1.8
4.42E-4	CE3	>2.2E-4	<2.0
1.79E-4	CE2	(4.45±0.13)E-4	0.402
8.58E-5	CE14	(5.77±0.17)E-4	0.149
2.76E-5	CE1	(2.32±0.07)E-4	0.119

FIGURE 5.10. ^{59}Ni Specific Activities in Spent Fuel Assembly Hardware

Combustion Engineering 14x14 Fuel Assembly, Calvert Cliffs Nuclear Power Plant

Predicted Ci/g-Nb	Sample Number	Measured Ci/g-Nb	Ratio: Predicted / Measured
1.35E-6	CE25	>3.2E-5	<0.042
4.62E-6	CE26	(1.27±0.22)E-5	0.364
3.82E-5	CE24	>2.9E-4	<0.13
7.81E-5	CE10	–	–
1.18E-3	CE9	(1.09±0.17)E-4	10.8
2.02E-3	CE8	–	–
2.57E-3	CE7	–	–
2.75E-3	CE6	–	–
3.19E-3	CE5	(1.19±0.23)E-4	26.8
2.86E-3	CE4	–	–
2.02E-3	CE3	(1.42±0.30)E-4	14.2
8.11E-4	CE2	(1.00±0.17)E-3	0.811
5.07E-4	CE14	>1.8E-4	<2.8
2.25E-4	CE1	>2.3E-5	<9.8

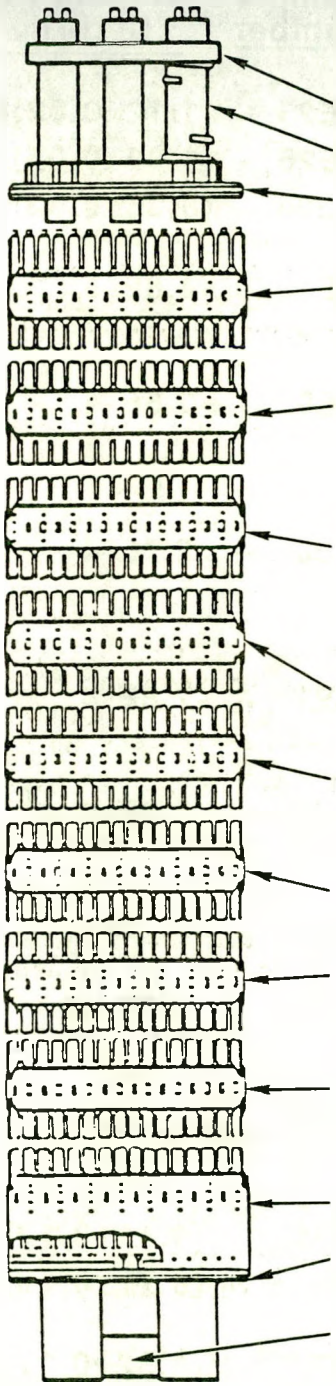

FIGURE 5.11. ^{94}Nb Specific Activities in Spent Fuel Assembly Hardware

fittings, the calculated ^{60}Co specific activities were in good agreement with the measured values. However, at the upper end fittings, the calculated values underestimated the actual ^{60}Co specific activities by about a factor of 10. Both the neutron flux and the energy spectrum undergo rapid reductions in this area, and this is the cause for the large discrepancies.

Figure 5.3 shows the measured versus calculated specific activities of ^{55}Fe in the Westinghouse assembly. The agreement for the fueled region of the assembly is excellent, with the predicted values averaging only about 12% lower than the measured activities over the entire fueled region. Again, larger variability exists at the end fittings. Figure 5.8 shows the ^{55}Fe specific activities in the Combustion Engineering assembly. Within the fueled region and the bottom end fitting the predicted values average about 2-fold lower than the measured activities. However, at the upper end fittings the calculated ^{60}Co activities are underestimated by about a factor of 10.

Figure 5.4 shows the calculated versus measured specific activities for ^{63}Ni in the Westinghouse assembly. Within the fueled region the calculated values averaged about a factor of 2.7 times lower than the measured activities, although in the middle of this region the difference is about 2.0. At the bottom and top end fittings the calculated values underestimated the ^{63}Ni activities by factors of 8 to 28. For the Combustion Engineering assembly (see Figure 5.9) the elemental nickel content of the Zircaloy spacer girds was too low to permit specific activity measurements, but the stainless steel end fittings had predicted values ranging from about 15 to 56 times lower than the measured values. Similar results were obtained for ^{59}Ni as shown in Figures 5.5 and 5.10. These discrepancies may be due to uncertainties in the available cross-section data. There are no available appropriate evaluated cross-sections for the $^{58}Ni(n,\tau)\ ^{59}Ni$ or the $^{62}Ni(n,\tau)\ ^{63}Ni$ reactions. Therefore, the cross section for natural nickel was used. This certainly affects the potential accuracy of the predictive calculations.

Figure 5.6 shows the measured and predicted ^{94}Nb specific activities for the Westinghouse assembly. Except for sample W11, which appears to be anomalous, possibly due to a very large analytical uncertainty in the elemental niobium measurement, the agreement between calculated and measured activities is quite good. In the fueled region of the assembly, the calculated values are underestimated by an average of only 25%, and at the end fitting they are underestimated by an average of only 6%, although the range is from 4% to 48%. The results for the Combustion Engineering assembly (Figure 5.11) are quite variable. For the fueled region, the calculations overestimated the ^{94}Nb activities by an average of a factor of 17, but at the end fittings the agreement is within a factor of 3. The reason for the anomalous results compared to the Westinghouse assembly is not known at this time.

The general indication of these analyses is that good agreement exists between calculational predictions of radionuclide inventories and measurements within the fueled region of the core. However, the further one goes from the fueled region, the greater the differences become. At this point it

is not certain why this discrepancy exists to the extent that it does. There are several areas currently being investigated to determine why the differences exist:

1. The calculation methods are not appropriate or were misapplied. The good agreement in the fueled region indicates that the calculations are sufficiently accurate in that region. However, the neutron flux is dropping off steeply at the end fittings and a small change in the slope would be significant.

2. The samples taken are not reflective of the average over the regions calculated. The calculations assume homogenous regions. Since the samples at the end fittings were primarily surface samples of castings, the elemental composition at the near-surface may not reflect the average in the component (e.g. the niobium may have precipitated to the surface during the casting process). Determining the curies of radionuclide in the sample per gram of parent nuclide in the sample should have accounted for this, but some other mechanism may be affecting the results.

3. As noted in 1) above, the slope of the flux is very steep outside the fueled region. The change over the upper end fitting alone is over an order of magnitude. A small shift in the sampling location could have a significant effect on the predicted radionuclide concentrations.

4. The uncertainties in the calculations may be greater than we believe. No quantitative estimate of the uncertainty due to the cross-sections used in the ANISN calculations is available. In particular, there are no appropriate evaluated cross-sections for the $^{58}Ni(n,\tau)\ ^{59}Ni$ or the $^{62}Ni(n,\tau)\ ^{63}Ni$ reactions available. Therefore, the cross-section for natural nickel was used would certainly affects the potential accuracy of the predictive calculations.

5. The relative location of control rods and burnable poisons with respect to these assemblies was not available. For PWRs, the control rods enter from the top of the assembly, thereby having a significant effect on the local flux. In general, the boron in the water has a more significant effect on the overall flux and reaction rates in the reactor core than do the control rods. However, the effect at a specific sample location may be large enough to account for the differences we are seeing.

All of these possible areas contribute to the overall uncertainty when comparing laboratory results to predictive calculations. At this point, it is not known if one dominates, or if all contribute somewhat equally. These uncertainties are presently being investigated to determine the relative error contributions.

5.2 GUNDREMMIGEN PRESSURE VESSEL

The radionuclide measurements of the Gundremmigen reactor pressure vessel steel described in Section 4 were compared with predictive calculations for the concentrations of ^{60}Co, ^{55}Fe, ^{63}Ni and ^{94}Nb. This comparison was made to evaluate the accuracy of predictive methods for calculating neutron activation product concentrations and inventories in decommissioned reactor pressure vessels. The comparison was conducted completely blind. Those conducting the measurements and the calculations were not informed of each others results until after all work was completed and submitted for comparisons. The calculated values in Table 5.4 even initially used estimated elemental concentrations of Fe, Co, Ni, and Nb for vessel steel taken from NUREG/CR-3474[12] and from Reference 18, instead of the actual measured concentrations in the specimens. For final comparisons, the initially calculated activation product concentrations in Table 5.4 were corrected for the actual elemental concentrations, and these values are given in Table 5.11.

The calculational methodology was conducted as follows. Previously determined neutron fluence values and the irradiation history[18] were used in the calculations. Activation cross sections for the precursor isotopes were generated using the XSDRN[19] neutronics code. The calculated activities are given in Table 5.4 at reactor shutdown (January 13, 1977).

The isotopes of interest are created by capturing a neutron in the naturally occurring isotopes of ^{54}Fe, ^{59}Co, ^{62}Ni, and ^{93}Nb. Neutron cross sections for these isotopes are not given in Reference 18, so values were generated starting from a 27-group library.[20] The neutron fluences are given in 35 energy groups which do not coincide with the 27 energy-group structure. The 27-group structure has fewer high-energy groups but more thermal groups. Groups 21 to 27 of the 27-group structure cover the same energy range (0.414 eV to 0 eV) as group 35 of the 35-group structure. A 27-group calculation was done from the core barrel, through the pressure vessel, and 10 cm into the concrete using the XSDRN code. Groups 21 to 27 were averaged into one group. The spectrum-averaged thermal group varies through the pressure vessel as shown in Table 5.5.

Cross sections for ^{54}Fe and ^{62}Ni do not exist on the 27-group library, so values for the elements (Fe and Ni) were obtained. The isotopes and elements all have thermal cross sections which are 1/v. Since most of the captures occur in group 35 as shown in Table 5.6 for one of the pressure vessel locations, use of the elemental cross sections with a normalization factor is a good approximation. The 2200 m/s cross sections and resonance integrals are given in Table 5.7. The XSDRN-weighted cross sections were transformed into 35-group cross sections by lethargy weighing the values above 0.414 eV. The values are given in Table 5.8.

For isotopes with a half-life less than 100 years, an appreciable fraction of the material decays away prior to reactor shutdown. Decay factors were generated using the irradiation history given in Table 10 of Reference 18. The equation given on page 9 of Reference 18 is missing a μT_m in the denominator. With the addition of μT_m in the denominator, the equation was

TABLE 5.4. Calculated Specific Activities in the Gundremmigen Vessel at Time of Reactor Shutdown[a]

	Fe-55 Activity, Ci/g			
Position	111.4	117.1	122.9	128.6
0 T	3.59E-04	3.26E-04	3.77E-04	4.39E-04
1/4 T	5.74E-05	5.18E-05	5.93E-05	6.83E-05
1/2 T	1.49E-05	1.38E-05	1.51E-05	1.70E-05
3/4 T	1.56E-05	1.49E-05	1.53E-05	1.62E-05
1 T	5.42E-05	5.26E-05	5.25E-05	5.30E-05

	Co-60 Activity, Ci/g			
Position	111.4	117.1	122.9	128.6
0 T	1.09E-05	9.91E-06	1.14E-05	1.33E-05
1/4 T	2.37E-06	2.16E-06	2.44E-06	2.79E-06
1/2 T	1.04E-06	9.65E-07	1.05E-06	1.16E-06
3/4 T	1.00E-06	9.55E-07	9.85E-07	1.04E-06
1 T	2.09E-06	2.02E-06	2.02E-06	2.05E-06

	Ni-63 Activity, Ci/g			
Position	111.4	117.1	122.9	128.6
0 T	7.89E-07	7.18E-07	8.28E-07	9.65E-07
1/4 T	1.23E-07	1.11E-07	1.27E-07	1.47E-07
1/2 T	3.00E-08	2.77E-08	3.04E-08	3.43E-08
3/4 T	3.17E-08	3.03E-08	3.13E-08	3.29E-08
1 T	1.17E-07	1.14E-07	1.13E-07	1.14E-07

	Nb-94 Activity, Ci/g			
Position	111.4	117.1	122.9	128.6
0 T	2.38E-11	2.18E-11	2.48E-11	2.86E-11
1/4 T	1.01E-11	9.29E-12	1.03E-11	1.15E-11
1/2 T	7.19E-12	6.70E-12	7.17E-12	7.88E-12
3/4 T	6.59E-12	6.25E-12	6.47E-12	6.88E-12
1 T	8.10E-12	7.78E-12	7.84E-12	8.04E-12

[a] Estimated elemental concentrations for vessel steel were taken from NUREG/CR-3474[12] and reference 18. The activities in this table were later corrected for the actual measured elemental concentrations, and these corrected values for calculated activities are listed in Table 5.11.

TABLE 5.5. Thermal Cross Sections in the Pressure Vessel, barns

Position	Fe	^{59}Co	Ni	^{93}Nb
0 T	1.482	21.57	2.646	0.666
1/4 T	1.384	20.13	2.469	0.622
1/2 T	1.226	17.84	2.188	0.551
3/4 T	1.324	19.28	2.364	0.595
1 T	1.536	22.35	2.741	0.690

TABLE 5.6. Activation by Energy Group at the Inner Surface of the Vessel (Angle = 111.4)

Group No	Fe	^{59}Co	Ni	^{93}Nb
1	1.03E-06	3.36E-07	8.22E-07	6.12E-06
2	2.41E-06	7.82E-07	1.91E-06	1.42E-05
3	4.72E-06	1.53E-06	3.75E-06	2.79E-05
4	6.52E-06	1.68E-06	7.95E-06	4.10E-05
5	1.72E-05	4.00E-06	2.37E-05	1.10E-04
6	2.77E-05	6.46E-06	3.82E-05	1.78E-04
7	1.77E-05	4.14E-06	2.45E-05	1.14E-04
8	4.26E-05	8.24E-06	7.65E-05	3.50E-04
9	1.40E-05	2.69E-06	2.51E-05	1.15E-04
10	1.37E-05	2.64E-06	2.47E-05	1.13E-04
11	8.23E-05	1.58E-05	1.57E-04	7.20E-04
12	7.86E-05	1.49E-05	1.53E-04	8.13E-04
13	1.58E-04	2.93E-05	2.62E-04	2.22E-03
14	2.43E-04	3.03E-05	2.57E-04	3.14E-03
15	3.71E-04	3.93E-05	3.24E-04	4.67E-03
16	3.29E-04	3.85E-05	2.98E-04	4.40E-03
17	2.22E-04	3.43E-05	2.25E-04	3.55E-03
18	3.68E-04	5.68E-05	3.73E-04	5.88E-03
19	2.96E-04	4.56E-05	2.99E-04	4.73E-03
20	6.14E-04	6.44E-05	8.94E-04	1.26E-02
21	3.02E-04	3.03E-05	4.49E-04	6.31E-03
22	7.65E-05	7.68E-06	1.14E-04	1.60E-03
23	9.71E-05	9.75E-06	1.44E-04	2.03E-03
24	3.57E-04	7.84E-05	6.14E-04	1.13E-02
25	4.84E-04	2.57E-04	1.12E-03	2.89E-02
26	4.04E-03	2.31E-04	1.25E-03	7.90E-02
27	5.67E-03	1.39E-02	8.81E-04	1.06E-01
28	1.45E-03	1.09E-01	1.48E-03	1.49E-01
29	2.04E-03	6.51E-03	2.06E-03	1.59E-02
30	4.05E-03	5.19E-03	4.08E-03	5.18E-03
31	4.19E-03	4.01E-03	4.21E-03	2.37E-03
32	7.20E-03	6.61E-03	7.23E-03	4.06E-03
33	1.29E-02	1.16E-02	1.30E-02	7.30E-03
34	5.85E-03	5.19E-03	5.89E-03	3.30E-03
35	9.48E-01	8.37E-01	9.54E-01	5.33E-01

TABLE 5.7. Comparison of Isotopic Cross Sections to Elemental Cross Sections

Cross Section	Cross Section, barns			
	^{54}Fe	Fe	^{62}Ni	Ni
2200 m/s	2.25	2.55	14.2	4.43
Res. Int.	1.2	1.4	6.8	2.2

used to calculate decay factors. The calculated decay factors are 0.373 for ^{55}Fe, 0.573 for ^{60}Co, and 0.968 for ^{63}Ni.

Atom densities for Fe and Ni are given in Reference 18. Atom densities for Co and Nb were obtained from NUREG/CR-3474[12] which shows a range of values for each impurity for various pressure vessels. The values used are 122 ppm for cobalt and 18.8 ppm for niobium.

Factors to normalize the activation calculations were generated with the following equation:

$$\frac{\text{(Cross Section Ratio)(Precursor Fraction)(Atom Density)(Decay Factor)(ln 2)}}{\text{(Half-Life)(Vessel Density)(Disintegrations/yr/Ci)}}$$

where the vessel density is 7.80 g/cm^3 and there are 1.168×10^{18} d/yr/Ci. The other values in the equation are isotope dependent and are given in Table 5.9. By multiplying the activation factor times the cross section times the neutron fluence, one obtains the specific activity in units of Ci/g of metal.

The resulting values (shown in Table 5.4) do not include axial form factors. From Figure 4 of Reference 18, axial form factors can be determined for fast neutrons (E > 1MeV). The deduced values are given in Table 5.10. From the thermal fluence (Tables 4 - 7 and Figures 15 - 18 of Reference 18) axial form factors have been generated (see Table 5.10). These values are good to 2 percent. Comparison of the thermal axial form factors to the fast axial form factors indicates a much different axial thermal flux shape.

As a check on the calculational approach described above, an attempt was made to reproduce the January 22, 1986 ^{54}Mn activities given in Reference 18. The activation factor is 1.25×10^{-15}. The results are 10-15% higher than the values given in Reference 18. The fast axial form factors were used for these comparisons. The cause of the discrepancy has not been determined; however, if the thermal axial form factors were used, the results would be 0-8% higher than the values given in Reference 18. Details on the published values are not given.

The final measured and predicted concentrations of ^{60}Co, ^{55}Fe, ^{63}Ni and ^{94}Nb are given in Table 5.11. The calculated activities given in Table 5.4 were corrected for the actual elemental concentrations of cobalt, iron,

TABLE 5.8. Multi-Group Section for Activity Calculations, barns

Group No	Fe	^{59}Co	Ni	^{93}Nb
1	3.49E-04	1.87E-03	4.92E-04	1.65E-03
2	3.49E-04	1.87E-03	4.92E-04	1.65E-03
3	3.49E-04	1.87E-03	4.92E-04	1.65E-03
4	5.36E-04	2.27E-03	1.16E-03	2.69E-03
5	6.66E-04	2.56E-03	1.63E-03	3.42E-03
6	6.66E-04	2.56E-03	1.63E-03	3.42E-03
7	6.66E-04	2.56E-03	1.63E-03	3.42E-03
8	1.12E-03	3.57E-03	3.57E-03	7.35E-03
9	1.13E-03	3.59E-03	3.61E-03	7.43E-03
10	1.13E-03	3.59E-03	3.61E-03	7.43E-03
11	1.37E-03	4.34E-03	4.65E-03	9.57E-03
12	1.90E-03	5.94E-03	6.55E-03	1.57E-02
13	2.55E-03	7.77E-03	7.48E-03	2.85E-02
14	4.04E-03	8.30E-03	7.57E-03	4.17E-02
15	4.92E-03	8.61E-03	7.63E-03	4.95E-02
16	5.06E-03	9.75E-03	8.12E-03	5.40E-02
17	5.62E-03	1.43E-02	1.01E-02	7.18E-02
18	5.62E-03	1.43E-02	1.01E-02	7.18E-02
19	5.62E-03	1.43E-02	1.01E-02	7.18E-02
20	1.10E-02	1.90E-02	2.84E-02	1.81E-01
21	1.19E-02	1.97E-02	3.14E-02	1.99E-01
22	1.19E-02	1.97E-02	3.14E-02	1.99E-01
23	1.19E-02	1.97E-02	3.14E-02	1.99E-01
24	1.23E-02	4.45E-02	3.75E-02	3.11E-01
25	1.36E-02	1.19E-01	5.58E-02	6.48E-01
26	8.01E-02	7.54E-02	4.38E-02	1.25E+00
27	1.27E-01	5.11E+00	3.49E-02	1.89E+00
28	2.74E-02	3.39E+01	4.96E-02	2.26E+00
29	5.56E-02	2.92E+00	9.95E-02	3.46E-01
30	9.17E-02	1.94E+00	1.64E-01	9.38E-02
31	1.63E-01	2.57E+00	2.91E-01	7.37E-02
32	2.22E-01	3.36E+00	3.96E-01	1.00E-01
33	4.10E-01	6.04E+00	7.33E-01	1.85E-01
34	5.44E-01	7.96E+00	9.72E-01	2.45E-01
35	1.48E+00	2.16E+01	2.65E+00	6.66E-01

nickel, and niobium measured in the samples (see Table 4.2). These corrections were made by multiplying the values in Table 5.4 by the ratio of the actual measured elemental concentration to the concentrations used in the initial calculations. These corrections amounts to factors of 2.78, 0.954, 1.031, and 0.53, respectively for the Co, Fe, Ni, and Nb.

TABLE 5.9. Factors for Activation Calculations

Description	^{55}Fe	^{60}Co	^{63}Ni	^{94}Nb
Precursor Fraction	0.058	1.0	0.036	1.0
Density, a/b-cm	0.0818	9.8E-06	6.4E-04	9.6E-07
Half-Life, yr.	2.7	5.272	100	20,000
Decay Factor	0.3733	0.5729	0.9681	0.9998
Cross Section Ratio	0.882	1.0	3.21	1.0
Activation Factor	4.40E-23	8.10E-26	5.45E-26	3.65E-30

TABLE 5.10. Axial from Factors for Gundremmigen

Trepan	E > 1 MeV	E > .4 eV
A,B,C,D	1.17	1.09
E,F,G,K	1.10	1.00
L,M,N,P	0.98	0.91

As shown in Table 5.11 the agreement between measured and calculated activities is quite good considering that the neutron flux varies by over two orders of magnitude through the reactor pressure vessel wall. The calculated ^{60}Co, ^{55}Fe, and ^{94}Nb concentrations were overestimated by an average factor of 1.9, 1.3, and >1.4, respectively. The calculated ^{63}Ni was underestimated by an average factor of 1.4. Thus, the agreement is quite good, and utilizing the methods for calculating neutron fluence[18] and vessel activation (this report) provides a reasonably good assurance that the calculational methods are producing reliable estimates of the concentrations of activation products in the reactor pressure vessel. This benchmarking will give confidence to similar methodology which will be used in future decommissioning assessments of commercial nuclear power stations.

TABLE 5.11. Comparison of Measured vs. Calculated Concentrations of Neutron Activation Products in Gundremmigen Pressure Vessel Steel

Radionuclide	Radiochemically Measured Concentration (Ci/g steel)[a]		Calculated Concentration (Ci/g steel)[a]		Ratio: Calculated/Measured	
	Sample #3 (0.41T)	Sample #4 (0.67T)	Sample #3 (0.41T)	Sample #4 (0.67T)	Sample #3	Sample #4
^{60}Co	2.53E-6	1.32E-6	4.53E-6	2.67E-6	1.79	2.02
^{63}Ni	1.14E-7	4.37E-8	7.53E-8	3.09E-8	0.662	0.709
^{55}Fe	2.91E-5	9.25E-6	3.29E-5	1.42E-5	1.13	1.54
^{94}Nb	<2.8E-12	<3.1E-12	4.4E-12	3.5E-12	>1.6	>1.1

(a) Decay corrected to reactor shutdown date of January 13, 1977.

6.0 SUMMARY AND CONCLUSIONS

Although this is an interim program report, there are significant results to date which have enhanced the radiological characterization associated with reactor decommissioning and related radioactive waste disposal.

6.1 RESEARCH FINDINGS AND REGULATORY IMPLICATIONS

The significant research findings can be grouped into two main areas: 1) the radiological assessments conducted during the Shippingport Station decommissioning, and 2) the radiological characterization of activated metal components.

6.1.1 Radiological Assessments During Shippingport Station Decommissioning

From a radiological standpoint, the decommissioning operations at Shippingport Station were extremely successful and have provided an optimistic and positive projection for the ultimate decommissioning of commercial reactor stations. One of the most significant observations at Shippingport Station was the fact that essentially all of the residual radionuclides were neutron activation products dominated by ^{60}Co. No significant concentrations of fission products or transuranic radionuclides were associated with the residual activity. This would be representative of the commercial nuclear power stations which have experienced little or no fuel cladding failures during their operations. Although the activation products ^{55}Fe, ^{63}Ni, ^{59}Ni, and ^{94}Nb were present with the ^{60}Co, their combined concentrations associated with the radioactive residues in piping, plant components, and other waste materials (excluding the pressure vessel internals) never exceeded the 10CFR61 Class A waste limit. Although the Shippingport Station was a DOE facility and not subject to the regulations contained in 10CFR61, the ramifications of the residual radioactivity levels in decommissioning wastes were of significance. First, it suggested that commercial stations having similar residual radionuclide inventories and distributions can expect to dispose of essentially most radioactive decommissioning materials and components (except reactor pressure vessel internals) as Class A waste. Secondly, this will greatly simplify the disposal methods and the dismantling options during decommissioning.

Another vanguard operation at Shippingport Station was the methodology developed by DOE and its subcontractors for characterization, packaging, shipment, and disposal of the reactor pressure vessel and internal components as an LSA, Type B package conforming to Department of Transportation and Nuclear Regulatory Commission regulations. The physical, chemical, and radiological characterization conducted by PNL of the radioactive corrosion film contained on the inside surfaces of the reactor pressure vessel and internal components showed that this material was extremely cohesive and would not be released under a variety of hypothetical severe accident conditions during transportation to the disposal facility.

Other important radiological "lessons learned" during the decommissioning of Shippingport Station as they apply to commercial stations are being assessed and will be presented in the final report for this project.

6.1.2 Radiological Characterization of Activated Metal Components

During the past year this work has involved the radiological characterization of activated metal components from three commercial fuel assemblies, and characterization of steel specimens from the Gundremmigen reactor pressure vessel. Particular emphasis has been in measuring and assessing the significance of the long-lived radionuclides specified in 10CFR61. This work has shown that the relatively high nickel and niobium content of Inconel, and the nickel content of stainless steel has resulted in ^{63}Ni, ^{59}Ni, and ^{94}Nb concentrations in some fuel assembly hardware components being over the Class C limit. This would require that these components be disposed of in a high-level waste repository or some other approved alternative facility.

It was discovered in this work that the concentrations of ^{93m}Nb, a 13.6 year half-life activation product, were present in the activated metal specimens at levels over 1800 times higher than previous calculations. To the best of our knowledge, these are the first actual measurements of ^{93m}Nb in activated metals. This radionuclide decays by emission of a 30-keV gamma-ray which is essentially all converted, and the predominant external radiation is due to the 16-keV Nb x-rays. This radionuclide has not even been considered in 10CFR61, and its long-term environmental significance will need to be assessed.

During the radiological characterization of the fuel assembly hardware it was possible to conduct separate detailed predictive calculations of radionuclide concentrations in the same material. A comparison of the measured versus calculated concentrations of ^{55}Fe, ^{60}Co, ^{59}Ni, ^{63}Ni, and ^{94}Nb in the fuel assembly hardware from Westinghouse and Combustion Engineering PWR fuel assemblies showed quite good agreement in most cases. The agreement between measured versus calculated values for these radionuclides in hardware from the fueled region of the assemblies were generally on the order of 10 to 50 percent, and never exceeded about a factor of two. As the neutron flux and energy spectrum drops rapidly between the fueled region and the end fittings of the assemblies, the uncertainties in the calculational methods become much larger and large differences in measured versus calculated activated were observed. The largest discrepancies were observed for the ^{59}Ni and ^{63}Ni activities at the end fittings of the fuel assemblies. Since no adequate isotopic cross-section data exist for the stable parent nickel isotopes, elemental cross-section data were used, and this may have introduced relatively large uncertainties in the calculated results.

The radionuclide measurements of the Gundremmigen pressure vessel steel were in very good agreement with a blind comparison of calculated activities. The average calculated-to-measured ratio for ^{55}Fe, ^{60}Co, and ^{63}Ni were 1.3, 1.9, and 0.69, respectively. The concentrations of the radionuclides were

all below Class A limits, indicating that the entire pressure vessel (not including internals) could have been disposed of as Class A waste in a low-level waste shallow land burial facility.

The measurements and calculational methods utilized in this work have lent confidence to calculational methods for predicting radionuclide inventories in activated metals, and have identified certain problem areas where better cross-section data or calculational methodology are needed.

7.0 FUTURE PLANNED WORK

With the completion of the Shippingport Station decommissioning and the radiological analyses of the spent fuel assembly hardware, the project will focus on the radiological characterization of spent PWR and BWR control rod assemblies and in addressing current issues/problems relating to reactor decommissioning, such as the adequacy of dose-to-curie conversion techniques, the adequacy of radiochemical methods for determining 10CFR61 radionuclides, and assessing alternative ways of disposing of greater-than-Class C radioactive materials.

The radiological characterization of spent control rods is a timely task because many nuclear utilities are in need of disposing of spent control rod assemblies and are faced with the difficult task of accurately determining the 10CFR61 radionuclide contents and associated waste classification of these materials prior to disposal. In our research task we have acquired specimens of the following spent control rods having well-known irradiation histories: 1) a BWR cruciform control rod from Duane Arnold Energy Center of Iowa Electric, 2) a rod cluster control assembly (RCCA) from Point Beach Nuclear Station of Wisconsin Electric, and 3) a burnable poison rod assembly (BPRA) also from Point Beach Nuclear Station. These control rods have been acquired under a separate DOE project and are presently stored in the hot cells at Pacific Northwest Laboratory (PNL). Extensive sampling of the various components of these control rods has commenced at PNL and detailed radiochemical analyses of the specimens will be conducted for all 10CFR61 radionuclides plus other long-lived activation products that are likely to be present, e.g., ^{108m}Ag, ^{113m}Cd, ^{93}Mo, ^{10}Be, and ^{14}C. This will be the first opportunity to conduct detailed laboratory sampling and analyses of the neutron activation products present in spent control rods. In addition to the laboratory measurements, direct assays of the radionuclide contents of the control rods by state of the art dose-to-curie conversion methods will be conducted to compare the accuracy of these techniques with the empirical measurements. Also, "blind" predictive modeling of the activation product contents of the spent control rods will be conducted to compare the accuracy of the calculational techniques with the empirical measurements. Thus, the adequacy of the two techniques (dose-to-curie conversion and modeling calculations) most commonly used for determining the waste classification of spent control rods will be assessed for the first time. This work will provide the first accurate measurements of the concentrations of neutron activation products in spent control rods and provide a degree of confidence in the direct assay and computational techniques presently being used by the utilities and their contractors for determining waste classification of these highly activated components. This work will also help to identify any shortcomings in these methods so that adequate corrections can be made to the existing techniques.

Future planned work will also provide an assessment of the adequacy of the radiochemical methods used for analyses of the 10CFR61 radionuclides and other long-lived radionuclides of interest. This assessment will involve an analysis of potential sources of error including dispersion, bias, repeatability, interfering radionuclides, and detection sensitivities. Special

consideration will be given to those difficult-to-measure radionuclides that have the greatest potential for analytical error, i.e., ^{59}Ni, ^{63}Ni, ^{129}I, ^{99}Tc, ^{14}C, ^{93}Mo, ^{10}Be and ^{93m}Nb. This work will also examine the potential errors contributed by the sampling of radioactive waste materials including sample representativeness, inhomogeneities, sample size, and sampling methods.

An assessment of the accuracy and potential sources of error associated with the direct assay and calculational methods for estimating the radionuclide contents of neutrons activated from reactor pressure vessels will be conducted. This assessment will include an analysis of errors associated with conducting dose measurements of extremely radioactive materials, uncertainties associated with irradiation histories, uncertainties associated with nuclear data and elemental concentration data used in calculations, uncertainties in dose-to-curie conversion factors, and other related parameters.

Finally, an assessment will be made of examining ways of minimizing the volume of greater-than-Class C waste generated at nuclear power stations, and methods to dispose of greater-than-Class C waste in ways not requiring disposal in a high-level waste repository. Such assessments would include methods of separating only those portions of irradiated components that actually exceed the Class C limit. For example, only a relatively small volume of certain spent fuel assembly hardware exceeds the Class C limit, while the majority of the hardware components may be below the limit. Also, ways of consolidating the greater-than-Class C waste into waste of lower specific activity by averaging the radionuclide concentrations over the entire volume of the waste component will be investigated.

8.0 REFERENCES

1. U.S. N.R.C., "General Requirements for Decommissioning Nuclear Facilities," Final Rule, 10 CFR Parts 30, 40, 50, 51, 70, and 72, Federal Register 53, No. 123, pp. 24018-24056, Monday, June 27,1988.

2. U.S. N.R.C., "Licensing Requirements for Land Disposal of Radioactive Wastes," 10 CFR 61. Federal Register, 46, No. 142, Friday, July 24, 1981, U.S. Nuclear Regulatory Commission, Washington, D.C.

3. Smith, R. I., G. J. Konzek and W. E. Kennedy, Jr., "Technology, Safety, and Costs of Decommissioning a Reference Pressurized Water Reactor Power Station," NUREG/CR-0130, Vols. 1 and 2, Prepared for the U.S. Nuclear Regulatory Commission by Pacific Northwest Laboratory, Richland, WA, June, 1978.

4. Luksic, A. T., et. al., "Spent Fuel Disassembly Hardware and Other Non-Fuel Bearing Components: Characterization, Disposal Cost Estimates, and Proposed Repository Acceptance Requirements," PNL-6046, Pacific Northwest Laboratory, October, 1986.

5. U.S. N.R.C., "Disposal of Radioactive Waste," Final Rule, 10 CFR 61, Federal Register 54, No. 100, pp. 22578-22583, Thursday, May 25, 1989.

6. Abel, K. H. et. al., "Residual Radionuclide Contamination Within and Around Commercial Nuclear Power Plant," NUREG/CR-4289, U.S. Nuclear Regulatory Commission, Washington, D.C., 1986.

7. Robertson, D. E., et. al., "Residual Radionuclide Contamination Within and Around Nuclear Power Plants: Origin, Distribution, Inventory, and Decommissioning Assessment," Rad. Waste Mgmt. Nucl. Fuel Cycle, 5, pp. 285-310, 1984.

8. Oak, H. D., G. M. Holter, W. E. Kennedy, Jr., and G. J. Konzek, "Technology Safety, and Costs of Decommissioning a Reference Boiling Water Reactor Power Station," NUREG/CR-0672, Vols. 1 and 2, Prepared for the U.S. Nuclear Regulatory Commission by Pacific Northwest Laboratory, Richland, WA, June, 1980.

9. Wittenbrock, N. G., "Technology, Safety, and Costs of Decommissioning Nuclear Reactors at Multiple-Reactor Stations," NUREG/CR-1755, Prepared for the U.S. Nuclear Regulatory Commission by Pacific Northwest Laboratory, Richland, WA, January, 1982.

10. Murphy, E. S. and G. M. Holter, "Technology, Safety, and Costs of Decommissioning Reference Light Water Reactors Following Postulated Accidents," NUREG/CR-2601, Vols. 1 and 2, Prepared for the U.S. Nuclear Regulatory Commission by Pacific Northwest Laboratory, Richland, WA, November, 1982.

11. Konzek, G. J., J. D. Ludwick, W. E. Kennedy and R. I. Smith, "Technology, Safety, and Costs of Decommissioning Reference Nuclear Research and Test Reactors," NUREG/CR-1756, Vols. 1 and 2, Prepared for the U.S. Nuclear Regulatory Commission by Pacific Northwest Laboratory, Richland, WA, March, 1982.

12. Evans, J. C., et. al., "Long-Lived Activation Products in Reactor Materials," NUREG/CR-3474, Prepared for the U.S. Nuclear Regulatory Commission by Pacific Northwest Laboratory, Richland, WA, August, 1984.

13. Evans, J. C., E. L. Lepel, R. W. Sanders, C. W. Thomas, D. E. Robertson, "Long-Lived Activation Products in Light-Water Reactor Construction Materials: Implications for Decommissioning," Rad. Waste Mgmt. Nucl. Fuel Cycle, 11 (1), pp. 1-39, 1988.

14. U.S. D.O.T., "Tests for Demonstrating the Ability of Type B and Fissile Radioactive Materials Packaging to Withstand Accident Conditions in Transportation," 49 CFR 173.469, Code of Federal Regulations, Ch. 1 (10-1-86 Edition), pp. 659-660, 1986.

15. Kea, K. I., "Reactor Pressure Vessel Preparation for Shipment and Burial," IN: 1987 International Decommissioning Symposium, October 4-8, 1987, Pittsburgh, PA, CONF-871018-Vol. 1, pp. II-31 to II-47, Gail A. Taft, Ed., Westinghouse Hanford Corporation, Richland, WA, 1987.

16. Westinghouse Hanford Company, "Safety Analysis Report for Packaging. Shippingport Reactor Pressure Vessel and Neutron Shield Tank Assembly," Shippingport Document SSDP-0050, Rev. 0, 7/1/88, Docket No. 87-7-9515, Westinghouse Hanford Company, Richland, WA, July, 1988.

17. Luksic, A. T., "Characterization of Activated Metals in Spent Fuel Hardware", J. Institt. Nucl. Mat. Mgmt. XVI, No. 3, 19-21, 1988.

18. Prillinger, G, "Neutron Spectrum Calculation for the Gundremmingen KRB/A Reactor," NUREG/CR-4791, Institute fur Kernenetgetik und Energiesysteme, November, 1986.

19. Greene, N. M. and C. W. Crave, Jr., "XSDRN: A Discrete Ordinates Spectral Averaging Code," ORNL-TM-2500, Oak Ridge National Laboratory, July, 1969.

20. Parks, C. V., "Summary Description of the SCALE Modular Code System," NUREG/CR-5033, Oak Ridge National Laboratory, December, 1977.

DISTRIBUTION

No. of
Copies

30 Pacific Northwest Laboratory

D. R. Haffner, K6-25
A. T. Luksic, K6-42
D. E. Robertson (20), P8-01
R. I. Smith, K6-25
N. L. Wynhoff, P8-08
Publishing Coordination
Technical Report Files (5)